PONTIFICIA UNIVERSIDAD CATOLICA DE CHILE
FACULTAD DE FISICA
INSTITUTO DE ASTROFÍSICA

Blue Stragglers in the Gaia Era: Galactic Open and Globular Clusters

by

Francisco Felipe Carrasco Varela

Thesis submitted to the Faculty of Physics, Institute of Astrophysics, of Pontificia Universidad Católica de Chile, as one of the requirements to qualify for the academic Master's degree in Astrophysics.

Supervisor	:	Thomas H. Puzia (PUC Chile)
Committee	:	Manuela Zoccali (PUC Chile)
		Rodrigo Contreras (PUC Chile)

October, 2023
Santiago, Chile

What people consider flaws are actually talents
they have yet to find a proper use for.

Abstract

Blue Straggler Stars (BSSs) are one of the keys to understand in a better way how stars evolve and interact with each other in different star clusters. They appear to be hotter and brighter than the Main Sequence Turn Off Point (MSTO) and, therefore, they should have evolved off the Main-Sequence branch. We properly select, for Open Clusters (OCs) and Globular Clusters (GCs), star cluster members based on proper motions and parallaxes provided by Gaia DR3. Using isochrones models and selection criteria from previous studies, we select and classify stars as BSS, Yellow Straggler Stars and Red Stragglers Stars (evolved BSSs). We identify BSSs to be present in all our GCs and in 42/129 ($\sim 33\%$) of OCs. We counted a total of 4399 BSSs; 434 ($\sim 10\%$) located in OCs and 3965 (90%) located in GCs. We obtain astrophysical parameters from 3 different methods (color–temperature relations, isochrone–fitting models and parameters from Gaia DR3 spectra) such as the effective temperature $T_{\rm eff}$, star mass M, and surface gravity $\log(g)$. We find values for BSS $T_{\rm eff}$ to be $\sim (6800 \pm 585)$ K in GCs and $\sim (7570 \pm 1400)$ K in OCs; and an average mass of $\langle M_{\rm BSS} \rangle = (1.75 \pm 0.45)\ M_{\odot}$ in OCs and $\langle M_{\rm BSS} \rangle = (1.02 \pm 0.1)\ M_{\odot}$ in GCs. Based on previous studies, we compute the value $\mathcal{M}_{\rm e}$ –the difference of the BSS mass and the MSTO mass, normalized by the MSTO mass– for every BSS. This parameter is classified as low–$\mathcal{M}_{\rm e}$ ($\mathcal{M}_{\rm e} < 0.5$, BSS likely formed through mass-transfer) and high–$\mathcal{M}_{\rm e}$ ($0.5 < \mathcal{M}_{\rm e} < 1.0$, BSS likely formed through mergers). For OCs we find a percentage 81.34% high–$\mathcal{M}_{\rm e}$ and 18.66% low–$\mathcal{M}_{\rm e}$. For GCs, we find 94.25% low–$\mathcal{M}_{\rm e}$ and 5.25% high–$\mathcal{M}_{\rm e}$. Comparing $\mathcal{M}_{\rm e}$ with BSSs age found from isochrones models we discover a double sequence in GC BSSs, where we conclude that these sequences correspond to a pre merger/closer-binary interaction and post merger/closer-binary interaction of BSS formation scenario.

Acknowledgment

A mi mamá, mi papá y Tobito: los mejores; siento que no los merezco.

A mis amigos del Discord (Rinconcito y Froggos): gracias por las risas.

Contents

Chapter 1

Introduction

1.1 What are Blue Stragglers?

Blue Stragglers Stars (BSSs) are stars that appear to be younger and more massive than the bulk of other stars of their host stellar population. They are characterized by their location on the Hertzsprung-Russell diagram (HR diagram) or Color-Magnitude Diagram (CMD), where they appear as hotter and bluer stars than their Main-Sequence (MS) neighbors.

1.2 Discovery

1.2.1 Globular Clusters

BSSs were first identified by Sandage (1953) through his observations of the Globular Cluster (GC) Messier 3 (M3). They were initially observed to be bluer and more luminous than other MS stars in the cluster, which led to their designation as "stragglers". M3 remained as the only GC in which BSSs were identified until 1971, when BSSs made their appearance again, but this time in the GC M71 (Arp and Hartwick, 1971). As time passed by, photometry improved, leading to the discovery of nearly 400 BSSs in the early 1990s for around 20 GCs (Fusi Pecci et al., 1993; Sarajedini, 1993).

1.2.2 Open Clusters

GCs were not the only places in our galaxy where BSSs were found in the 1950s. Their first official discovery in an Open Cluster (OC) was made by Burbidge and Sandage (1958), even when a couple of years earlier Johnson and Sandage (1955) also discovered some BSSs; however, the authors thought these new unknown blue stars could be anomalous MS stars or they could be confusing them with Blue Horizontal Branch (BHB) stars.

An interesting case is the OC NGC6791, which is one of the oldest OCs known with age ~ 7.22 Gyr and [Fe/H] ~ 0.4 (Dias et al., 2021; Cordoni et al., 2023), where not only BSSs were identified, but the sequence is more yellow than blue; which started giving some hints about BSSs evolution.

In a similar way that more and more BSSs were being identified for GCs, the same happened for OCs. For example, Ahumada and Lapasset (1995) provided a catalogue of BSSs for almost ~ 960 objects for 390 OCs; with an updated version in 2007 with almost ~ 1900 BSSs for 427 OCs (Ahumada and Lapasset, 2007).

1.2.3 Other structures

Additionally, BSSs started being identified in another places/structures such like the field (Bond and MacConnell, 1971; Preston et al., 1994), OB Associations (Schild, 1985; Mathys, 1987), and even dwarf galaxies (Da Costa, 1984; Momany et al., 2007; Mapelli et al., 2009).

1.3 Formation Mechanisms

1.3.1 Mass-Transfer

The appearance of BSSs in different places/structures puts above the table that there might be a common process happening that creates these stars. One of the first explanations in the early 1960s was that BSSs could be Algol-type Eclipsing Binaries (Hoyle, 1955) proposed by Eggen and Sandage in 1962 (published later as Eggen and Sandage, 1964). These types of stars are eclipsing binaries with a short period where the brighter

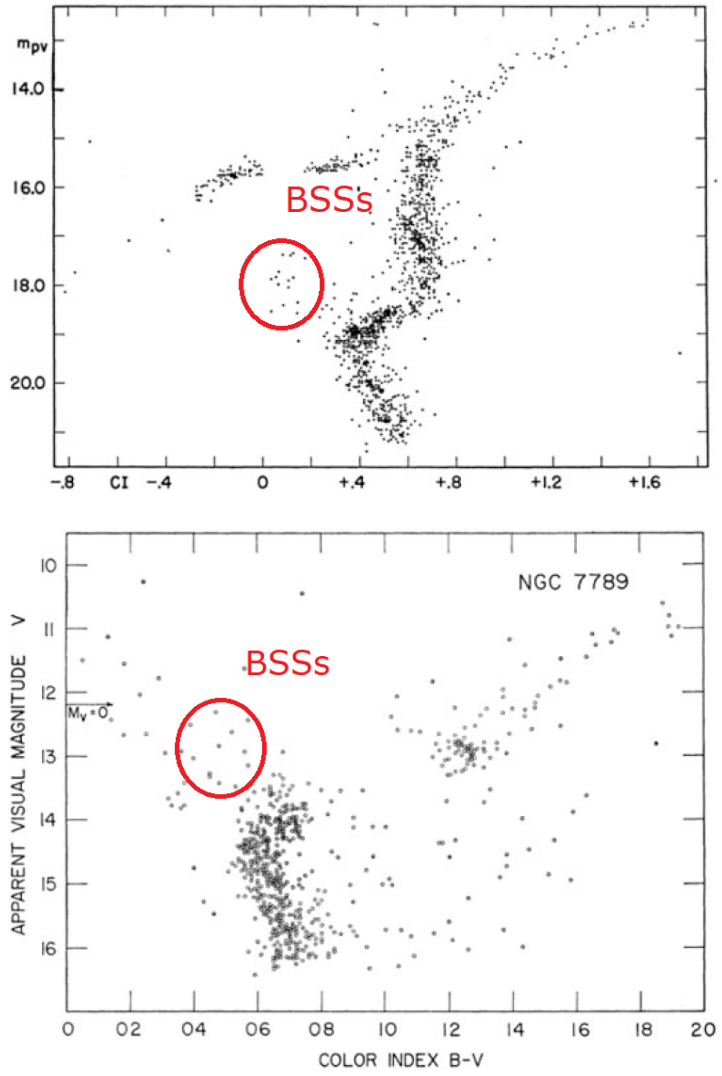

Figure 1.1: First discoveries of Blue Stragglers Stars in Galactic Clusters. *Top*: CMD for Globular Cluster M3 by Sandage (1953). *Bottom*: CMD for Open Cluster NGC7789 by Burbidge and Sandage (1958). BSSs are enclosed in a red cirle.

star is located near the Zero-Age Main-Sequence (ZAMS) and the fainter companion looks apparently more evolved, i.e., older.

However, it was not until the work of McCrea (1964) that a theory of mass-transfer (MT) was formally introduced. In this theory, the primary star transfers material/mass to the secondary one via the inner Lagrangian point when its Roche lobe is filled. Assuming this scenario, the secondary star becomes a more massive MS star, which extends its life by a factor of ~ 2 if we compare it with a common star with a similar mass.

When the material is transferred from one star to another, we may also expect chemical anomalies in the secondary star; the one receiving the material. This is due to the fact that the accreted material is expected to lie on the secondary star surface, which comes from the inner region of the donor star and, therefore, we may expect material/elements that should not be present in the secondary star (Sarna and De Greve, 1996).

1.3.2 Collisions

On the other hand, it has been proposed that BSSs could be also formed through collisions (Hills and Day, 1976). Contrary to the chemical anomalies expected in the MT scenario, we do not expect chemical anomalies for BSSs formed through this scenario (Lombardi et al., 1995). In this scenario, we expect BSSs that are formed through collisions (COL) predominantly in a high-density environment, where collisions between stars are most probable to occur (Mapelli et al., 2004, 2006).

1.3.3 Hierarchical Triple Systems

Hurley et al. (2005) through `N-Body` simulations suggested that most of the MT-BSSs should be formed in the inner regions of the clusters. But this was in contradiction with the observations which showed that MT-BSSs do exist much further in the cluster outskirts than they should be (Geller et al., 2008). Tokovinin et al. (2006), based on 2-MASS data, have shown that most of binary systems with a period $P < 3$ days, around 96%, had distant tertiary components. Based on the discrepancy between the models and the observations for MT-BSSs (binaries) and this observational evidence of binary periods and the presence of third companions, Perets and Fabrycky (2009) proposed a new formation channel for BSSs: triple hierarchical systems. This would explain why some MT-BSSs are where they "should not be" (based on the models mentioned previously) and, would also contribute to explain their unique period–eccentricity distribution for observations.

Chapter 2

State of Art

2.1 Catalogues

2.1.1 Globular Clusters

For GCs, Simunovic and Puzia (2016) have provided a BSSs Catalogue for 38 GCs. Using proper motions derived from HST data using "*The ACS Survey of Galactic Globular Clusters*" (Sarajedini et al., 2007) and "The HST Legacy Survey of Galactic Globular Clusters: Shedding UV Light on Their Populations and Formation" (Piotto et al., 2015). However, it is important to note that this is an optical-filter driven catalogue, which may lead to biases and systematics when identifying BSSs using other filter combinations such as UV filters (see section 2.4 for more details).

2.1.2 Open Clusters

As mentioned in section 1.2.2, one of the first catalogues for BSSs in OCs was provided by Ahumada and Lapasset (1995), updated in Ahumada and Lapasset (2007) for 390 clusters based on the Open Cluster Database WEBDA (Mermilliod and Paunzen, 2003).

In the last decade, the Gaia mission (Gaia Collaboration et al., 2016) has provided proper motions and parallaxes for more than 1.3 billion stars in its second data release (Gaia Collaboration et al., 2018). Using Gaia Data Release 2 photometry and new machine-learning based catalogues (Cantat-Gaudin et al., 2018, 2020) a new "Gaia-based" catalogue

for 408 Galactic OCs was generated by Rain et al. (2021), who successfully identified 897 BSSs in 111 of the analyzed clusters. In addition to providing identified BSSs, they found that OCs younger than $\sim$ 500 Myr do not host any BSSs.

More recently, Li et al. (2023) made a new "Gaia-based" catalogue, but this time using Gaia Data Release 3 also for OCs. In addition to selecting clusters of previous Gaia DR2 based studies (Rain et al., 2021; Jadhav and Subramaniam, 2021), they identify new OCs not added/identified in previous OC BSSs catalogues (e.g. Cantat-Gaudin and Anders, 2020; Cantat-Gaudin et al., 2020). They have studied 101 new OCs and, within this new sample, they found 138 new BSSs in 50 OCs that have not been previously reported.

2.2 Double Sequence of Blue Stragglers

Ferraro et al. (2009) presented for the very first time the discovery of two sequences of BSSs in the GC M30. A red sequence of BSSs and a blue sequence of BSSs. They suggest that red-BSSs are formed through the MT scenario whereas blue-BSSs are formed through collisions.

Some years later, Dalessandro et al. (2013) discovered a Double Sequence of BSSs in the GC NGC362 as well. They found that blue-BSSs are well reproduced by collision isochrone models from Sills et al. (2009), with a 200 Myr collisional isochrone; whereas red-BSSs lie in the region expected for MT-BSSs based on a model from Tian et al. (2006). Therefore, they suggest that blue-BSSs are formed through collisions whereas red-BSSs are formed via MT.

Simunovic et al. (2014) have also found a double sequence of BSSs in the GC NGC1261. In short, they fit an isochrone collision model for these two sequence of BSSs. Unlike the two previous studies mentioned, they find that both sequences are well reproduced by collisional isochrones. The bluer sequence fits well with a 200 Myr collision model whereas the red sequence of BSSs is in agreement with a collisional isochrone model of a 2 Gyr old population. This indicates the presence of a post-core-collapse event in this cluster that triggers a sudden formation of BSSs and, therefore, they observe two sequences of BSSs indicating that two different formation events have occurred in the past.

These results have also been discovered in the GC M15 by Beccari et al. (2019), reaffirming the idea that BSSs can be a great indicator that a core-collapse event have occurred in the cluster's dynamical evolution history.

More recently, Rao et al. (2023a) have also shown a double sequence of BSSs, but this time they have found this double sequence in an OC, an environment less dense than a GC. Therefore, collisional BSSs are not expected to be present in such low-stellar density environments; or at least not in such a large fraction. They could not provide an explanation for this.

2.3 Importance and Utility of Blue Stragglers

Based on the works of Lanzoni et al. (2007) and Contreras Ramos et al. (2012), Ferraro et al. (2012) have analyzed the radial distribution of BSSs and classified the dynamical evolution of the cluster based on this parameter. Using the minimum distance from the cluster center for this radial distribution $r_{\rm min}$, Ferraro et al. (2012) have used this parameter as a chronometer to measure the dynamical ages of GCs. In some way $r_{\rm min}$ is an indicator of the mass segregation of the cluster. In general, small values for $r_{\rm min}$ are found in dynamically young clusters, whereas large values are found in dynamically old clusters. For non-extreme values of $r_{\rm min}$, Ferraro et al. (2012) expect a dynamically middle-age cluster. In order to quantify this "BSSs mass segregation" indicator parameter, Alessandrini et al. (2016) defined the parameter A^+ and refined by Lanzoni et al. (2016) as:

$$A^+_{\rm rh}(x) = \int_{x_{\rm min}}^{x} \phi_{\rm BSS}(x') - \phi_{\rm ref}(x')dx' \tag{2.1}$$

where $x = \log(r/r_{\rm hm})$ is the decimal logarithm of the distance from the cluster center normalized by $r_{\rm hm}$, the half-mass radius. $x_{\rm min}$ is the minimum value sampled. $\phi_{\rm BSS}$ is the cumulative radial distribution for BSSs, while $\phi_{\rm ref}$ is the cumulative radial distribution for a reference population (which could be MS, Sub-Giant Branch [SGB], RGB and/or HB stars). To measure the mass segregation parameter A^+ in equal conditions Lanzoni et al. (2016) slightly refined the definition from Alessandrini et al. (2016) and only consider stars within the half-mass radius.

Using this parameter, Ferraro et al. (2018) have shown the correlation between $A^+_{\rm rh}$ and the logarithm of $N_{\rm relax} = t_{\rm GC}/t_{\rm rc}$ –the dynamical age of the system quantified by the number of current central relaxation times ($t_{\rm rc}$) that have occurred since the epoch of cluster formation ($t_{\rm GC}$)–. Additionally, they have shown how $A^+_{\rm rh}$ relates to some parameters that are expected to change with the cluster age: the core radius and central luminosity density. In particular, it was found that $A^+_{\rm rh}$ shows an anti-correlation with the cluster core-radius and a correlation with the central luminosity density.

Using Gaia DR2 data, Rao et al. (2021) measured the A^+_{rh} for 11 OCs and more recently Rao et al. (2023b) –using Gaia Early Data Release 3 (Gaia Collaboration et al., 2021, EDR3)– have measured this parameter for 12 more OCs (23 in total) where they have found a similar relation for $A^+_{\rm rh}$ against other cluster parameters which are in agreement with the Ferraro et al. (2018, 2023) GC results.

These conclusions indicate how strongly related BSSs are to their parent cluster's dynamical evolution, their stellar dynamics parameters and their mass segregation.

2.4 Blue Stragglers at Different Wavelengths

Planck's function describes the spectral energy density radiated by a blackbody (an idealized object that absorbs and emits all incident radiation), which is described as a function of temperature and frequency as:

$$I(\nu, T) = \frac{2h\nu^3}{c^2}\left(\frac{1}{e^{h\nu/k_bT} - 1}\right) \tag{2.2}$$

where T is the blackbody temperature in K, ν the frequency in Hz, $h \simeq 6.626\times10^{-34}$J·s is the Planck's constant, $k_b \simeq 1.38 \times 10^{-23}$ J $\cdot$ K^{-1} is the Boltzmann constant, and $c \simeq 2.997 \times 10^8$ m $\cdot$ s^{-1} is the speed of light. Or as a function of temperature and wavelength (λ):

$$I(\lambda, T) = \frac{2hc^2}{\lambda^5}\left(\frac{1}{e^{hc/\lambda k_bT} - 1}\right) \tag{2.3}$$

Now, in a simplified binary star system, consider a star A with an effective temperature

T_A and a star B with an effective temperature T_B, where $T_B > T_A$; meaning Planck's function for star B will have its peak/maximum at higher frequencies (or lower wavelengths) compared with star A based on Wien's displacement law:

$$\lambda_{\max} \times T = 2.8978 \times 10^{-3}\ \mathrm{m} \cdot \mathrm{K} \tag{2.4}$$

where T is the black body's effective temperature, m is meters and K represents Kelvin.

Assuming a non-eclipsing binary system, and also that we cannot resolve it, we expect to observe the spectral energy distribution of both stars as a composite spectrum. In our simplified model we expect the spectral energy distribution for the binary system to be:

$$I(\lambda, T_{\mathrm{A}}, T_{\mathrm{B}})_{\mathrm{binary}} \simeq I_A(\lambda, T_{\mathrm{A}}) + I_B(\lambda, T_{\mathrm{B}}) \tag{2.5}$$

or using equation (2.3) in (2.5):

$$I(\lambda, T_{\mathrm{A}}, T_{\mathrm{B}})_{\mathrm{binary}} \simeq \frac{2hc^2}{\lambda^5}\left(\frac{1}{e^{hc/\lambda k_b T_A} - 1} + \frac{1}{e^{hc/\lambda k_b T_B} - 1}\right) \tag{2.6}$$

We additionally assume that our system irradiates isotropically[1], so we assume that the relation between the flux and the specific intensity is $F = \pi I$. Now, for illustration purposes, we normalize the flux by its maximum for each spectrum. Finally, we combine (or add) these spectra based on equation (2.5). The results for the Spectral Energy Distributions (SEDs), assuming $R_{\mathrm{B}} \ll R_{\mathrm{A}}$– are shown in the bottom panel of Figure 2.1. Upper panel shows transmission curves extracted from the Spanish Virtual Observatory (SVO) (Rodrigo et al., 2012; Rodrigo and Solano, 2020) for Gaia DR3 filters, which are the ones that will be used in this work (see Section 3 for more details).

As can be observed at the bottom panel, we obtain a "double peak" curve, each peak corresponding to the single-star SED that contribute to the composite spectrum. However, in this specific problem where we have a very hot star (with $T_{\mathrm{eff,B}} = 15\ 500$ K) and a more "common" star ($T_{\mathrm{eff,A}} = 5\ 000$ K) represents a problem for Gaia for two reasons. First of all, based on our model, the coverage range of Gaia filters, including them all, is from

[1]Radiation emission is emitted with the same intensity in all directions. In other words, the radiation is distributed uniformly in a spherical pattern around the source.

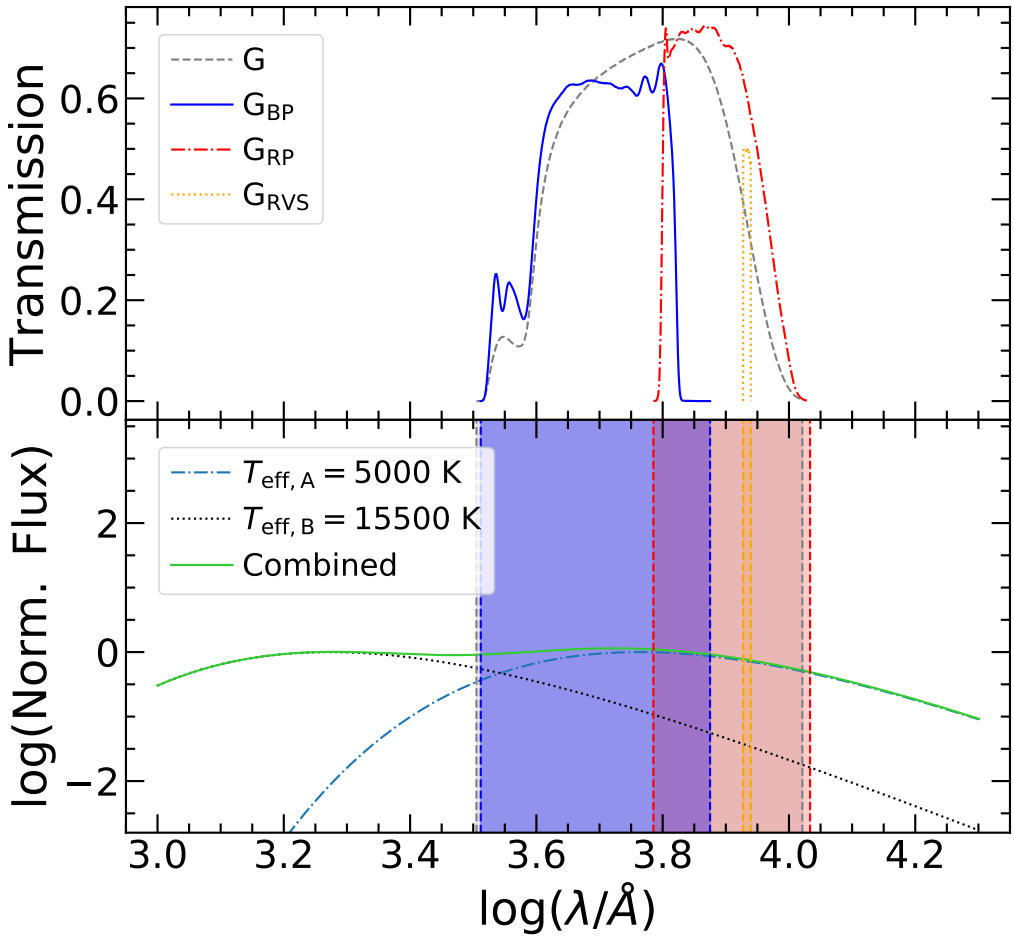

Figure 2.1: Simple binary SED model in Gaia DR3 filters. *Top*: Transmission curves extracted from SVO (Rodrigo et al., 2012; Rodrigo and Solano, 2020) for Gaia DR3 filters as a function of decimal logarithm of wavelength (in Å). G, G_{BP}, G_{RP} and G_{RVS} (Gaia's spectroscopic instrument, the Radial-Velocity Spectrometer) are plotted in dashed gray, solid blue, dot-dashed red and orange dotted lines, respectively. *Bottom*: Normalized and combined spectra, as a function of the decimal logarithm of wavelength (in Å), for a non-eclipsing binary system model for a pair of stars with effective temperature $T_{eff,B} = 15\ 500$ K and $T_{eff,A} = 5\ 000$ K –with $R_B \ll R_A$– plotted in dashed black line and dot-dashed blue line, respectively. Combined spectrum is plotted as a solid green line. Areas shaded, with their respective colors, represent the wavelength coverage range for every Gaia DR3 filter from top panel.

$\log(\lambda/\text{Å}) \sim 3.5$ (or 3 160 Å) to $\log(\lambda/\text{Å}) \sim 4.05$ (or 11 200 Å). For a very hot star, with an effective temperature around $T_{eff} = 15\ 500$ K, it will have its Planck's law peak around $\lambda \sim 1\ 932$Å, based on equation (2.4), which is clearly outside Gaia's wavelength

range coverage. This is one of the main reasons why studying our binary model using Far-Ultraviolet (FUV) filters is almost mandatory, if we want to extract parameters from the hotter companion for our binary system; unless the temperature for the binary stars in the system is more or less the same, with an effective temperature $T_{\rm eff,B} = 5\ 000$ K, which is a reasonable assumption if we consider that both stars were born from the same cloud and do have similar ages and their spectra peak within the Gaia wavelength coverage.

Remember that $F \propto \sigma T^4$. Thus, the hotter component will always dominate the flux of the binary composite spectrum, even if we observe it at the Rayleigh-Jeans tail of its SED. The second problem is that if we attempt to fit, for example, atmospheric parameters such as the surface gravity (log[g]), metallicity ([M/H]) or the effective temperature ($T_{\rm eff}$) using different models to a spectrum obtained within the Gaia wavelength coverage we might only get the parameters for the hotter star in the binary system since the spectrum of the cooler companion will contribute less to the composite spectrum. However, if we assume that one of the stars is much smaller ($R_B \ll R_A$) by a big fraction, the luminosity of the hotter companion will also decrease since $L = 4\pi R^2 \sigma T_{\rm eff}^4$. Because of this we must consider that our model parameter approximate a binary and, therefore, we might be overestimating some parameters –such as absolute luminosity– due to the fact that we cannot resolve the system. Finally, we also have to keep in mind that in the specific case of BSSs we are talking about "weird" stars, so traditional spectrum models could slightly diverge from our real data spectrum.

In the last decades, it was proposed that the best way to study BSSs is through the so called "UV-Route" (Ferraro et al., 1997, 2001, 2018). In GCs/old stellar systems, most of the cluster brightness will be dominated by a population of red and bright stars with luminosities around $\sim 10^2 L_\odot$ and effective temperatures between 3500 and 5000 K. Therefore identifying BSSs becomes a difficult task for the most-crowded regions in these clusters. However, when we plot CMDs using filter combinations that include the UV, BSSs are clearly separated from other stellar evolutionary phases within the same cluster. Particularly, Raso et al. (2017) have shown that selecting BSSs using optical and UV filters leads to "intruders" stars that lie in the region where BSSs are usually identified; i.e., a BSS could be/not be a BSS depending on which filter/wavelength range we are observing

them with/in. These "intruders" are more recently known as "blue lurkers" (Subramaniam et al., 2020)[2]. As a brief summary, Raso et al. (2017) compare BSSs selected using the UV-Route method and optical filters. They use data obtained from "*HST UV Globular Cluster Survey*" *("HUGS")* (Piotto et al., 2015; Nardiello et al., 2018) –using `F275W` vs `F275W−F336W` combination filters for CMD– and compared them with those BSSs obtained from HST optical filters from Simunovic and Puzia (2016) –using `F814W` vs `F606W−F814W` combination filters for CMD–. They found that $\sim 20\% - 60\%$ of BSSs obtained through the UV Route are missing in the optical sample for BSS from Simunovic and Puzia (2016) for diferent GCs. Additionally, some of the BSSs selected with the optical filter sample lie on the MS and less bright Red Giant Branch (RGB) stars when they are observed with UV filters.

Last, but not least, when we observe and analyze BSSs spectra using UV filters, we might find some interesting phenomena occurring as demonstrated by Gosnell et al. (2015). Using FUV HST photometry they analyzed the excess of color/brightness in this wavelength regime for all their identified BSSs; where they have found that some models for BSS+White Dwarfs (WDs) matched with the observations for their blue stars; stars that where much bluer than they should be in the FUV regime. Therefore, concluding that some BSSs in their study do host a WD companion. In more recent examples using spectroscopy, based on ASTROSAT/Ultra Violet Imaging Telescope (UVIT) data, Subramaniam et al. (2016) discovered a post AGB/horizontal branch (HB) star as a companion of a BSS. More recently, also using UVIT data, Sindhu et al. (2019) reported and confirmed an observed WD companion of a BSS in the GC NGC2682 (M67) analyzing the SED of the binary system. In the last months, as of the date of writing of this thesis, Dattatrey et al. (2023) have analyzed the SEDs of multiple BSSs in the GC NGC362. They found that more massive (and also bluer) BSSs do not show any evidence of hot companions, whereas BSSs that do show the evidence of a companion are located on a "redder" BSSs sequence. Therefore, they suggest that most massive (bluer) BSSs could be formed through a collisional process whereas less massive (redder) BSSs that do show the evidence of a WD companion are

[2]Stars that, when observed with visual filters, belong to the MS branch in optical CMDs. However, when observed with UV filters they lie in the BSS region. This may indicate the presence of a MS star with a WD companion.

formed through a mass-transfer process; which is in agreement with the theory/explanation presented by Ferraro et al. (2009) for GC M30 and Dalessandro et al. (2013), trying to explain the presence of a Double Sequence of BSS in the GC NGC362 as well.

Since GC BSS have been poorly studied with Gaia, since this mission does not work very well for overcrowded regions such as GC centres, our goal is to provide and identify BSSs using Gaia to complement HST-based studies for BSSs in the form of a master catalog. Additionally, and based on Gaia data, we want to provide astrophysical parameters for these stars, in OCs and GCs, that could be useful for their future study.

Chapter 3

Gaia Data and Blue Stragglers Stars selection

3.1 Gaia Data Release 3 Cluster Membership

To properly select member stars for each cluster in this study we start our clusters sample selection based on previous Gaia studies.

For GCs we focus our attention on clusters studied by Vasiliev and Baumgardt (2021). However, instead of using their identified star sample we only select GCs with $N_{\rm members} \geq 1000$ from their catalogue, since we expect them to keep a similar number of cluster members after applying our selection criteria, which will be explained later in this section.

For OCs we use the catalogue provided by Dias et al. (2021) and we focus our attention on those clusters with cluster star member samples $N_{\rm members} \geq 350$. Additionally, we are only capable to extract data from OCs with an apparent size smaller than $\sim$90 arcmin in diameter. We prefer Dias et al. (2021) over Cantat-Gaudin et al. (2018) due to the fact that the provided number of OCs is slightly higher than in the older catalogue.

Once we have a initial list of targets we obtain their apparent size using SIMBAD Astronomical Database - CDS (Strasbourg)[1]. We then apply the following procedure for every cluster candidate in our list:

[1] https://simbad.cds.unistra.fr/simbad/

1. Select Gaia Data Release 3 (Gaia Collaboration et al., 2023, GDR3) data centered on the coordinates provided by the respective catalogue -Vasiliev and Baumgardt (2021) for GCs or Dias et al. (2021) for OCs- in a cone search around their center using `TOPCAT`[2] (Taylor, 2005).

2. Discard all data that does not meet the following conditions:

   - Its error in proper motion (Right Ascension or Declination component) is higher than 0.35 mas $\cdot$ yr^{-1}
   - Its magnitude in the G band is higher than 19.5 mag. This is to avoid faint stars whose proper motion could be less reliable. However, and as there will be explained and justified later, for a few GCs we decided to extend this cut down to 21.5 mag in the G band (Fabricius et al., 2021).
   - Its magnitude in the G band is lower than $\sim$ 10.5 mag to avoid bright/saturated stars (Fabricius et al., 2021).
   - Data whose `ruwe`[3] ≥ 1.4.

3. In the data Vector Point Diagram (VPD; Proper Motion RA vs. Proper Motion DEC) we draw an ellipse centered on, as a first guess, the coordinates provided by Vasiliev and Baumgardt (2021) for GCs or Dias et al. (2021) for OCs.

4. In a MonteCarlo (MC) process, we change the minor axis, mayor axis and inclination (with respect to y-axis) of this VPD ellipse. We keep the values that maximizes the number of stars within the ellipse.

5. From now, we work based on the algorithm provided by Cordoni et al. (2018) to extract cluster members with data within the VPD ellipse. For the data set Cordoni et al. (2018) define a new parameter called $\mu_{\rm R}$ as:

$$\mu_{\rm R} = \sqrt{\left(\mu_\alpha \cos\delta - \langle \mu_\alpha \cos\delta \rangle\right)^2 + \left(\mu_\delta - \langle \mu_\delta \rangle\right)^2} \tag{3.1}$$

[2] https://www.star.bris.ac.uk/~mbt/topcat/

[3] `ruwe` is the "Renormalised Unit Weight Error" which is a kind of χ^2 between Gaia models and astrometric observations. This parameter indicates how well/bad the astrometric observation fits a single-model star. A value above 1.0 could mean it is a non-binary and/or problematic for astrometric solutions.

where $\mu_\alpha \cos\delta$ is the proper motion along RA component, μ_δ is the proper motion along DEC component, $\langle \mu_\alpha \cos\delta \rangle$ is the median of the proper motion along RA component for the data within the ellipse and $\langle \mu_\delta \rangle$ is the median of the proper motion along DEC component of the data within the ellipse. Note that equation (3.1) is the equation of the distance between two points on a Cartesian plane. So, basically, $\mu_{\rm R}$ is the distance between a point in the VPD and the ellipse center.

6. We plot G vs. $\mu_{\rm R}$ and divide the data into $N_{\rm bins} = 20$ bins of $\sim$0.45 mag bin width, from 10.5 mag to 19.5 mag in the G band. Let us call the current bin "N". If we do not obtain at least 2 stars per bin, we reduce $N_{\rm bins}$ by 1 until we get at least 2 stars for every bin.

7. Now that we have our data divided into bins, we compute parameters for every bin. Only considering data within the "N-th" bin, we compute the median $\rm G_N$ mag, the median $\mu_{\rm R,N}$ and the standard deviation $\sigma_{\mu_R,N}$. We then define a point for the "N-th" bin with the coordinates as:

$$\text{Point Bin}_{\rm N,\mu_R} = [\text{Median}(\rm G_N),\ \text{Median}(\mu_{\rm R,N}) + 3 \times \sigma_{\mu_R,N}]. \tag{3.2}$$

I.e., we compute the median magnitude for the "N-th" bin to get the Y-axis coordinate. To get the X-axis coordinate of this point for this bin we compute the median value for μ_R and then add 3 times the standard deviation of this parameter.

8. We repeat the last step for all the bins, so every bin has an associated reference point.

9. Once we have defined all the points for all the bins we interpolate them. If the data has lower values in $\mu_{\rm R}$ than this reference interpolation then the data is kept. Otherwise it is discarded.

10. We repeat step 7, but this time we use as a parameter the parallax (ϖ) instead of $\mu_{\rm R}$, creating reference points similar to (3.2):

$$\text{Point Bin}_{\rm N,\varpi} = [\text{Median}(\rm G_N),\ \text{Median}(\varpi_N) \pm 3 \times \sigma_{\varpi,N}] \tag{3.3}$$

Note that now we have used the symbol "±" to create an upper and a lower boundary instead of only an upper boundary like was done for (3.2). Similar to the previous points, we interpolate them and we keep all the data that is between our upper and lower boundaries for all the bins.

11. We then re-compute the ellipse center and repeat the process from step 5 until we reach 3 iterations.

In summary, for a cluster we select Gaia DR3 data between a range of magnitudes where it is not saturated or it is not too faint, so we can avoid significant systematic errors (Fabricius et al., 2021). Based on the Cordoni et al. (2018) algorithm, we then select data inside an ellipse in the VPD and we keep its median values for both axes ($\mu_\alpha \cos\delta$ and μ_δ). Next, divide this data into bins/section along G magnitude and, for every bin, we compute their median values for G magnitude, $\mu_{\rm R}$ parameter and parallax (ϖ). We then interpolate the median values for G mag vs. $\mu_{\rm R}$ and then for G mag vs. ϖ (parallax) for all the bins and keep the data below this interpolation/threshold. With the filtered data we re-compute the VPD ellipse center and repeat the process until we reach three (3) iterations. A flowchart for our cleaning procedure method/selecting cluster members algorithm can be seen in Figure 3.4.

We apply and repeat this process/algorithm for all our target clusters. As a special mention, clusters larger than ~ 90 arcmin in diameter were especially difficult to observe due to their large area coverage in the sky. If the cluster is too big we might not be able to extract all the necessary data to properly obtain the "initial" cluster guess/extraction in the VPD and, therefore, the following steps for the classification algorithm fail. This is the reason why we only kept OCs with an apparent size smaller than ~ 90 arcmin in diameter. We point out that Cordoni et al. (2018) do apply differential reddening corrections as a final step for their identified cluster sample, following the procedure of Milone et al. (2012a). However, we decided to skip this step and apply a uniform extinction to each cluster in our sample in the following analyzes (see Sections 3.2.1 and 3.2.2 for more details).

Applying this algorithm to our raw sample data (cluster members mixed with field/non-member stars) leads to a cleaned sample of *bona-fide* cluster member stars.

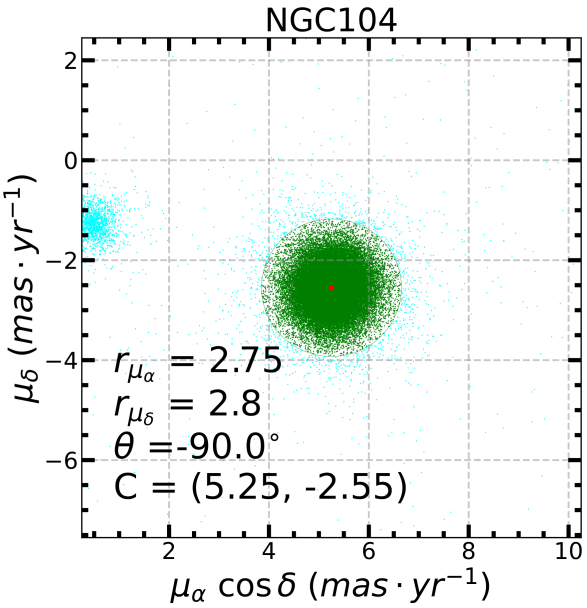

Figure 3.1: Ellipse selection for Gaia DR3 in VPD for NGC 104. Data without being filtered are shown cyan dots. Computed selection ellipse and data are displayed in green. Red dot indicates the ellipse center computed by Vasiliev and Baumgardt (2021).

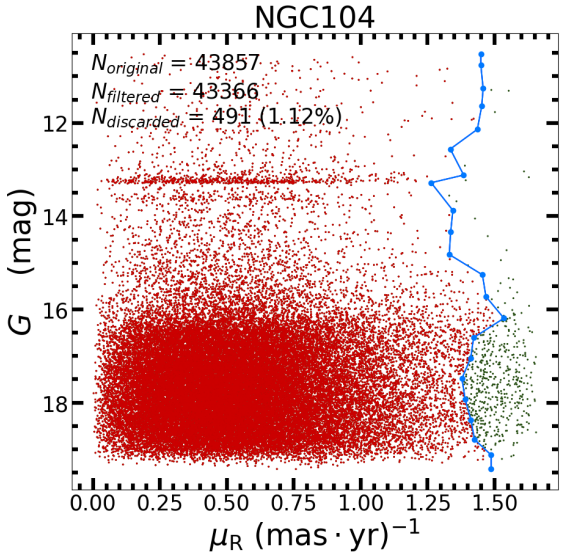

Figure 3.2: Criteria selection for G mag vs. μ_R. The data has been divided into 20 bins along G magnitude. Values in dark-green are outside the interpolation/selection criteria and are discarded. Data in red is kept for the next iteration.

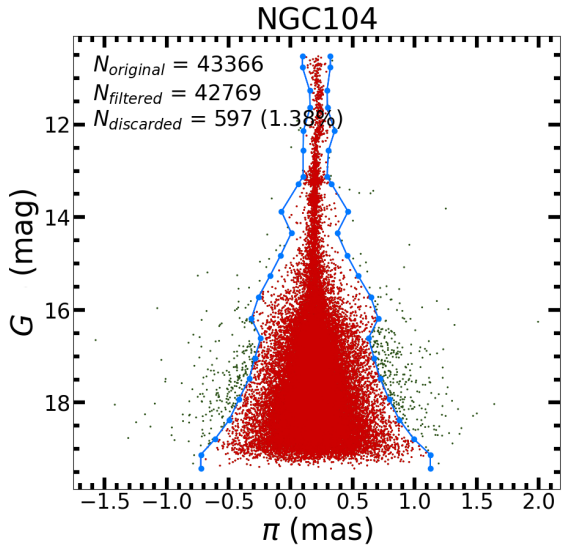

Figure 3.3: Same as Figure 3.2, but for parallax –which in this individual case is denoted as π–.

A closer look at our procedure combined with the Cordoni et al. (2018) algorithm can be observed at Figures 3.1, 3.2 and 3.3. It can be appreciated how we applied a single border as a delimiter for G vs. μ_{R} (upper limit) and two borders have been applied to data in G vs. parallax (lower and upper limits).

We must mention that there are some exception in the upper-cut limit in magnitudes for GCs since we are not able to identify the MSTO despite the photometric data reaching down to G $\approx$ 19.5 mag. These exceptional GCs are: NGC1261, NGC5024, NGC5466, NGC5897, NGC6093, NGC6101 and NGC6144. For this exceptional clusters we have applied an upper limit at G $\approx$ 20 mag. We also increased the tolerance in proper-motion errors, in both components, up to 0.5 mas $\cdot$ yr^{-1} as the error in proper motion grows with the magnitude (Riello et al., 2021). Implications of these assumptions are discussed in Section 4.3.

All these figures and selections have been generated using `astrogaia`; an open source software developed by the author of this thesis (see Appendix C for details).

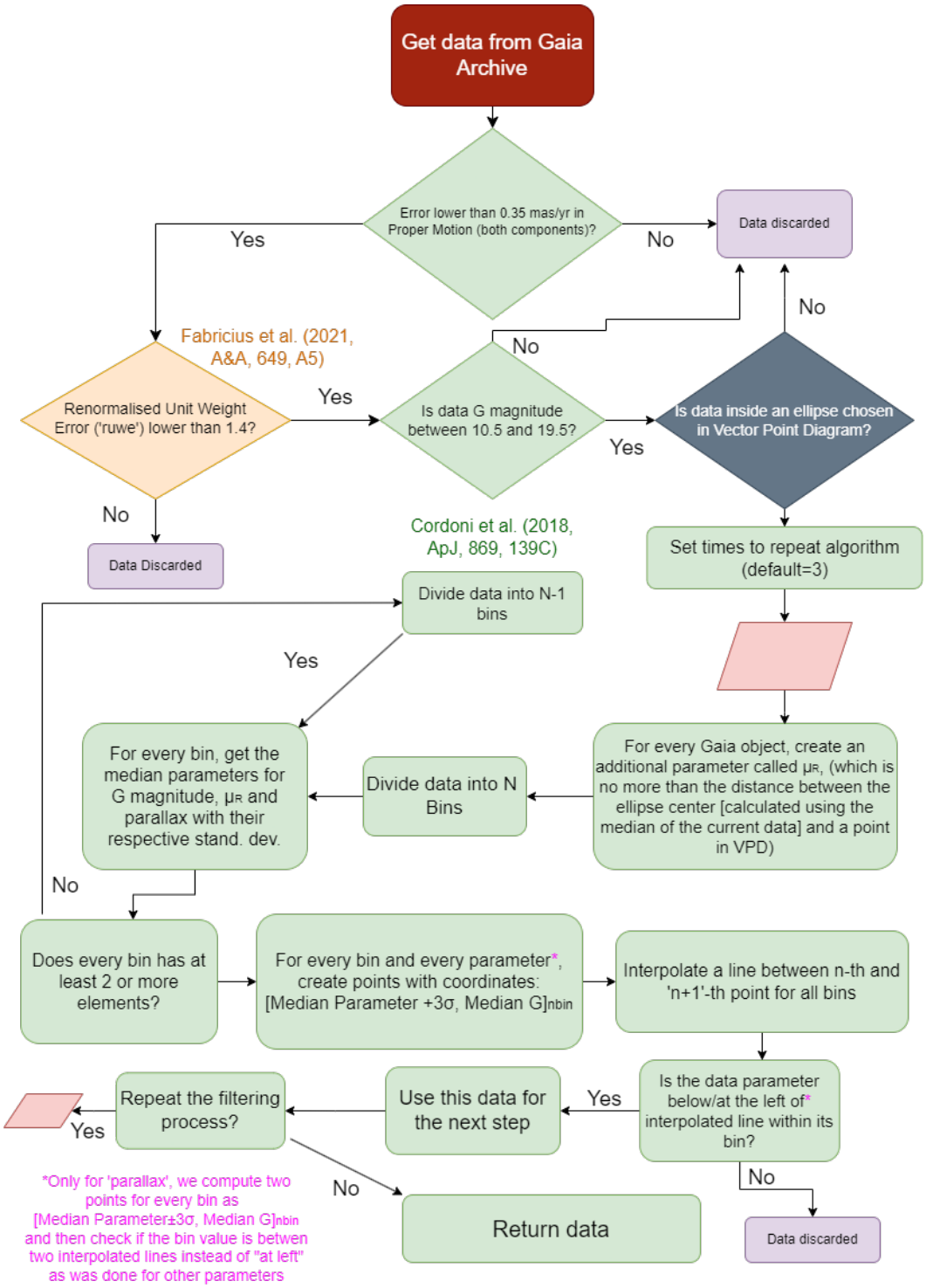

Figure 3.4: Flowchart for algorithm used to extract and filter objects from Gaia DR3. Suggestion in orange -work with a Renormalised Unit Weight Error ('`ruwe`') lower than 1.4- was taken from Fabricius et al. (2021) and cells in green are steps based on Cordoni et al. (2018).

As result, we successfully were able to extract and identify cluster members for 170 targets. 41 of the total were GCs ($\sim$ 24%) and 129 of the total were OCs ($\sim$ 76%). The distribution of numbers of clusters based on their confirmed cluster members can be seen in Figure 3.5.

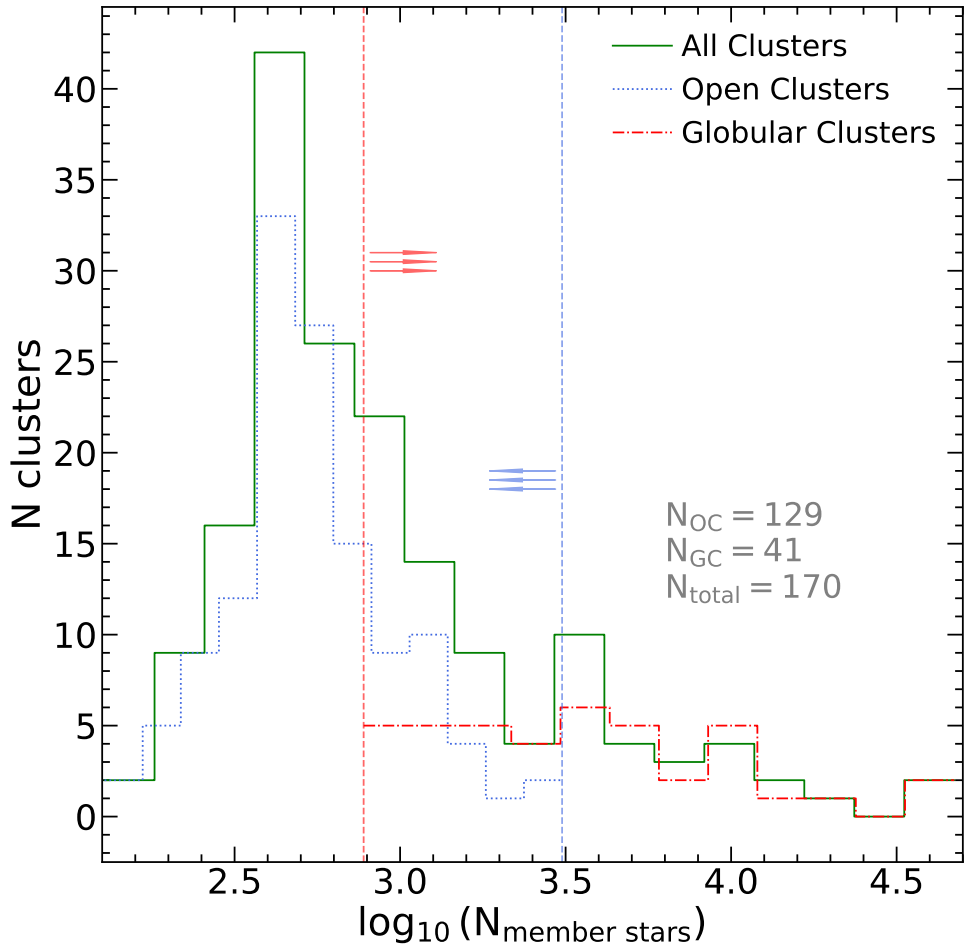

Figure 3.5: Histogram of our final sample of clusters analyzed for this work. We have analyzed a total of 41 GCs and 129 OCs; this yields to a total of 170 clusters analyzed. All clusters/total sample is shown as a solid green line, OCs are shown as a blue dotted line and GCs are shown as a dashed-dotted red line. The vertical red line denotes the minimum member stars identified for GCs ($\sim$ 800) while the blue vertical line shows the limit for the maximum member stars identified for OCs ($\sim$ 3100).

3.2 Blue Straggler Stars selection

To properly identify and select BSSs for every cluster we must first identify the key reference point in the corresponding CMD: the Main-Sequence Turn-Off Point (MSTO). Since we assume that BSSs are stars that are slightly bluer and equally/slightly brighter than the MSTO, we first must properly identify it. For this reason we have decided to use isochrone stellar models for several reasons:

- They will allow us to easily identify the MSTO for established GC/OC parameters.
- Since isochrones are iso-age curves constructed from stellar evolutionary tracks for stars of a given mass from stellar evolution models, we can use this as an advantage and extract the astrophysical parameters for the MSTO.
- We can self-consistently use the isochrones to set limits for the BSSs selection region as has been previously done in Gaia-based studies (e.g. Rain et al., 2021; Jadhav and Subramaniam, 2021).

For these reasons we have decided to use PARSEC isochrone models (Bressan et al., 2012)[4] as they cover broad stellar population parameters with sufficiently fine parameter sampling. We follow the next procedure to select BSSs for every of our sample cluster:

1. First we must obtain the empirical ridge-line for the cluster. We manually select a the best-fitting MS, Sub-Giant Branch (SGB) and Red Giant Branch (RGB) using `TOPCAT` for each cluster with their confirmed members in the CMD using G_{BP} vs. $G_{BP} - G_{RP}$. We use G_{BP} along the magnitude axis in the CMD for the reason presented in Section 2.4 since G_{BP} is the most UV-like available filter for Gaia.
2. Divide this data into bins (from 10 to 20) along the G_{BP} axis (Y-axis in the CMD) and keep their median for color and magnitude.
3. For each bin we apply a σ-clipping, with $3 \times \sigma$ for the color.
4. Iterate and repeat this process (step 3) a total of three (3) times.

[4] https://stev.oapd.inaf.it/cmd/

5. Once we have obtained the ridge-line for every cluster we are able to request PARSEC isochrones with parameters based on previous studies. As reference parameters we obtain the distance from Baumgardt and Vasiliev (2021), the metallicites and ages from Baumgardt et al. (2023)[5], and color excess from Harris (2010) for GCs. For OCs we use values from Dias et al. (2021) for metallicity, distance and extinction.

6. We then request a series of PARSEC isochrones based on our reference parameters with values from ± 0.01 in log(Age)[6] in steps of 0.001 in log(Age). For metallicity we vary our parameters from our reference value ± 0.3 dex in steps of 0.05 dex. For example, if our cluster is solar-like and 12 Gyr old then our reference value for age is log(Age) = 10.079 and metallicity [M/H] = 0.0. Therefore we request PARSEC isochrones in the range of 10.079 ± 0.01 for log(Age) and 0.0 ± 0.3 for metallicity.

   To fit the data between PARSEC isochrone models –that are in absolute magnitudes and derredened colors– and observational Gaia DR3 data we assume a color-extinction relation given by Cardelli et al. (1989):

$$R_{\mathrm{V}} = \frac{A_{\mathrm{V}}}{\mathrm{E(B-V)}} \tag{3.4}$$

   with $R_{\mathrm{V}} = 3.1$.

   To convert from the extinction A_{V} to the Gaia extinction coefficients we assume the relations (Marigo et al., 2008; Evans et al., 2018):

$$A_{\mathrm{G}}/A_{\mathrm{V}} = 0.85926 \tag{3.5}$$

$$A_{\mathrm{BP}}/A_{\mathrm{V}} = 1.06794 \tag{3.6}$$

$$A_{\mathrm{RP}}/A_{\mathrm{V}} = 0.65199 \tag{3.7}$$

7. From all our isochrone model candidates we do a least-square fit against the ridge-

[5]They do not explicitly provide the metallicity [M/H] (abundance of elements heavier than Helium), instead they provide [Fe/H] (iron abundance) and extinction is taken from Harris (2010). We use these values as an "initial guess".

[6]Hereafter every time we refer to log(Age) we mean log(Age/yr), the decimal logarithm of the age in year units.

line obtained previously and keep the isochrone that minimizes the distance between the points of the isochrone and the ridge-line.

8. Using the metallicity found for the best fit, we request isochrones from log(Age) = 6.0 to log(Age) = 10.13 in steps of 0.1 for log(Age). We then use these isochrones to create a Zero-Age Main Sequence (ZAMS) track. Based on the ideas from Rain et al. (2021); Jadhav and Subramaniam (2021), we will use the ZAMS to select the BSSs region as will be shown later, but it will be used slightly differently compared to the previously mentioned studies.

3.2.1 Globular Cluster BSSs selection

Once we have properly obtained isochrone models we use them to set a region where BSSs are expected.

1. We plot the confirmed cluster members in a CMD and select MS stars. Divide the selected MS stars into 10 to 20 bins along the $G_{\rm BP}$ magnitude (Y-axis of the CMD).

2. Centering our attention on the bin that contains most MS stars and compute its dispersion/standard deviation along the color axis. We refer to this parameter $\sigma_{\rm bin,color}$.

3. Similar to step 1, we select SGB stars and divide the data along the $\rm G_{BP} - G_{RP}$ axis (X-axis in CMD) in ~ 5 bins.

4. We focus again on the bin that contains most SGB stars, compute its dispersion along the magnitude axis and use this value to shift the isochrone along the $\rm G_{BP}$–axis. We call this parameter $\sigma_{\rm bin,mag}$.

5. Shift the best-fitting isochrone in a quantity $3 \times \sigma_{\rm bin,color}$ along the $\rm G_{BP} - G_{RP}$ axis to bluer colors and in a quantity $4 \times \sigma_{\rm bin,mag}$ along the $\rm G_{BP}$ axis to brighter magnitudes. This will create the lower–right boundary for our BSS selection region. Typical values for $3 \times \sigma_{\rm bin,color}$ are in the range of $\sim [0.1, 0.2]$ mags and $\sigma_{\rm bin,mag} \sim [0.2, 0.3]$ mags.

6. Shift the ZAMS along along the $\rm G_{BP} - G_{RP}$ axis by $\sim 6 \times \sigma_{\rm bin,color}$ to bluer colors. This will create our lower–left boundary of the BSS selection region.

7. Set an upper–limit to the magnitude that consists of the MSTO G_{BP} magnitude subtracted by $\sim$ 2 magnitudes. This upper magnitude limit is based on previous selections by Leigh et al. (2011).

8. Set a lower–limit which is equal to the MSTO magnitude.

9. To avoid selecting BHB and more evolved stars from our sample we set a left (blue) limit in color that is $([G_{BP} - G_{RP}]_{MSTO} - x_{lower})$ magnitudes. With typical values of x_{lower} of 0.5 mag $\leq x_{lower} \leq$ 0.6 mag.

10. We then connect all the defined lines and set a region to select BSSs. All stars that lie inside this area are considered Straggler Stars candidates.

11. To distinguish between BSSs, Yellow Straggler Stars (YSSs) –which could be evolved BSSs– and Red Straggler Stars (RSSs) –evolved YSSs– we apply the following simple criteria to stars inside our selection area: if the star is bluer (hotter) than the MSTO color it is selected as a BSS. If the star is colder (redder) than the MSTO color and it is in the bottom half of the selection area (i.e. fainter stars) it is selected as a YSSs. If the star is colder than the MSTO color and is in the upper half of the selection area then it is selected as a RSSs.

Selection criteria described here and applied to GC NGC104 (47 Tuc) are illustrated in Figure 3.6.

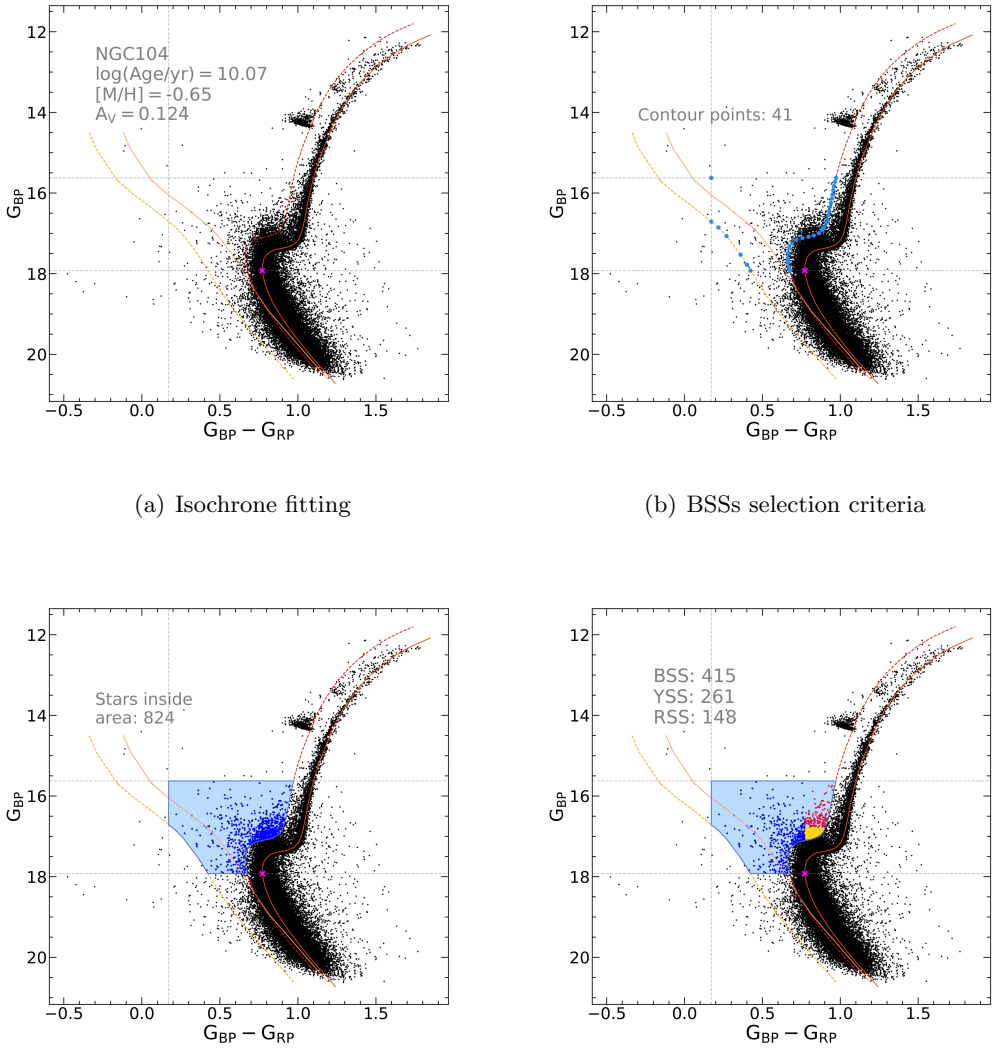

(a) Isochrone fitting

(b) BSSs selection criteria

(c) Stragglers Stars selection

(d) BSSs, YSSs and RSSs selection

Figure 3.6: Selection process to select BSSs, YSSs and RSSs for GCs in CMD. a) Isochrone fitting process for NGC104 (47 Tuc). Cluster members stars are denoted as black points. The orange solid line denotes the best isochrone fitting line for our sample, while the red dashed line shows the same isochrone shifted along temperature and magnitude (see text for details) to create the lower-right boundary for the Straggler Stars selection region. The yellow solid line marks the ZAMS with the metallicity of the best isochrone fitting line. Dashed yellow lines denote the ZAMS shifted (see text for details) to create the lower–right boundary for the selection region. Identified MSTO of the isochrone is marked as a magenta cross symbol. Vertical and horizontal dashed gray lines demarcate the left and upper boundaries for the selection region, respectively. b) Contour points for the selection area. Points are marked as light-blue dots. c) Confirmed cluster member stars that lie inside the area are classified as "Straggler Stars"; marked as blue points. d) Stars classified as BSS are marked as blue points, YSS as yellow points and RSS as red points depending on their position with respect to the MSTO (see text for details).

3.2.2 Open Clusters BSSs selection

The criteria to select BSSs in OCs is similar to the one explained in the previous section, but with a few differences:

- We additionally set a right-boundary limit to the selection criteria. This right (red) boundary is defined as the $([G_{BP} - G_{RP}]_{MSTO} + \sigma_{bin,color})$ magnitudes. Since OCs are younger than GCs, if we follow the selection criteria applied to GCs we might be selecting stars close to the RGB-Bump. To avoid selecting these stars we add this extra limit for the selection region to OCs.

- We do not apply a vertical left-edge cut in color since we do not expect stars in their last stellar phases. Only shifted–ZAMS delimits the left contour side.

- We set the upper magnitude limit to ~ 3 mag brighter than the MSTO magnitude. Since OCs are much younger than GCs we do not expect them to have BHB stars that could contaminate our BSSs sample and, therefore, we find it is acceptable to extend this upper limit. Additionally, Rain et al. (2021) and Jadhav and Subramaniam (2021) have not set an upper limit to their selection criteria. Jadhav and Subramaniam (2021) estimates that only about $\sim 1.4\%$ of their sample might be BHB contaminating it. Even though we expect not many BHB stars, we apply this additional criterion to avoid BHBs in our sample (see Section 3.2). We point out that also this criterion is limited by the cut in brightness we have applied in the cluster membership selection process, since all stars with magnitudes brighter than $G \approx 10$ mag were discarded.

In Figures 3.7 and 3.8 we show the final results of our selection criteria for cluster membership and BSSs we show the results for GC NGC6205 and OC NGC188, respectively. Similar figures for all the clusters analyzed in this work, with their respective member stars and identified BSSs, are presented in Appendix A.

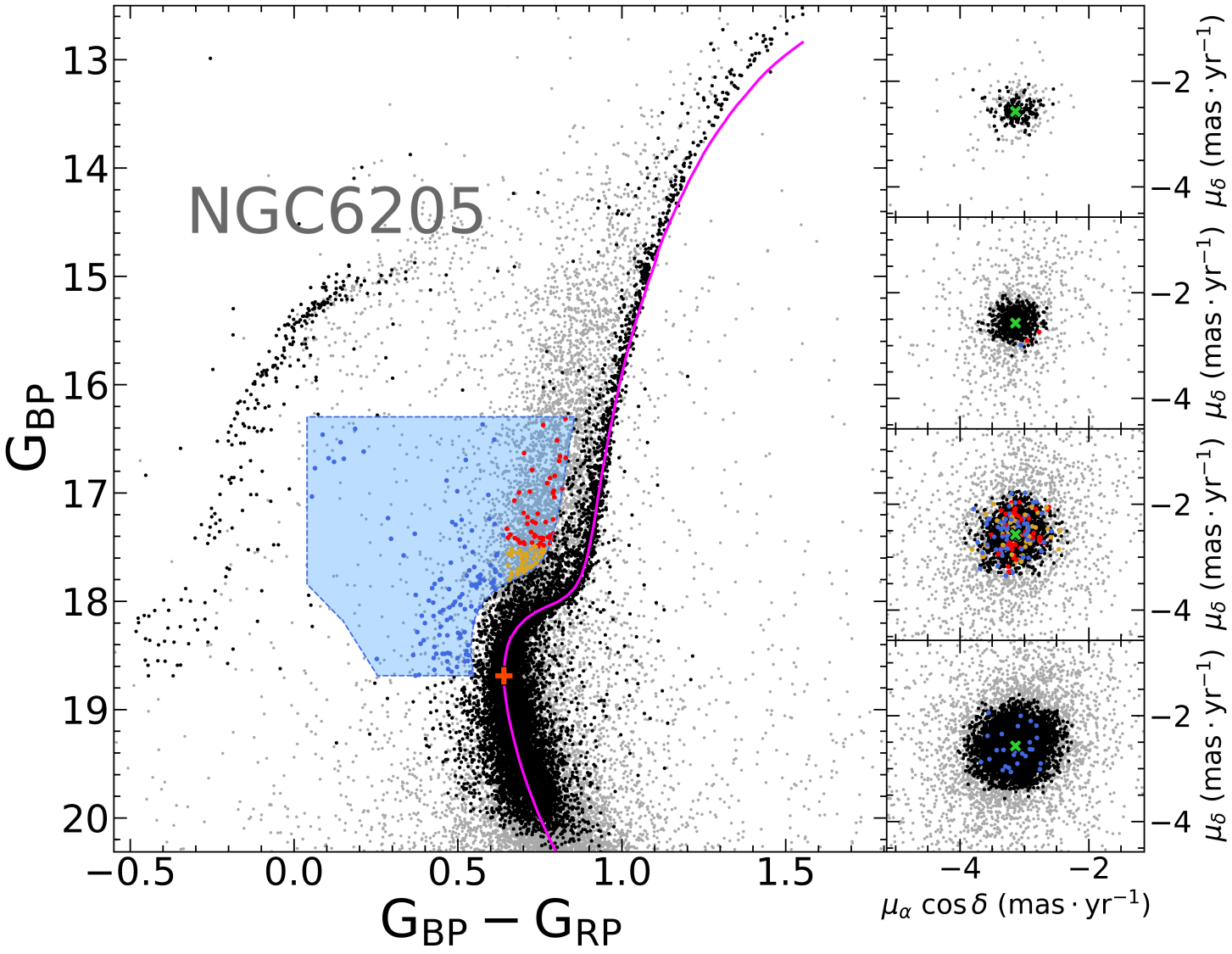

Figure 3.7: Selection of BSSs for GC NGC 6205. Discarded stars are shown as gray dots, whereas confirmed cluster members are shown as black dots. The best-fitting isochrone is shown as a magenta solid curve. The MSTO is marked by an orange plus (+) symbol. The area containing BSSs, YSSs, and RSSs is denoted as a transparent blue area with dashed line borders. BSSs, YSSs, and RSSs are marked as blue, yellow, and red points, respectively. In the right-hand side panels, the VPDs are displayed for stars of the corresponding magnitude bins with respect to the CMD. The green cross shows the median of the ellipse for $\mu_\alpha \cos\delta$ and μ_δ found for cluster members (see Section 3.1 for details).

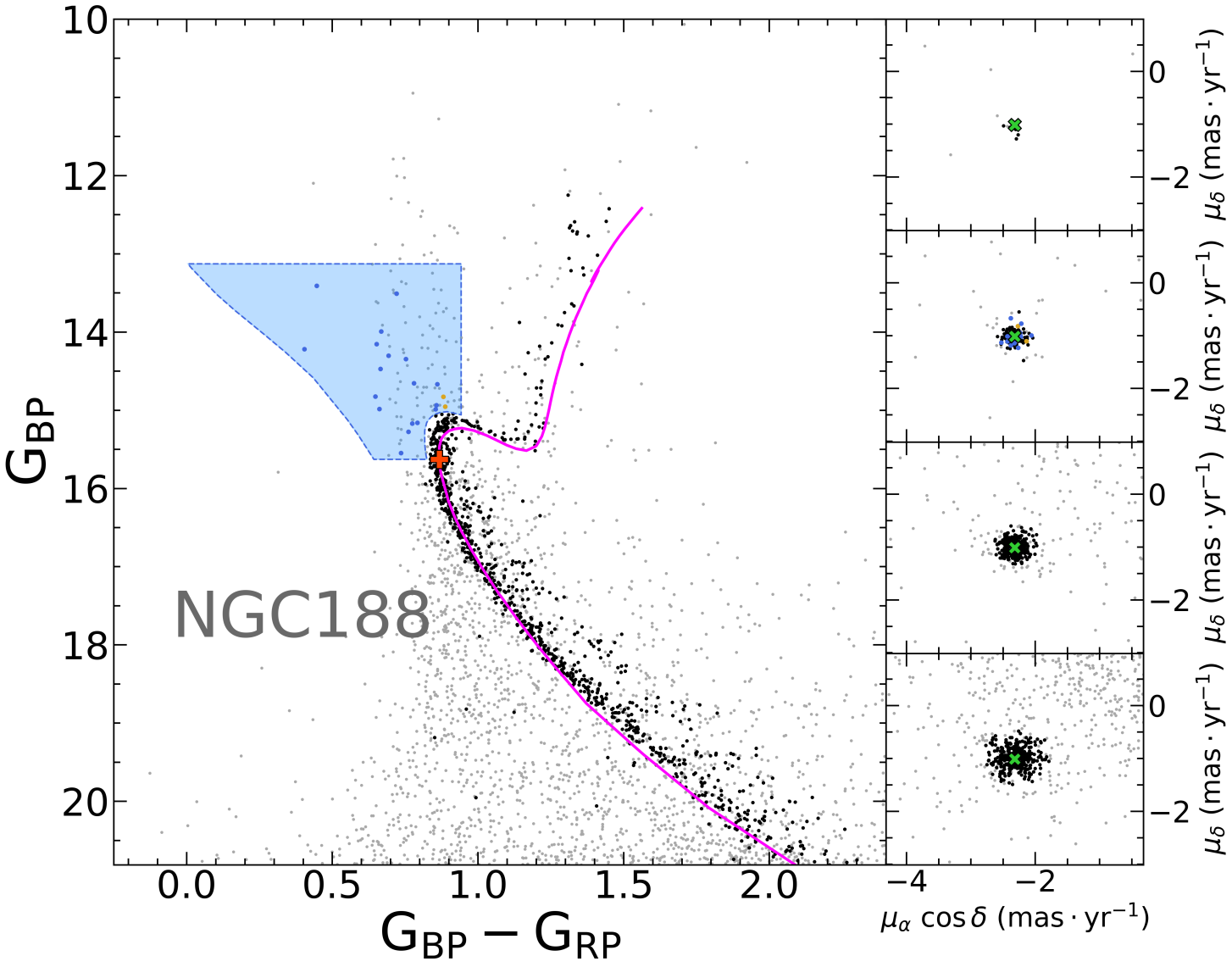

Figure 3.8: Similar as Figure 3.7, but for OC NGC188. Note that now we have added a right-border to the Straggler Stars selection area to avoid selecting RGB stars.

3.3 Blue Straggler Stars Astrophysical Parameters

For a deeper analysis of the selected BSSs, we measure their properties using three different approximations: color-temperature relations, isochrone-fit models and, if available, spectroscopic data from GDR3.

3.3.1 Color-Temperature Relations

As a first approximation to estimate BSSs effective temperatures ($T_{\rm eff}$) we use color–temperature relations provided by Mucciarelli et al. (2021) for Gaia EDR3. Using the infrared flux method (IRFM) by González Hernández and Bonifacio (2009) for effective temperatures, Mucciarelli et al. (2021) computed the best-fitting polynomial relating color and temperature leading to the equation:

$$\theta = b_0 + b_1 C + b_2 C^2 + b_3 [\mathrm{Fe/H}] + b_4 [\mathrm{Fe/H}]^2 + b_5 [\mathrm{Fe/H}] C \tag{3.8}$$

where $\theta = 5040\ \mathrm{K}/T_{\rm eff}$, C is the dereddened color and [Fe/H] is the metallicity. b_i coefficients, with $1 \leq i \leq 5$ are shown in Table 3.1 for dwarf stars (first row) and giant stars (second row). We use metallicity [Fe/H] values from Carretta et al. (2009) for GCs and Dias et al. (2021) for OCs.

It is important to note that our sample of selected BSSs, YSSs and RSSs might lie outside the range of magnitudes described on Table 3.1. For these stars we extrapolate their $T_{\rm eff}$.

Color range (mag)	$\sigma_{T_{\rm eff}}$ (K)	N	b_0	b_1	b_2	b_3	b_4	b_5
[0.39–1.5]	61	436	0.4929	0.5092	–0.0353	0.0192	–0.0020	–0.0395
[0.33–1.81]	83	209	0.5323	0.4775	–0.0344	–0.0110	–0.0020	–0.0009

Table 3.1: Color-temperature relations derived by Mucciarelli et al. (2021) for dereddened color $(G_{BP} - G_{RP})_0$. First row are the values obtained using dwarf stars; whereas the second row denotes the values obtained using giant stars. Columns are as follows: 1) color range of the stars used to derive the relation, 2) $T_{\rm eff}$ dispersion of the fit residuals, 3) numbers of stars used to obtain the relation, 4–9) coefficients for equation (3.8).

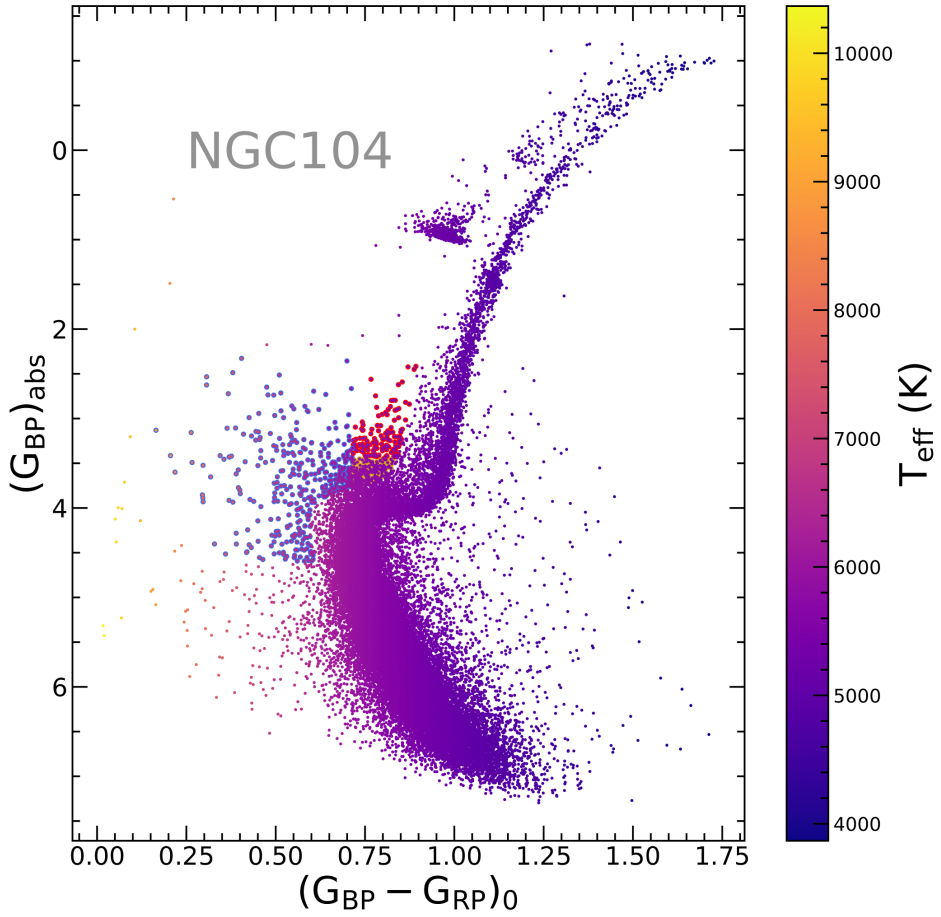

Figure 3.9: Color-temperature relations found for the GC NGC 104 (47 Tuc) CMD using the relations from Mucciarelli et al. (2021). BSSs, YSSs and RSSs are enclosed in blue, yellow and red colors, respectively.

3.3.2 Isochrone Fitting-Models

As a second method to obtain astrophysical parameters for BSS we will make use of isochrone models, similar to what has been done in previously mentioned studies (Jadhav and Subramaniam, 2021; Dattatrey et al., 2023). For this we use again PARSEC isochrones (Bressan et al., 2012). For GCs we use isochrones from 150 Myr up to the best-fitting isochrone age identified for the respective cluster in steps of 50 Myr. For OCs we repeat

the process, but the minimum age requested is now 100 Myr in steps of 25 Myr. We keep the metallicity found for the best-fitting isochrone for all the clusters –GCs and OCs– assuming a simple stellar population (SSP). It is important to note that metallicity can lead to degeneracies in the models and to keep it simple we have chosen to consider the cluster metallicity as homogeneous even when it has been found more recently that, especially GCs, are good approximations of but not exactly SSPs; they are rather Multiple Stellar Populations (Milone et al., 2012b, 2015, MSP).

We then sample the isochrone models along the CMD for every cluster and we choose the 3 closest isochrone–model points to each selected star. The astrophysical parameters are then computed as the average of these 3 points; and their standard deviation as their error for the respective parameter.

3.3.3 Spectroscopy from Gaia DR3

Gaia DR3 has provided spectroscopy for over 220 billion stars (Gaia Collaboration et al., 2023). They provide atmospheric parameters parameters such as effective temperature and $\log(g)$; measuring radial velocities; and interstellar parameters such as extinction. The spectra provided by Gaia are low-resolution spectra –BP/RP spectra (hereafter called 'XP' spectra)–, with resolution values between $R \sim 50 - 160$ in the range of 640 up to 1050 nm (De Angeli et al., 2023; Montegriffo et al., 2023). Andrae et al. (2023) used different methods, such as isochrone fitting, A and OB stars and extinction laws to fit the spectra with observational measurements. However, these techniques are highly sensitive to calibration inaccuracies and systematics. For this reason Zhang et al. (2023) decided to train a machine-learning model that, based on high-resolution spectra, "downgrades" those spectra to XP spectra resolution. Since high-resolution spectra allow one to measure astrophysical parameters with higher accuracy, training a machine-learning model that learns from reliable measurements and then learns how the spectra change when the spectral resolution changes to that of XP spectra permits somewhat higher accuracy measurements and helps to find systematic errors in XP spectra, which have been already reported in De Angeli et al. (2023). These authors use data from LAMOST DR8 (Wang et al., 2022; Xiang et al., 2022) which is at higher resolution and then convert them to XP spectra resolution.

Additionally, infrared photometry data from 2MASS (Skrutskie et al., 2006) and WISE (Schlafly et al., 2019) is analyzed to break the degeneracy between $T_{\rm eff}$ and extinction. The authors also provide a custom parameter called `quality_flag`. This parameter is an integer between 0 and 9. The closer this value is to 0, the more reliable the result is. For all these reasons we have decided to work with XP spectra Parameters (hereafter XPP) from Zhang et al. (2023) instead of those provided directly by Andrae et al. (2023) with General Stellar Parameterizer from Photometry (GSP-Phot). It is important to mention that most of the parameters are obtained for stars with G $<$ 19 mag. For GCs that are too faint we expect that most of the cluster members do not have parameters measured from XPP. However, since BSSs are equally or slightly brighter than the MSTO and due to the high numbers of BSSs present in GCs we expect that a substantial percentage of our BSSs, YSSs and RSSs sample does have spectroscopic parameters measured.

To achieve this goal we request `XPP` data via `TOPCAT` selecting the same region requested as described in Section 3.1. We already have selected cluster members, so we match the data using their `Gaia Source ID`[7]. Additionally, we only select data whose `quality_flag` parameter is ≤ 4 to continue the subsequent analysis with only the most reliable values.

[7]A unique identifier for every object in GDR3.

Chapter 4

Results

4.1 Number of Blue Straggler Stars

Only 42/129 ($\sim$ 33%) of OCs show the presence of BSSs. On the other side, all GCs (41) show the presence of BSSs. This leads to a total of 83 clusters whose BSSs members could be identified. The total number of BSSs is shown in Figure 4.1 compared against other Gaia–based works (Rain et al., 2021; Jadhav and Subramaniam, 2021; Cordoni et al., 2023; Li et al., 2023). It is clear that the number of BSSs increases with the age of the cluster, modestly inverted when considering GCs only. We have found a total of 4399 BSSs. In our BSSs sample, 434 ($\sim$ 10%) are linked to OCs. In the case of GCs we were able to identify 3965 BSSs ($\sim$ 90%).

4.2 Astrophysical Parameters of BSSs

We now present the results obtained with our 3 different methods explained in Section 3.3. Hereafter, the "IRFM" label is related to results obtained with color-temperature relations, "isochrone" label is related to results obtained with best-fitting isochrone methods and "XPP" is related to matched spectroscopic data from (Zhang et al., 2023).

From color-temperature relations we are only able to extract $T_{\rm eff}$ for our sample stars. For PARSEC isochrone models, we can extract many more parameters such as the stellar mass, luminosity, age and surface gravity, among other parameters, that are considered

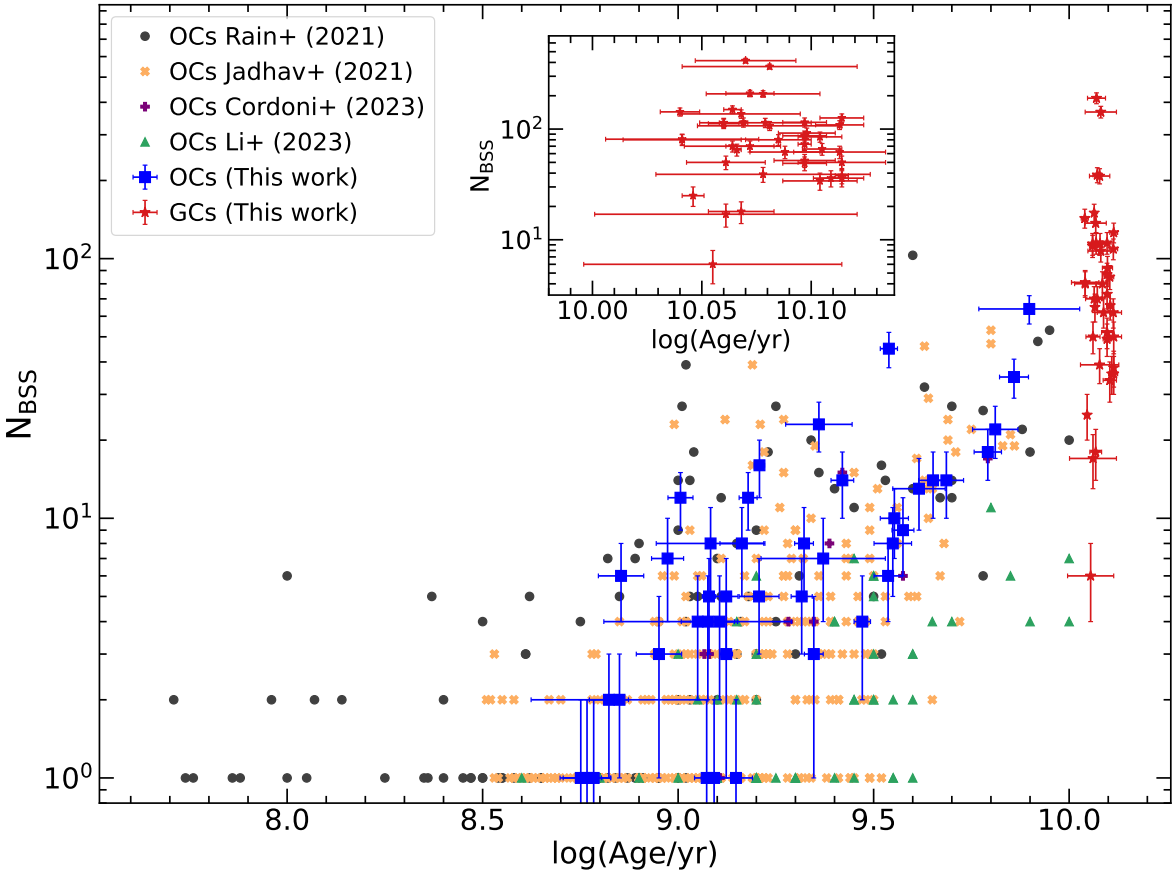

Figure 4.1: Total number of identified BSSs for different Gaia-based studies vs. cluster age. We note that, similar to the previous studies, BSSs start to appear for an age of $\sim$ 500 Myr. Apparently, there is a correlation between the number of BSSs and the cluster age. The smaller inset plot shows the number of BSSs in GCs, where the trend shown for OCs agrees in the mean, but appears to be modestly inverted when considering GCs only. Errors in the numbers of BSS are Poisson uncertainties. For OCs age errors are based on those provided by Dias et al. (2021), whereas for GCs age errors are the difference between the cluster age found for our best-fitting method and those provided by Baumgardt et al. (2023).

beyond the scope of this work. XPP comes with 2 useful parameters for us: $T_{\rm eff}$ and surface gravity $\log(g)$. To test whether the parameters extracted with our different methods are consistent with each other, we compare each pair of them. We have $T_{\rm eff}$ measured for all our methods; $\log(g)$ is available for isochrone and XPP methods. In the following sub-sections we provide their comparisons and relations.

4.2.1 Effective Temperature of Blue Straggler Stars

Figure 4.2 shows the comparison between $T_{\rm eff}$ found for isochrones against the other two methods for all stars with an error below 300 K. It is clear that when $T_{\rm eff}$ obtained through the color-temperature relations and $T_{\rm eff}$ obtained from XPP are compared against this same parameter measured with best-fit isochrone models, results in a linear relation, close to 1 : 1. Therefore, we can say that results obtained from different methods are consistent with each other.

For BSSs, we applied a least square method –including errors in both components– to derive the relations between $T_{\rm eff}$ obtained with color–temperature relations ($T_{\rm eff,\ IRFM}$) against $T_{\rm eff}$ obtained with isochrones ($T_{\rm eff,\ isochrone}$); and $T_{\rm eff}$ obtained from XPP ($T_{\rm eff,\ xpp}$) against $T_{\rm eff}$ from isochrones are given, respectively, in units of K, by:

$$T_{\rm eff,\ IRFM} = 1.074\ \times T_{\rm eff,\ isochrone} - 585 \tag{4.1}$$

$$T_{\rm eff,\ xpp} = 0.842\ \times T_{\rm eff,\ isochrone} + 1092 \tag{4.2}$$

Cluster type	Method	$\langle T_{\rm eff}\rangle$ (K)	Median $T_{\rm eff}$ (K)	$\sigma_{T_{\rm eff}}$ (K)	Max. $T_{\rm eff}$ (K)	Min. $T_{\rm eff}$ (K)
OC + GC	Color–Temperature	6853	6671	795	11 889	5221
OC + GC	Isochrone–fitting	6900	6782	687	12 217	5298
GC	Color–Temperature	6772	6648	630	9849	5221
GC	Isochrone–fitting	6829	6762	529	9467	5298
OC	Color–Temperature	7598	7199	1476	11 889	5558
OC	Isochrone–fitting	7549	7208	1331	12 217	5636

Table 4.1: Values found for BSS $T_{\rm eff}$. Columns are as follow: 1) Cluster type for the corresponding data sample, 2) Method applied to obtain the values. 3) average BSS $T_{\rm eff}$, 4) median mass $T_{\rm eff}$ of BSSs, 5) dispersion in $T_{\rm eff}$ for BSSs, 6) maximum $T_{\rm eff}$ found for BSSs in data sample, 7) minimum $T_{\rm eff}$ found for BSSs in data sample.

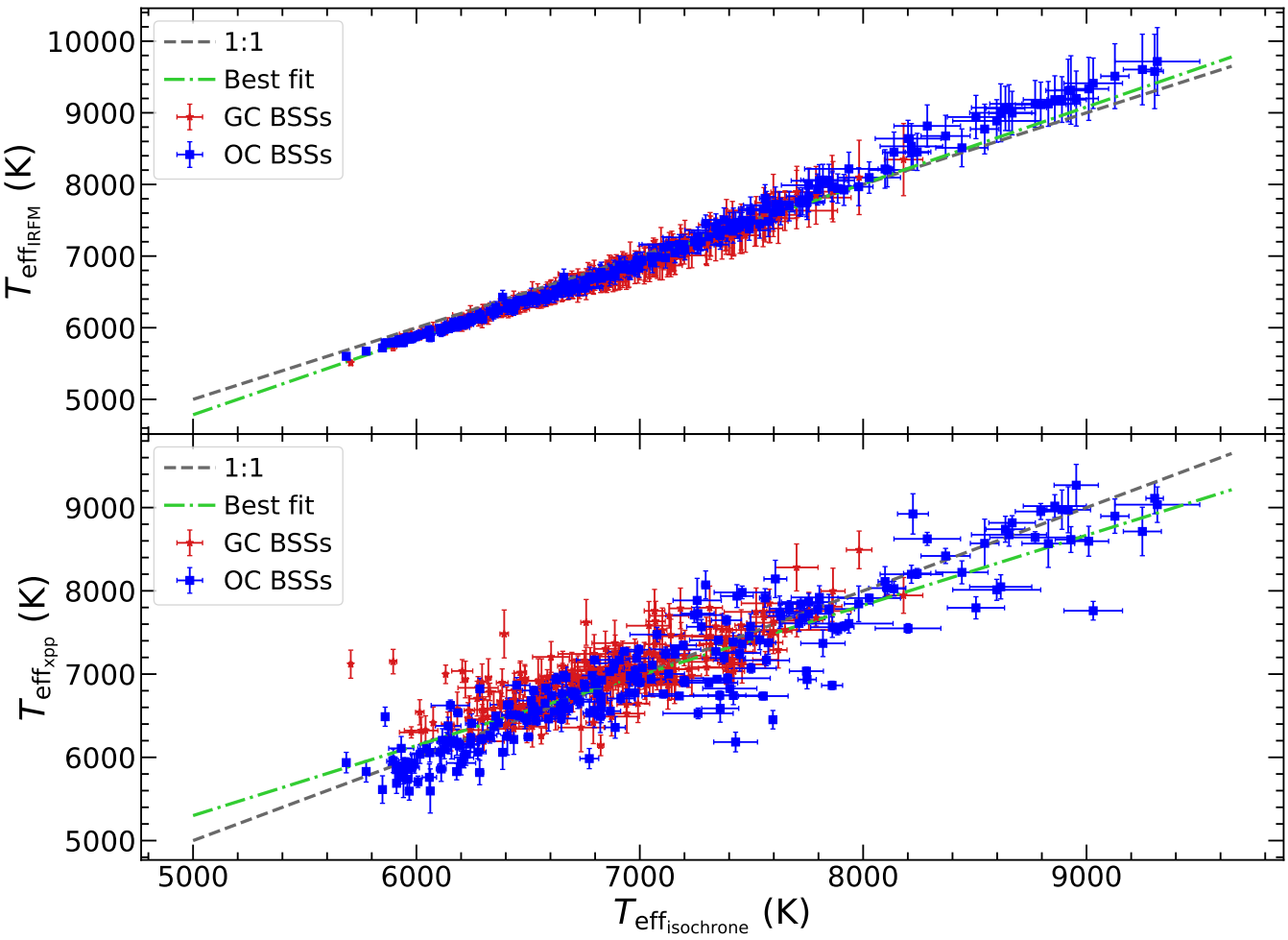

Figure 4.2: Comparison of $T_{\rm eff}$ obtained using different methods. *Top*: comparison between $T_{\rm eff}$ obtained from the color-temperature (IRFM) relation vs. $T_{\rm eff}$ found for isochrone-based models. The figure shows all the results for BSSs with an error below 300 K in both methods compared. Dashed gray lines show $1:1$ relations. Dotted-dashed green lines show the best fit –considering errors– using the least-squares method for all the data (OCs + GCs). BSSs for GCs and OCs are denoted as red stars and blue squares, respectively. *Bottom*: Same as top figure, but comparing $T_{\rm eff}$ found using XPP vs. isochrone-based models.

Equations (4.1) and (4.2) are the best-fit for the top and bottom of Figure 4.2, respectively.

We also compare the $T_{\rm eff}$ obtained with color–temperature relations against those found

in XPP. We repeat the same method we applied to obtain equations (4.1) and (4.2) and we derive the relations for BSSs –shown in Figure 4.3–, in units of K, as:

$$T_{\text{eff, xpp}} = 0.735 \times T_{\text{eff, IRFM}} + 1870 \tag{4.3}$$

The corresponding comparison relations for YSSs and RSSs –for T_{eff} using the different methods like (4.1), (4.2) and (4.3)– can be found in Appendix B.1.

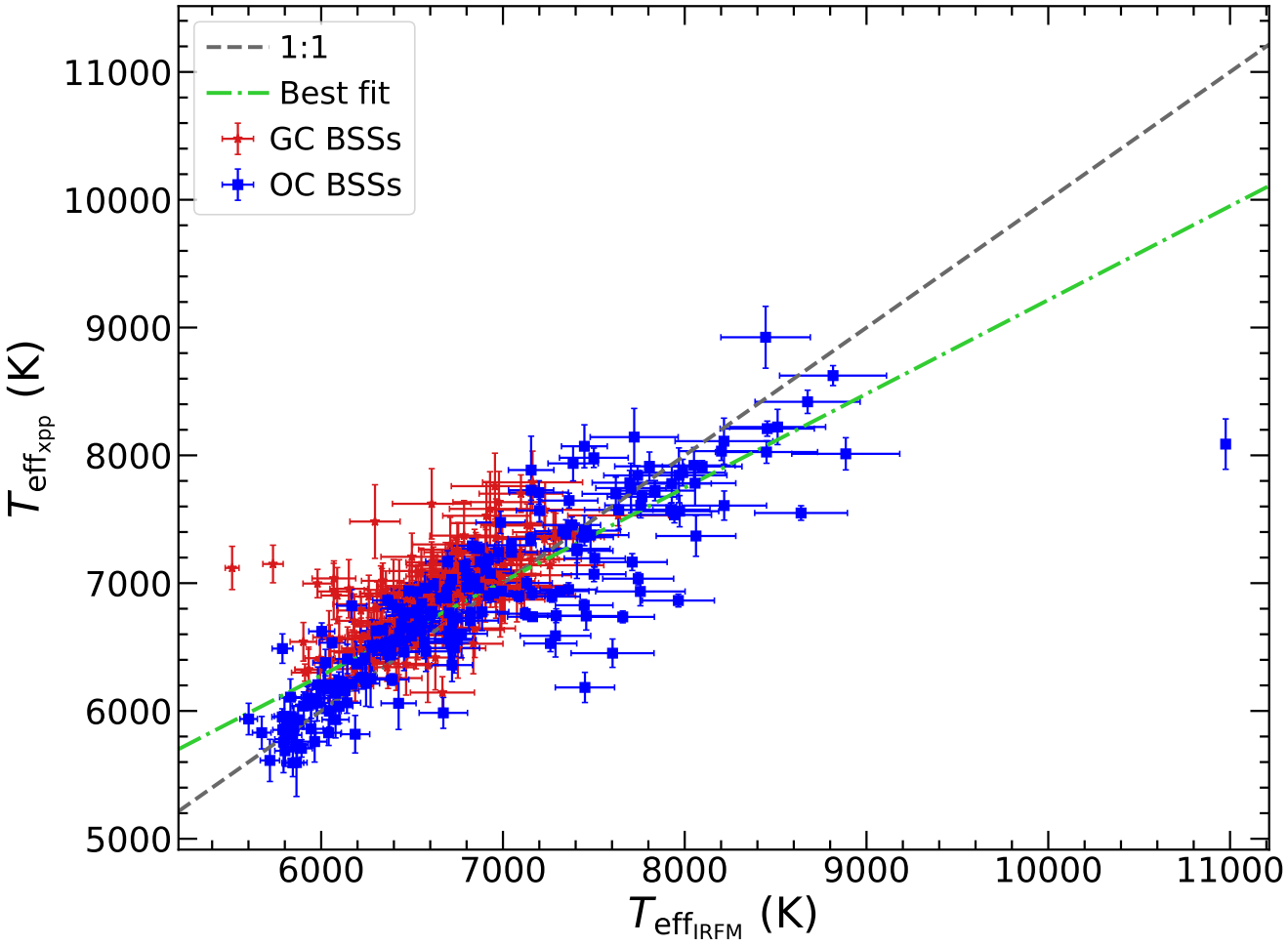

Figure 4.3: Same as Figure 4.2, but for T_{eff} obtained from color–temperature relations against those found in XPP for BSSs.

4.2.2 Surface gravity of Blue Straggler Stars

As was mentioned earlier, from isochrone parameters and XPP we do have a second common parameter that we can compare: surface gravity, $\log(g)$. Following the same procedure as before, we now test the consistency between the surface gravity values found with isochrones and those found from XPP. The results for all the data with an error under 0.2 for $\log(g)$ in both components are shown in Figure 4.4. From this figure we derive the relation for $\log(g)$ obtained with isochrones and XPP for BSSs –with g in units of $\mathrm{cm}\cdot\mathrm{s}^{-2}$– as:

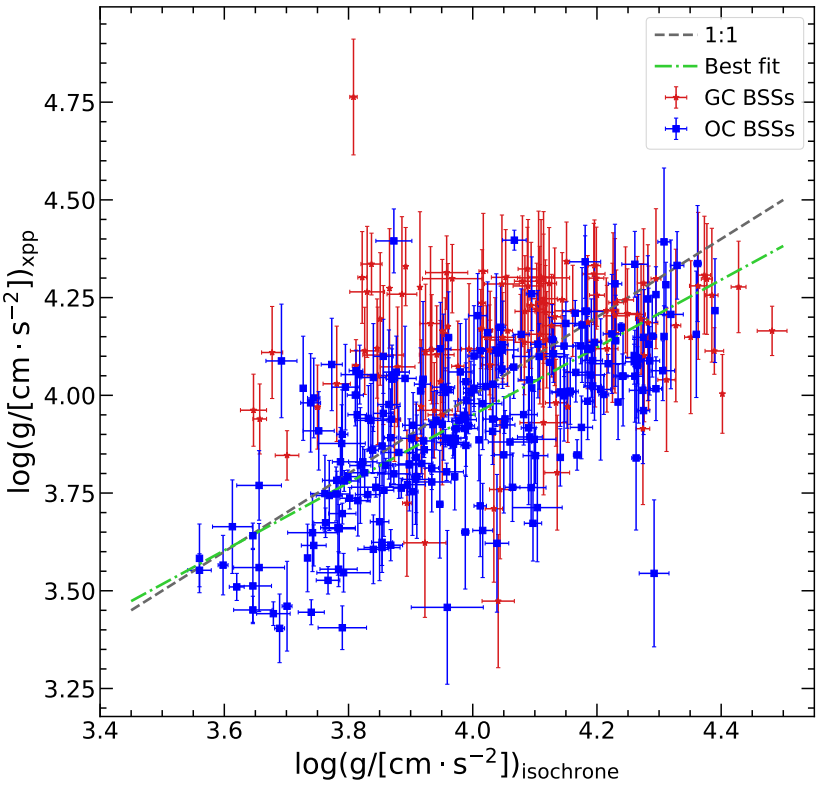

Figure 4.4: Comparison of log(g) obtained using different methods: log(g) obtained from XPP vs. log(g) obtained with isochrones. The figure shows all the results for BSSs with an error below 0.2 in both methods compared. Dashed gray lines show $1:1$ relations. Dotted-dashed green lines show the best fit –considering errors– using least-squares method for all the data (OCs + GCs). BSSs for GCs and OCs are shown as red stars and blue squares, respectively.

$$\log(g)_{\rm xpp} = 0.865 \times \log(g)_{\rm isochrone} + 0.49. \tag{4.4}$$

We can appreciate that we still have an acceptable concordance for $\log(g)$ for values obtained from isochrones and from XPP. However, we note that on average, $\log(g)$ obtained with isochrone models are slightly inferior than those obtained from spectra/XPP.

4.2.3 Masses of Blue Straggler Stars

Last, but not least, we extract the mass of BSSs only based on isochrone models, since it is the only method that directly provides this parameter. However, we must keep in mind that BSSs could be binary or even multiplet systems. Therefore, and due to Gaia filter limitations that do not allow us to characterize robustly cool companions for the stars, as shown in Figure 2.1, we could be overestimating the mass of the star since we are considering the mass of the binary system as the total mass. Some statistics found for our identified BSS mass sample is shown in Table 4.2. We find that, within our entire sample, the average mass of the blue stragglers is $\langle M_{\rm BSS,all} \rangle = (1.09 \pm 0.28)\ M_{\odot}$. As expected OCs/younger clusters show a higher average-mass with $\langle M_{\rm BSS,OC} \rangle = (1.75\ \pm 0.45)\ M_{\odot}$ and GCs show a lower average-mass with $\langle M_{\rm BSS,GC} \rangle = (1.02 \pm 0.1)\ M_{\odot}$. We also note that the dispersion is much smaller in GCs compared to that found for OCs. A deeper analysis of these results can be found at Section 4.3.

Cluster type	$\langle$Mass$\rangle$ ($M_{\odot}$)	Median Mass ($M_{\odot}$)	$\sigma_{\rm Mass}$ ($M_{\odot}$)	Max. Mass ($M_{\odot}$)	Min. Mass ($M_{\odot}$)
OC + GC	1.09	1.01	0.28	3.38	0.84
OC	1.75	1.65	0.45	3.38	1.18
GC	1.02	1.0	0.1	1.5	0.84

Table 4.2: Statistics of masses derived to BSSs from isochrone models. The first, second and third row show the data for all clusters (OCs + GCs), OCs and GCs, respectively. Columns are as follow: 1) Cluster type for the corresponding data sample, 2) average of mass of BSSs, 3) median mass of BSSs, 4) dispersion in the mass for BSSs, 5) maximum mass found for BSSs in data sample, 6) minimum mass found for BSSs in data sample.

4.3 Analysis and Discussion

To observe how $T_{\rm eff}$ changes with the cluster age, we display these results into Figure 4.5. Similar to what has been done to the mass parameter, we see if there are any correlations between the difference of BSS $T_{\rm eff}$ and MSTO $T_{\rm eff}$, hereafter $\Delta T_{\rm eff}$, and the cluster age. At the top of this figure we can appreciate that, in average, $\Delta T_{\rm eff}$ decreases with the cluster age. This trend can be appreciated in OCs and GCs. This means that as time passes BSSs cooldown in a faster way than the MSTO does. This is not a surprising result since BSSs are more massive stars compared to those around the MSTO. Since BSSs are more massive they evolve faster, reaching post MS phases such as SGB and RGB sooner where they slowly start to cooldown in contrast with less massive stars that take more time to reach those stages. Therefore, we can expect this difference in temperature to "shrink" with the cluster age. This correlation is even more clear when we normalize $\langle \Delta T_{\rm eff} \rangle$ with respect to the MSTO eff. We also show the dispersion in $T_{\rm eff}$ of the BSSs against the cluster age. We put our attention on OCs, since their dispersion clearly decreases with the cluster age; this means that, even if new BSSs are being formed, they tend to be closer to the MSTO. Nevertheless, this clear trend in the dispersion in OCs cannot be appreciated in GCs. We must remember that in our BSS selection criteria for GCs we selected stars with $\sim [0.5-0.6]$ mags bluer than the MSTO to avoid selecting stars in later stellar phases compared to the MS. We then expect an "upper" cut value in $T_{\rm eff}$ dispersion for BSSs. However, this means that, for GCs, as the cluster gets older BSSs are more-less equally disperse in $T_{\rm eff}$. Sindhu et al. (2019) found $T_{\rm eff}$ for the old OC M67 in ranges around 7500–8700 K. These results are in agreement with our average value found for $T_{\rm eff}$ obtained from different methods in OCs; $\langle T_{\rm eff} \rangle = (7598 \pm 1476)$ K derived from color–temperature relations and $\langle T_{\rm eff} \rangle = (7549 \pm 1331)$ K from isochrone fittings. Dattatrey et al. (2023) have classified BSSs in GC NGC 362 depending if they find a hotter companion based on their SED. They report $T_{\rm eff}$ of 7500–9250 K for BSSs that did not show evidence of a hotter companion and 6200–8250 K for BSSs that did. The authors show and demonstrate that BSSs without companions live in a "bluer" BSS sequence –probably formed through collisions– and stars with a WD companion lie in a "redder" BSS sequence. Our results

for GCs show a better agreement with those temperatures found for BSSs with a WD neighbor.

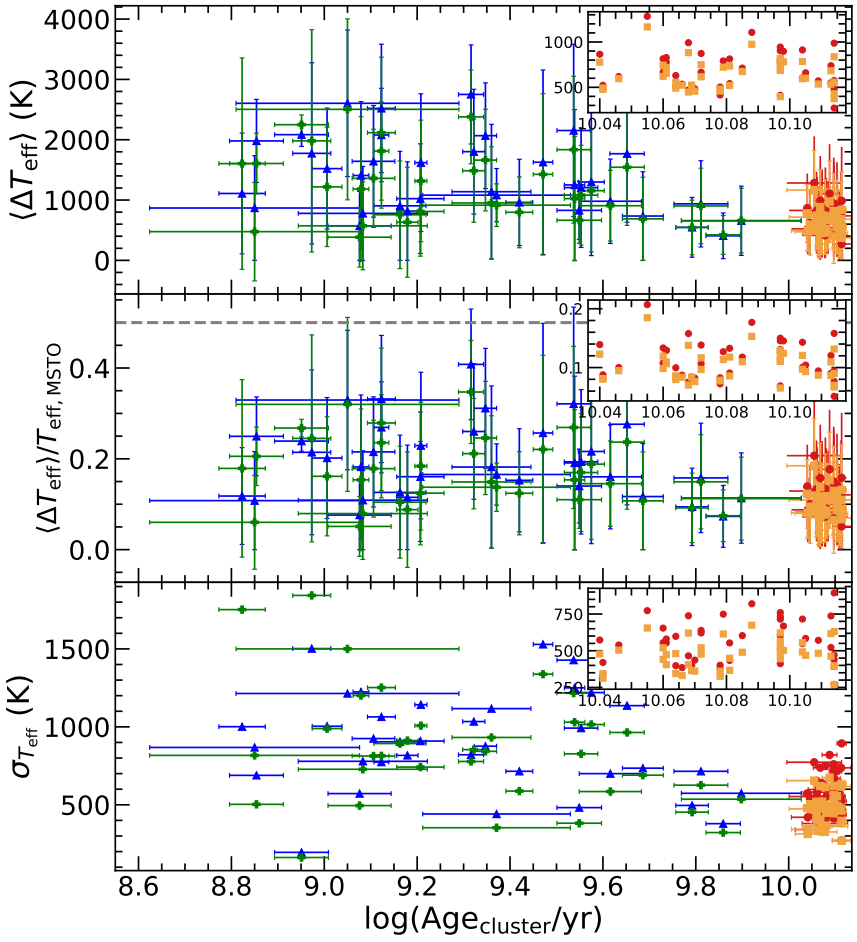

Figure 4.5: $T_{\rm eff}$ vs. cluster age. *Top*: $\langle \Delta T_{\rm eff} \rangle$ –the average of the difference between BSS $T_{\rm eff}$ and MSTO $T_{\rm eff}$ for stars within the same cluster– vs. cluster age. Blue triangles and red dots represent $T_{\rm eff}$ obtained from color–temperature relations for OCs and GCs, respectively. Green plus symbol (+) and orange squares represent $T_{\rm eff}$ derived from isochrone models for OCs and GCs, respectively. At the top right corner we show the results only for GCs without error bars for a better appreciation, keeping the same axes from the major plot. Error bars show the dispersion of BSSs $T_{\rm eff}$. *Middle*: $\langle T_{\rm eff} \rangle$ normalized by the MSTO temperature –found with the same method–. Horizontal gray line indicates BSS $T_{\rm eff}$ = 1.5 × MSTO $T_{\rm eff}$. *Bottom*: Dispersion of BSS $T_{\rm eff}$ vs. cluster age.

For the GC average-mass of our BSSs sample, we find this value –$\langle M_{\rm BSS,GC}\rangle = (1.02 \pm 0.1)\ M_{\odot}$– to differ from those found by Shara et al. (1997); Baldwin et al. (2016); who reported a BSS Mass of $M_{\rm BSS} = (1.7 \pm 0.4)\ M_{\odot}$ and $\langle M_{\rm BSS}\rangle = (1.22 \pm 0.12)\ M_{\odot}$, respectively. We could explain this difference based on two factors: i) Where are the BSSs located with respect to the cluster core center and, ii) Data limitations by Gaia. Contreras Ramos et al. (2012) and Ferraro et al. (2012) have shown that BSSs tend to sink to the inner parts of the cluster. However, Gaia Mission itself is capped in overcrowded regions such as GC centre; whereas the two previously mentioned studies are based on HST observations. This implies that our data sample is based on regions outside $\sim r_{\rm h}$, the half-light radius, which would explain our average value is different from HST-based studies. Nevertheless, our results are agreement with those measured by Simunovic (2017) ($\langle M_{\rm BSS}\rangle \sim 1\ M_{\odot}$), Fiorentino et al. (2014) ($\langle M_{\rm BSS}\rangle = 1.06 \pm 0.09$) and Stępień and Kiraga (2015) ($\langle M_{\rm BSS} \sim (1 - 1.1)\ M_{\odot}$). Values compared with Simunovic (2017) are the most significant ones, since he extracted the parameters from 38 GCs using isochrone fittings as well; which makes this study statistically more comparable to our GC sample. Compared with OCs, our average-mass value obtained for BSSs –$\langle M_{\rm BSS,OC}\rangle = (1.75 \pm 0.45)\ M_{\odot}$– is lower to those found by Jadhav and Subramaniam (2021). They report an average-mass value of $\langle M_{\rm BSS}\rangle = (2.67 \pm 1.2)\ M_{\odot}$ if we consider they confirmed BSSs and $\langle M_{\rm BSS}\rangle = (2.49 \pm 1.13)\ M_{\odot}$ if we consider their confirmed and candidate/probable BSSs. Nevertheless, we focus that our average-mass value is within their range considering the errors in both cases. Our dispersion in data is also smaller than those provided by Jadhav and Subramaniam (2021). However, and as was explained previously, this gap between our results is expected since we might have added a cut at the moment to select Gaia G magnitude range, discarding all stars with magnitudes below $G_{\rm BP} \sim 10$ as they could be saturated and, therefore, their Gaia parameters could contain systematic errors. This would not only explain the difference between our results, but also why our dispersion for OCs is smaller.

Even so, these values are also in agreement with simulations for old open clusters from Tian et al. (2006), who simulated a binary system with a mass $(1.4 + 0.9) M_{\odot}$.

BSSs are expected to gain mass in their MS lifetime. This means that the "excess" between their current mass and the mass of the MSTO could give a hint about their formation pathways. Recall that, based on previous observations (Dalessandro et al., 2013; Dattatrey et al., 2023), more massive (bluer) BSSs are likely to be formed through collisions whereas less massive (redder) BSSs are likely to be formed by MT. Even though this is not a strict statement, it could be considered a first indication for the formation channel for the particular BSS. Trying to provide a quantity that could give a hint about which pathway could predominate Jadhav and Subramaniam (2021) defined a parameter called the "Fractional Mass Excess", or $\mathcal{M}_e$. This quantity is defined as:

$$\mathcal{M}_e = \frac{M_{BSS} - M_{MSTO}}{M_{MSTO}} \tag{4.5}$$

where M_{BSS} is the mass of the BSS and M_{MSTO} is the mass at the MSTO, which in our case are obtained from isochrone models. In simple words, this $\mathcal{M}_e$ factor is the excess of mass between the BSS mass and MSTO mass, normalized by the MSTO mass. Note that $\mathcal{M}_e = 0.5$ can be intepreted as $M_{BSS} = 1.5 \times M_{MSTO}$, and $\mathcal{M}_e = 1.0$ represents $M_{BSS} = 2 \times M_{MSTO}$. By definition, this "fractional mass excess" is roughly equivalent to the MT efficiency if we assume that both participants of the system, the donor and the secondary star, are MS stars (Shao and Li, 2016). Based on $\mathcal{M}_e$ value, Jadhav and Subramaniam (2021) decided to divide it into 3 different regimes: low–$\mathcal{M}_e$ ($\mathcal{M}_e < 0.5$), high–$\mathcal{M}_e$ ($0.5 < \mathcal{M}_e < 1.0$) and extreme–$\mathcal{M}_e$ ($\mathcal{M}_e > 1.0$) where, as a first approximation, formation pathways that predominate are MT, collisions and multiple-mergers/MT, respectively.

We test this parameter against the cluster age, which is displayed in Figure 4.6. First of all we note that, as expected, the younger clusters show BSSs with a higher mass; mass that decreases with cluster age. This means that younger clusters will tend to have BSSs with higher masses compared to their older counterparts. However, this is expected for stellar evolution for the lifetime of a star, τ, since $\tau \propto \frac{M}{L} = \frac{1}{M^3}$. I.e., more massive stars have decreased τ by $\sim$3 orders of magnitude compared to less massive stars, which correspondingly translates to the absolute BSS mass as a function of cluster age.

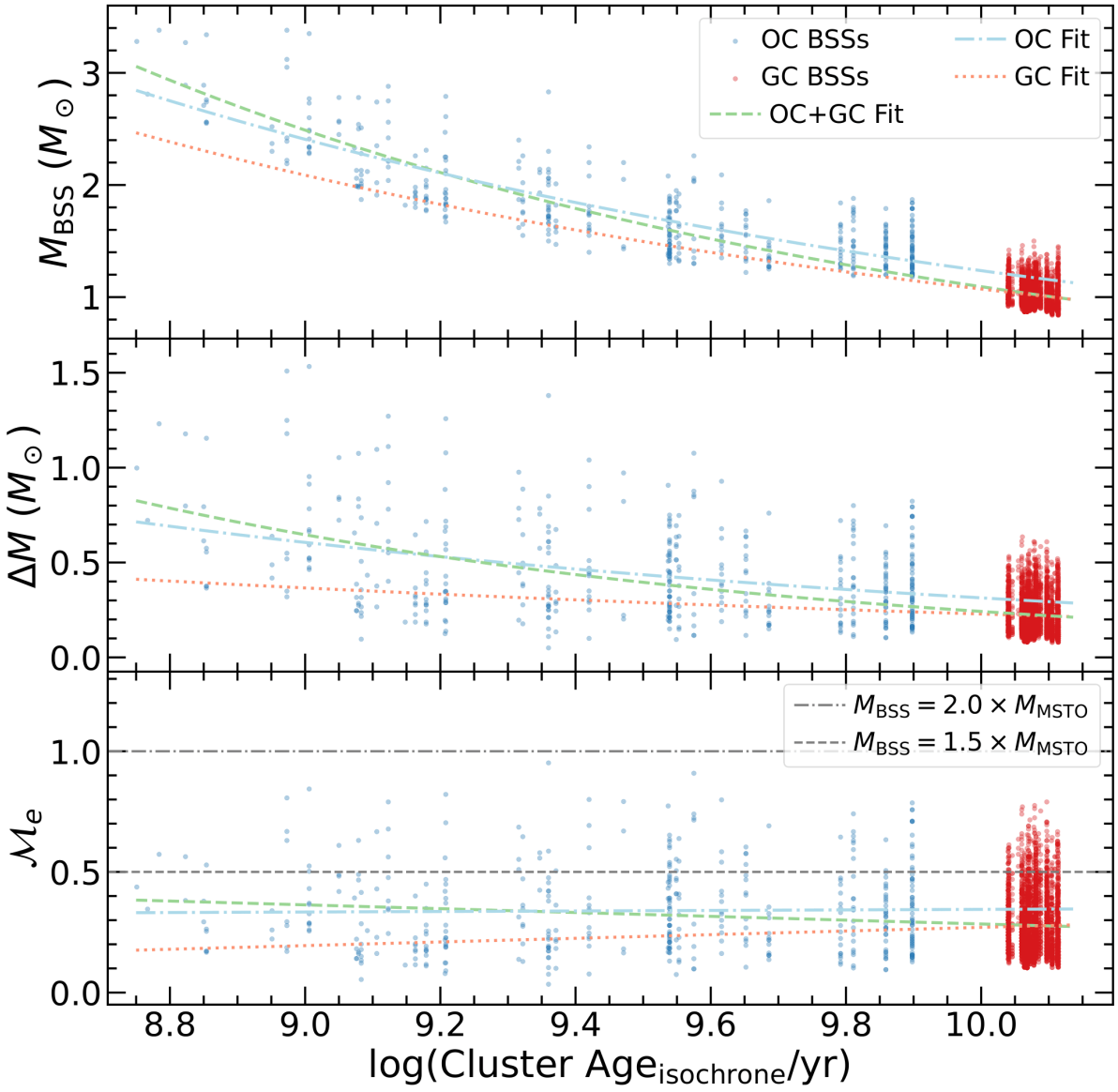

Figure 4.6: Mass parameters vs. log(cluster age). *Top*: Mass of BSSs vs. cluster age. Semi-transparent red dots show the mass of BSSs from GC and semi-transparent blue dots show the mass of BSSs from OCs. Green dashed lines show the best fit for all the clusters, dashed-dotted light-blue lines show the best fit for OCs and dotted orange lines show the best fit for GCs. *Middle*: Difference between $M_{\rm BSS}$ and $M_{\rm MSTO}$ vs. cluster age. *Bottom*: $\mathcal{M}_{\rm e}$ vs. cluster age. The dashed-dotted gray line shows the limit where $M_{\rm BSS} = 2.0 \times M_{\rm MSTO}$ and dashed gray line shows the limit for $M_{\rm BSS} = 1.5 \times M_{\rm MSTO}$.

Figure 4.6 also shows that the difference between the mass of BSSs and the mass that corresponds to the MSTO decreases with cluster age. As explained before, this is expected since more massive stars will end their life earlier and MSTO mass decreases slower with increasing age. We expect that $M_{\rm BSS} - M_{\rm MSTO}$ shrinks as time advances. We find no significant trend of $\mathcal{M}_{\rm e}$ with cluster age. However, we observe that the fraction of high-$\mathcal{M}_{\rm e}$ BSSs is higher in GCs than in OCs, which may indicate that the collisional formation channel is more pronounced in old star cluster. This is turn might be related to sufficiently old dynamical ages of star cluster, which can in principle have undergone one or more core collapse, boosting the stellar encounter rates and thus the formation of collision-induced BSS formation. We find to be $\sim 81.34\%$ and $\sim 18.66\%$ the percentages for low and high–$\mathcal{M}_{\rm e}$, respectively, for OCs. In GCs, we find these proportions to be $\sim 94.25\%$ and $\sim 5.75\%$ for low and high–$\mathcal{M}_{\rm e}$, respectively. Considering all clusters, the percentage of low–$\mathcal{M}_{\rm e}$ is $\sim 93\%$ and for high–$\mathcal{M}_{\rm e}$ we obtain $\sim 7\%$. We do not find BSSs for clusters younger than ~ 300 Myr; supporting the results found by Rain et al. (2021); Jadhav and Subramaniam (2021); Cordoni et al. (2023). More specifically, within our sample, BSSs start to appear at ages ~ 500 Myr.

Apart from our direct comparison of OCs and GCs, the difference between our results and those provided by Jadhav and Subramaniam (2021) is that we were not able to find any stars with $\mathcal{M}_{\rm e} > 1.0$ and, therefore, be located in the extreme–$\mathcal{M}_{\rm e}$ regime. An explanation is our Gaia DR3 selection criteria. As was specified in section 3.1, we applied a cut along G magnitudes between 10.5 mag $\leq$ G $\leq$ 20.5 mag. We skipped too bright/saturated stars (to avoid systematic errors) which may have been classified as more massive by our models. Nevertheless, our cut could have also added a bias in the selection where we do not consider extremely massive stars, especially for OCs.

Additionally, we test the BSSs mass parameters vs. log(BSSs age), i.e. the individual ages of our sample BSSs. Results are displayed in Figure 4.7. The relations for $M_{\rm BSS}$ and ΔM –the difference between the mass corresponding to the MSTO and the BSS mass– against BSSs age are broadly similar to those found against the cluster age, i.e. both of these parameters decrease as a function of age. In addition, we see various sequences appearing in the two upper panels. The main difference, however, is in $\mathcal{M}_{\rm e}$

against log(BSSs age): as BSSs become older and older, $\mathcal{M}_e$ also starts to decrease.

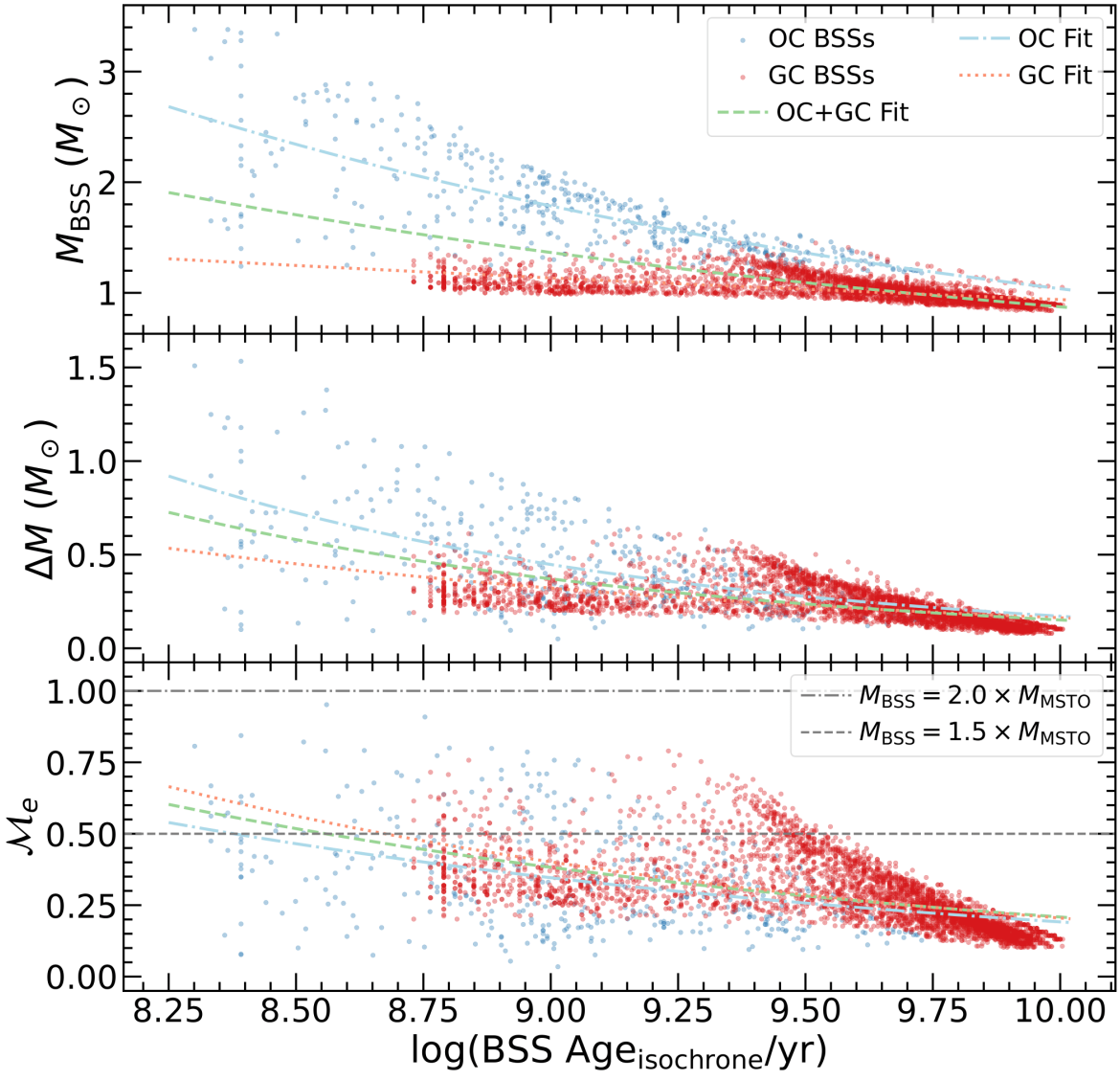

Figure 4.7: Same as Figure 4.6, but age is computed from isochrone models.

We can have two main scenarios for MT-efficiency: one conservative scenario where efficiency > 0.5 for close binaries that could end in a merger; or a non-conservative scenario where efficiency < 0.5 binary interactions can leave a remnant of the donor (Shao and Li, 2016). As was stated by Jadhav and Subramaniam (2021), we could assume $\mathcal{M}_{\rm e}$ to be roughly similar to MT-efficiency. We can interpret this as the older the BSS is, the more likely it is to be formed via MT; or as BSSs gets older, MT is more inefficient –likely leaving remnants of the donor–.

We find this relation between $\mathcal{M}_{\rm e}$ and $\log(\mathrm{Age_{BSS}})$ for all clusters, GCs and OCs to be, respectively:

$$\mathcal{M}_{\rm e,all} = (89.65 \pm 11.19) \times \exp(-[0.606 \pm 0.013] \times \log[\mathrm{Age_{BSS}/yr}]) \tag{4.6}$$

$$\mathcal{M}_{\rm e,GC} = (171.15 \pm 23.46) \times \exp(-[0.672 \pm 0.014] \times \log[\mathrm{Age_{BSS}/yr}]) \tag{4.7}$$

$$\mathcal{M}_{\rm e,OC} = (71.07 \pm 41.83) \times \exp(-[0.591 \pm 0.065] \times \log[\mathrm{Age_{BSS}/yr}]) \tag{4.8}$$

Figure 4.8 shows the percentage of low–$\mathcal{M}_{\rm e}$ and high–$\mathcal{M}_{\rm e}$ against log(Age) of BSSs. For OCs, it is clear that high–$\mathcal{M}_{\rm e}$ fraction decreases between the ages of BSSs of $\sim$ 1 Gyr–2 Gyr, whereas the low–$\mathcal{M}_{\rm e}$ fraction dominates, with a percentage $> 90\%$, for BSSs older than 2.5 Gyr. On other hand, we observe that high–$\mathcal{M}_{\rm e}$ is relatively stable for ages between $\sim$ 600 Myr–1.5 Gyr, with values $\sim 10\%$. But this value increases up to $\sim 30\%$ between for BSSs ages between $\sim$ 1.5–2.5 Gyr. Simunovic et al. (2014) fitted collisional isochrones (Sills et al., 2009) to Blue-Sequence BSSs (as presented in Section 2.1.1) finding that their age is $\sim$ 2 Gyr, which is within the range of ages found for BSSs where high–$\mathcal{M}_{\rm e}$ fraction increases/low–$\mathcal{M}_{\rm e}$ fraction decreases. For GCs older than $\sim$ 3.5 Gyr the high–$\mathcal{M}_{\rm e}$ fraction rapidly decreases to values under 10% similar to those that can be appreciated for OCs. Overall, it can be observed for all BSSs in our sample low/high–$\mathcal{M}_{\rm e}$ fraction is dominated by OCs for younger BSSs ages ($\sim 250 - 600$ Myr) and by GCs for older BSSs ages ($\sim$ 1.5–10 Gyr) as expected by their population number (Section 4.1).

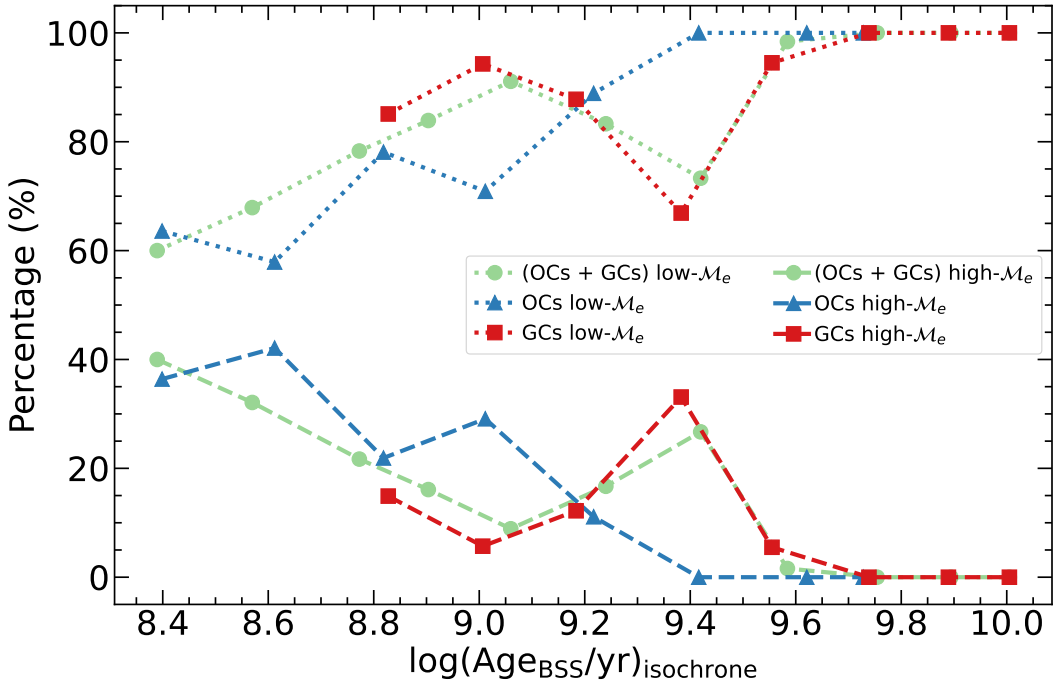

Figure 4.8: Low/High–$\mathcal{M}_e$ percentage vs. log(Age$_{BSS}$). Green dots, red squares and red triangles represent all clusters, GCs and OCs, respectively. Dotted line indicates low–$\mathcal{M}_e$ and dashed line indicates high–$\mathcal{M}_e$ values.

$\mathcal{M}_e$–type	Cluster type	$\langle G_{BP,abs} \rangle$ (mag)	M ($G_{BP,abs}$) (mag)	$\sigma_{G_{BP,abs}}$ (mag)	$\langle (G_{BP} - G_{RP})_0 \rangle$ (mag)	M [$(G_{BP} - G_{RP})_0$] (mag)	$\sigma_{(BP-RP)_0}$ (mag)
high–$\mathcal{M}_e$	GC	2.57	2.52	0.46	0.29	0.26	0.16
low–$\mathcal{M}_e$	GC	3.5	3.5	0.49	0.51	0.51	0.12
high–$\mathcal{M}_e$	OC	1.11	1.43	0.93	0.16	0.11	0.22
low–$\mathcal{M}_e$	OC	2.23	2.33	1.04	0.41	0.45	0.22

Table 4.3: Statistics of BSSs, with their respective $\mathcal{M}_e$ classified as high/low, in CMD. Columns are as follow: 1) $\mathcal{M}_e$ classification, 2) Cluster type, 3) average of the absolute G_{BP} magnitude, 4) median of the absolute G_{BP} magnitude, 5) dispersion of the absolute G_{BP} magnitude, 6) Average derredened color. 7) Median of derredened color. 8) Dispersion of derredened color.

BSSs classified as Low–$\mathcal{M}_e$ and high–$\mathcal{M}_e$ statistics in CMD–space are displayed in Table 4.3 and shown in Figure 4.9. We find the same trend shown in Figure 6 from Jadhav and Subramaniam (2021): BSSs with $\mathcal{M}_e$ classified as high–$\mathcal{M}_e$ do not show a difference in color –however, high–$\mathcal{M}_e$ BSSs are slightly bluer than low–$\mathcal{M}_e$ by $\sim$ 0.2mag–. The difference is in the absolute magnitude where they show $\sim$ 1.0, i.e., high–$\mathcal{M}_e$ are, approximately, 10 times brighter than low–$\mathcal{M}_e$ BSSs. This difference is appreciable for both type of clusters, GCs and OCs. This separation between different BSSs and their $\mathcal{M}_e$ classification is clear in Figure 4.9.

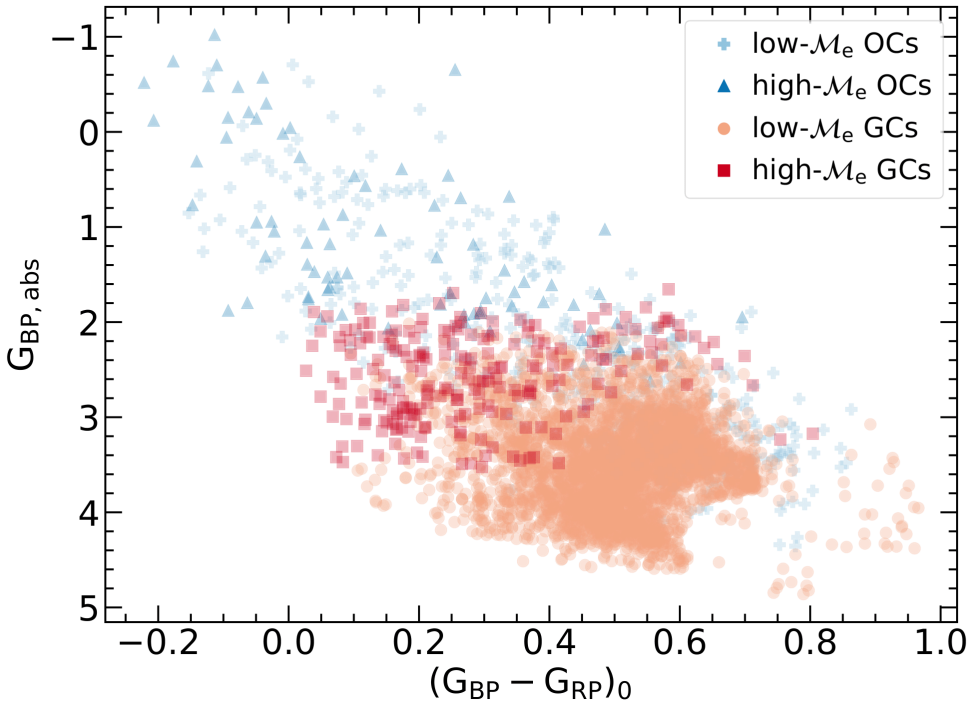

Figure 4.9: CMD for all our analyzed BSSs; G_{BP} absolute magnitude vs. derredened color. BSSs marked as light-blue plus (+) symbol, blue triangle, orange dot and red square denote low–$\mathcal{M}_e$ BSSs in OCs, high–$\mathcal{M}_e$ BSSs in OCs, low–$\mathcal{M}_e$ BSSs in GCs and high–$\mathcal{M}_e$, respectively.

We finally focus attention on the bottom of Figure 4.7: we can see something similar to a double-sequence[1]. To keep it simple, we set a linear function that separates these two sequences as "upper" and "lower" sequence. This linear function is defined as:

[1]Do not confuse it with double sequences of BSSs since we are not in the CMD–space.

$$\mathcal{M}_{\rm e} = -0.539 \times \log(\mathrm{Age_{BSS}/yr}) + 5.475 \tag{4.9}$$

Values above equation (4.9) are classified as "upper"–sequence and for values lower than the mentioned equation we classify them as "lower"–sequence. After classifying BSSs with this new label, we then display them in a CMD. Selection criteria and CMD can be observed at Figure 4.10.

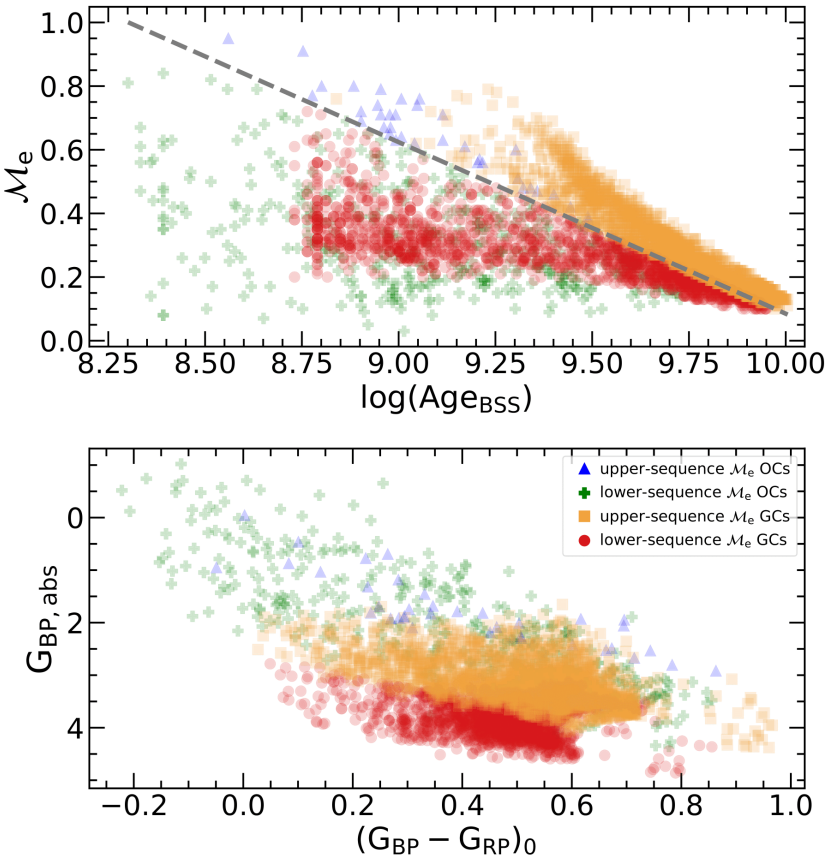

Figure 4.10: *Top*: Same as Figure 4.7, but classifying stars depending if they lie above or under the grey dashed separation represented by equation (4.9). Blue triangles, green plus (+) symbol, orange squares and red point represent OC BSSs located above the separation, OC BSSs located under the separation, GC BSSs located above the separation and GC BSSs located under the separation, respectively. *Bottom*: BSSs classified by the criteria shown in upper figure displayed along the CMD.

We explain these final results as follows: from a binary perspective, the higher $\mathcal{M}_e$, the more efficient the MT process is. Since the MT is more efficient this yields to more accreted mass and hence more fuel for the star receiving the material, extending its life (McCrea, 1964). Assuming the scenario of a common-envelope evolution, the separation between the stars of the binary system eventually decreases. This could end in two scenarios: they could end in a merge or one of the binaries could be ejected from the system; with the first scenario being the more probable to occur (Hurley et al., 2002). As a result of this merger scenario, the secondary star now is more massive. Considering that $\tau \propto M^{-3}$, this triggers the evolution to be faster and, thus, be located at older ages in $\mathcal{M}_e$ vs. $\log(\mathrm{Age}_{\mathrm{BSS}}/\mathrm{yr})$ with isochrone evolutionary tracks. Ergo, we interpret these two sequences as post-merger/close-binary interaction sequence ("upper" sequence) and pre-merger/close-binary interaction sequence ("lower" sequence).

It is important to mention, and as Jadhav and Subramaniam (2021) have warned, that the "fractional mass excess" $\mathcal{M}_e$ is not a strict/rigid parameter that states exactly how BSSs were formed. This parameter *suggests* how a BSS could likely be formed. For deeper analysis, which escapes from Gaia limitations, we do need FUV observations (Sindhu et al., 2019; Dattatrey et al., 2023, for example) to be able to distinguish the presence or absence of a companion.

Chapter 5

Conclusions

We summarize the progress and results of this thesis as follows:

1. Using Gaia DR3 and Cordoni et al. (2018) algorithm we have successfully identified cluster members for 41 GCs and 129 OCs. In the case of GCs we are only able to extract data outside $\sim r_{\rm h}$ due to Gaia problems with overcrowded regions.

2. We used PARSEC isochrones (Bressan et al., 2012) with the identified cluster members to properly determine the cluster MSTO point. Based on this point as a reference and dispersion of the cluster along color and magnitude, we shifted the best-fitting isochrone, ZAMS and BSSs area limitations from previous studies (Leigh et al., 2011) to set a region and extract BSSs for GCs and OCs to select and classify stars as BSS, YSS or RSS. We were able to recognize BSSs in all GCs and 42/129 ($\sim$ 33%) OCs in our sample. We counted a total of 4399 BSSs; 434 ($\sim$ 10%) located in OCs and 3965 (90%) located in GCs.

3. The number of BSSs increases with the cluster age in OCs; this trend is not clear in GCs –remembering that we are sampling outer regions of the cluster for GCs–. We do not see the presence of BSSs in clusters younger than $\sim$ 300 Myr, in agreement with previous Gaia-based studies for BSSs (Rain et al., 2021; Jadhav and Subramaniam, 2021; Cordoni et al., 2023). We note that BSSs start to appear at cluster with ages $\sim$ 500 Myr in our sample.

4. Using color–temperature relations, isochrone–fittings and parameters from Zhang et al. (2023, called "XPP") –which is based on spectra provided by Gaia DR3– we were able to determine astrophysical parameters for all our BSSs sample. We obtain $T_{\rm eff}$ from color–temperature relations; $T_{\rm eff}$, mass, luminosity and $\log(g)$ from isochrone–fittings; and $T_{\rm eff}$ and $\log(g)$ from XPP. We find a good agreement between measurements obtained through different methods. We provide these parameters for YSSs and RSSs as well.

5. Focusing on $T_{\rm eff}$ we find effective temperatures for BSSs $\langle T_{\rm BSS}\rangle = (6853 \pm 795)$ K from color–temperature relations and $\langle T_{\rm BSS}\rangle = (6900 \pm 687)$ K from isochrone–fitting for all our BSS sample. $T_{\rm eff}$ found in OC BSSs are $\langle T_{\rm BSS}\rangle = (7598 \pm 1476)$ K and $\langle T_{\rm BSS}\rangle = (7549 \pm 1331)$ K from color–temperature and isochrone–fitting methods, respectively. BSSs in GCs present $\langle T_{\rm BSS}\rangle = (6772 \pm 630)$ K derived from color–temperature relations and $\langle T_{\rm BSS}\rangle = (6829 \pm 529)$ K. Overall, the difference in $T_{\rm eff}$ found from isochrone–fittings are ~ 50 K hotter than those obtained from color–temperature relations. These values are in agreement with previous studies (Sindhu et al., 2019; Dattatrey et al., 2023).

6. Based on the isochrone–fitting method, we find the mass of all our BSSs to be, approximately, $\langle M_{\rm BSS}\rangle = (1.09 \pm 0.28)\ M_{\odot}$. In OCs, we find the mass of BSSs to be $\langle M_{\rm BSS}\rangle = (1.75 \pm 0.45)\ M_{\odot}$. For GCs we obtain a BSS mass around $\langle M_{\rm BSS}\rangle = (1.02 \pm 0.1)\ M_{\odot}$. Results for OCs are inferior to those found by Jadhav and Subramaniam (2021), but our results still their error range.Even so, masses in OCs are in agreement with binary simulations (Tian et al., 2006). GC BSS mass is slightly inferior to some HST-based studies such as Shara et al. (1997); Baldwin et al. (2016), but are in agreement with BSS mass measured to multiple GCs as well (Simunovic, 2017).

7. We observe that $\Delta T_{\rm eff}$, the difference between the BSS $T_{\rm eff}$ and $T_{\rm eff}$ corresponding to the MSTO (measured with the same method), decreases with the cluster age. We find these results for $T_{\rm eff}$ obtained with color–temperature relations and isochrone–fitting models. This means that the difference in temperature between the BSSs and the MSTO do change with the time; which is expected since BSSs are supposed to

be more massive MS stars than the MSTO and, therefore, they evolve to post-MS phases faster than those stars located around the MSTO –which are less massive compared to BSSs–. We find this trend for OCs and GCs. We also observe that the dispersion of BSSs of $\Delta T_{\rm eff}$ tends to decrease with the cluster age. We do not find this trend in GCs, where we had to applied a cut along the color axis (and hence, in the temperature) to avoid selecting much more evolved stars.

8. We follow the definition provided by Jadhav and Subramaniam (2021) for the "fractional mass excess", or $\mathcal{M}_{\rm e}$. This parameter is the difference between the BSS mass and the mass that corresponds to the MSTO –this last based on isochrone-fittings–, normalized by the MSTO mass. This parameter is roughly equal/proportional to the MT efficiency in a binary system. These authors classify $\mathcal{M}_{\rm e}$ in three (3) regimes; each regime giving hints about which could be the formation pathway for the BSS: i) low–$\mathcal{M}_{\rm e}$ ($\mathcal{M}_{\rm e} < 0.5$, likely to be formed via MT), high–$\mathcal{M}_{\rm e}$ ($0.5 < \mathcal{M}_{\rm e} < 1.0$, likely to be formed from mergers/collisions) and extreme–$\mathcal{M}_{\rm e}$ ($1.0 < \mathcal{M}_{\rm e} < 1.5$, likely to be multiple-MT systems.). In our sample, we do not find any (0%) extreme–$\mathcal{M}_{\rm e}$, where we explain this could be due to a bias error applied to our data since we skipped stars brighter than $G_{\rm BP} \sim 10$ –to avoid Gaia systematic errors– that could have been more massive. In all our sample, $\sim 7\%$ is classified as high–$\mathcal{M}_{\rm e}$ and 93% as low–$\mathcal{M}_{\rm e}$. For OCs this proportion is $\sim 81.34\%$ and $\sim 18.66\%$ for high–$\mathcal{M}_{\rm e}$ and low–$\mathcal{M}_{\rm e}$, respectively. For BSSs in GCs, we find these percentages to be $\sim 94.25\%$ for low–$\mathcal{M}_{\rm e}$ and $\sim 5.25\%$ for high–$\mathcal{M}_{\rm e}$. This suggest that, in summary, MT is the preferred formation method for BSSs; but OCs do present a higher fraction of BSSs that could have likely been formed through mergers compared to GC BSSs.

9. We do not find a clear trend for $\mathcal{M}_{\rm e}$ against the cluster age. These results are similar to those provided by Jadhav and Subramaniam (2021) for OCs.

10. For OCs we see that high–$\mathcal{M}_{\rm e}$ fraction decreases with the BSS age (obtained with isochrone–fittings). This means that, in OCs, older BSSs are more likely to be formed through MT. GCs showed a similar trend to that mentioned before, with the great exception that we find a "boost" in high–$\mathcal{M}_{\rm e}$ fraction around ~ 2 Gyr. This age is in

agreement with ages found from collisional isochrones that explain blue sequences of BSSs in clusters with a double sequence of BSSs (Simunovic et al., 2014; Dattatrey et al., 2023).

11. Finally, we observe a double sequence in $\mathcal{M}_e$ vs. $\log(\mathrm{Age}_{\mathrm{BSS}})$ in GCs: one corresponding to an "upper" sequence, with higher $\mathcal{M}_e$ along the BSS age; and another "lower" sequence, linked to smaller $\mathcal{M}_e$ along the BSS age. We plot BSSs labeled by their associated sequence, identified for OCs and GCs, along a CMD and we find a clear division between these branches; especially for GCs. BSSs located at the "upper" sequence are brighter than those located at the "lower" sequence. From binary-evolution perspective, the distance between the binaries could eventually decrease, the star receiving the material will gain mass but shorten its life and, hence, will appear as an "older" star in the isochrone tracks. Finally, we consider these "upper" and "lower" sequences as post-merger/closer-binary interaction and pre merger/closer-binary sequences.

Bibliography

J. Ahumada and E. Lapasset. Catalogue of blue stragglers in open clusters. , 109:375–382, Feb. 1995.

J. A. Ahumada and E. Lapasset. New catalogue of blue stragglers in open clusters. *Astronomy & Astrophysics*, 463(2):789–797, Feb. 2007. doi: 10.1051/0004-6361:20054590.

E. Alessandrini, B. Lanzoni, F. R. Ferraro, P. Miocchi, and E. Vesperini. Investigating the Mass Segregation Process in Globular Clusters with Blue Straggler Stars: The Impact of Dark Remnants. *The American Astronomical Society*, 833(2):252, Dec. 2016. doi: 10.3847/1538-4357/833/2/252.

R. Andrae, M. Fouesneau, R. Sordo, C. A. L. Bailer-Jones, T. E. Dharmawardena, J. Rybizki, F. De Angeli, H. E. P. Lindstrøm, D. J. Marshall, R. Drimmel, A. J. Korn, C. Soubiran, N. Brouillet, L. Casamiquela, H. W. Rix, A. Abreu Aramburu, M. A. Álvarez, J. Bakker, I. Bellas-Velidis, A. Bijaoui, E. Brugaletta, A. Burlacu, R. Carballo, L. Chaoul, A. Chiavassa, G. Contursi, W. J. Cooper, O. L. Creevey, C. Dafonte, A. Dapergolas, P. de Laverny, L. Delchambre, C. Demouchy, B. Edvardsson, Y. Frémat, D. Garabato, P. García-Lario, M. García-Torres, A. Gavel, A. Gomez, I. González-Santamaría, D. Hatzidimitriou, U. Heiter, A. Jean-Antoine Piccolo, M. Kontizas, G. Kordopatis, A. C. Lanzafame, Y. Lebreton, E. L. Licata, E. Livanou, A. Lobel, A. Lorca, A. Magdaleno Romeo, M. Manteiga, F. Marocco, N. Mary, C. Nicolas, C. Ordenovic, F. Pailler, P. A. Palicio, L. Pallas-Quintela, C. Panem, B. Pichon, E. Poggio, A. Recio-Blanco, F. Riclet, C. Robin, R. Santoveña, L. M. Sarro, M. S. Schultheis, M. Segol, A. Silvelo, I. Slezak, R. L. Smart, M. Süveges, F. Thévenin, G. Torralba Elipe, A. Ulla,

E. Utrilla, A. Vallenari, E. van Dillen, H. Zhao, and J. Zorec. Gaia Data Release 3. Analysis of the Gaia BP/RP spectra using the General Stellar Parameterizer from Photometry. *Astronomy & Astrophysics*, 674:A27, June 2023. doi: 10.1051/0004-6361/202243462.

H. C. Arp and F. D. A. Hartwick. A Photometric Study of the Metal-Rich Globular Cluster M71. *The American Astronomical Society*, 167:499, Aug. 1971. doi: 10.1086/151047.

A. T. Baldwin, L. L. Watkins, R. P. van der Marel, P. Bianchini, A. Bellini, and J. Anderson. Hubble Space Telescope Proper Motion (HSTPROMO) Catalogs of Galactic Globular Clusters. IV. Kinematic Profiles and Average Masses of Blue Straggler Stars. *The American Astronomical Society*, 827(1):12, Aug. 2016. doi: 10.3847/0004-637X/827/1/12.

H. Baumgardt and E. Vasiliev. Accurate distances to Galactic globular clusters through a combination of Gaia EDR3, HST, and literature data. *Monthly Notices of the Royal Astronomical Society*, 505(4):5957–5977, Aug. 2021. doi: 10.1093/mnras/stab1474.

H. Baumgardt, V. Hénault-Brunet, N. Dickson, and A. Sollima. Evidence for a bottom-light initial mass function in massive star clusters. *Monthly Notices of the Royal Astronomical Society*, 521(3):3991–4008, May 2023. doi: 10.1093/mnras/stad631.

G. Beccari, F. R. Ferraro, E. Dalessandro, B. Lanzoni, S. Raso, L. Origlia, E. Vesperini, J. Hong, A. Sills, A. Dieball, and C. Knigge. Discovery of a Double Blue Straggler Sequence in M15: New Insight into the Core-collapse Process. *The American Astronomical Society*, 876(1):87, May 2019. doi: 10.3847/1538-4357/ab13a4.

H. E. Bond and D. J. MacConnell. The Nature of the Field Blue-Straggler Stars. *The American Astronomical Society*, 165:51, Apr. 1971. doi: 10.1086/150875.

A. Bressan, P. Marigo, L. Girardi, B. Salasnich, C. Dal Cero, S. Rubele, and A. Nanni. PARSEC: stellar tracks and isochrones with the PAdova and TRieste Stellar Evolution Code. *Monthly Notices of the Royal Astronomical Society*, 427(1):127–145, Nov. 2012. doi: 10.1111/j.1365-2966.2012.21948.x.

E. M. Burbidge and A. Sandage. The Color-Magnitude Diagram for the Galactic NGC 7789. *The American Astronomical Society*, 128:174, Sept. 1958. doi: 10.1086/146535.

T. Cantat-Gaudin and F. Anders. Clusters and mirages: cataloguing stellar aggregates in the Milky Way. *Astronomy & Astrophysics*, 633:A99, Jan. 2020. doi: 10.1051/0004-6361/201936691.

T. Cantat-Gaudin, C. Jordi, A. Vallenari, A. Bragaglia, L. Balaguer-Núñez, C. Soubiran, D. Bossini, A. Moitinho, A. Castro-Ginard, A. Krone-Martins, L. Casamiquela, R. Sordo, and R. Carrera. A Gaia DR2 view of the open cluster population in the Milky Way. *Astronomy & Astrophysics*, 618:A93, Oct. 2018. doi: 10.1051/0004-6361/201833476.

T. Cantat-Gaudin, F. Anders, A. Castro-Ginard, C. Jordi, M. Romero-Gómez, C. Soubiran, L. Casamiquela, Y. Tarricq, A. Moitinho, A. Vallenari, A. Bragaglia, A. Krone-Martins, and M. Kounkel. Painting a portrait of the Galactic disc with its stellar clusters. *Astronomy & Astrophysics*, 640:A1, Aug. 2020. doi: 10.1051/0004-6361/202038192.

J. A. Cardelli, G. C. Clayton, and J. S. Mathis. The Relationship between Infrared, Optical, and Ultraviolet Extinction. *The American Astronomical Society*, 345:245, Oct. 1989. doi: 10.1086/167900.

E. Carretta, A. Bragaglia, R. Gratton, V. D'Orazi, and S. Lucatello. Intrinsic iron spread and a new metallicity scale for globular clusters. *Astronomy & Astrophysics*, 508(2): 695–706, Dec. 2009. doi: 10.1051/0004-6361/200913003.

R. Contreras Ramos, F. R. Ferraro, E. Dalessandro, B. Lanzoni, and R. T. Rood. The Unimodal Distribution of Blue Straggler Stars in M75 (NGC 6864). *The American Astronomical Society*, 748(2):91, Apr. 2012. doi: 10.1088/0004-637X/748/2/91.

G. Cordoni, A. P. Milone, A. F. Marino, M. Di Criscienzo, F. D'Antona, A. Dotter, E. P. Lagioia, and M. Tailo. Extended Main-sequence Turnoff as a Common Feature of Milky Way Open Clusters. *The American Astronomical Society*, 869(2):139, Dec. 2018. doi: 10.3847/1538-4357/aaedc1.

G. Cordoni, A. P. Milone, A. F. Marino, E. Vesperini, E. Dondoglio, M. V. Legnardi, A. Mohandasan, M. Carlos, E. P. Lagioia, S. Jang, and T. Ziliotto. Photometric binaries, mass functions, and structural parameters of 78 Galactic open clusters. *Astronomy & Astrophysics*, 672:A29, Apr. 2023. doi: 10.1051/0004-6361/202245457.

G. S. Da Costa. The age (s?) of the Sculptor dwarf galaxy. *The American Astronomical Society*, 285:483–494, Oct. 1984. doi: 10.1086/162523.

E. Dalessandro, F. R. Ferraro, D. Massari, B. Lanzoni, P. Miocchi, G. Beccari, A. Bellini, A. Sills, S. Sigurdsson, A. Mucciarelli, and L. Lovisi. Double Blue Straggler Sequences in Globular Clusters: The Case of NGC 362. *The American Astronomical Society*, 778 (2):135, Dec. 2013. doi: 10.1088/0004-637X/778/2/135.

A. K. Dattatrey, R. K. S. Yadav, S. Rani, A. Subramaniam, G. Singh, S. Sahu, and R. S. Singh. GlobULeS. IV. UVIT/AstroSat Detection of Extremely Low Mass White Dwarf Companions to Blue Straggler Stars in NGC 362. *The American Astronomical Society*, 943(2):130, Feb. 2023. doi: 10.3847/1538-4357/acade0.

F. De Angeli, M. Weiler, P. Montegriffo, D. W. Evans, M. Riello, R. Andrae, J. M. Carrasco, G. Busso, P. W. Burgess, C. Cacciari, M. Davidson, D. L. Harrison, S. T. Hodgkin, C. Jordi, P. J. Osborne, E. Pancino, G. Altavilla, M. A. Barstow, C. A. L. Bailer-Jones, M. Bellazzini, A. G. A. Brown, M. Castellani, S. Cowell, L. Delchambre, F. De Luise, C. Diener, C. Fabricius, M. Fouesneau, Y. Frémat, G. Gilmore, G. Giuffrida, N. C. Hambly, S. Hidalgo, G. Holland, Z. Kostrzewa-Rutkowska, F. van Leeuwen, A. Lobel, S. Marinoni, N. Miller, C. Pagani, L. Palaversa, A. M. Piersimoni, L. Pulone, S. Ragaini, M. Rainer, P. J. Richards, G. T. Rixon, D. Ruz-Mieres, N. Sanna, L. M. Sarro, N. Rowell, R. Sordo, N. A. Walton, and A. Yoldas. Gaia Data Release 3. Processing and validation of BP/RP low-resolution spectral data. *Astronomy & Astrophysics*, 674:A2, June 2023. doi: 10.1051/0004-6361/202243680.

W. S. Dias, H. Monteiro, A. Moitinho, J. R. D. Lépine, G. Carraro, E. Paunzen, B. Alessi, and L. Villela. Updated parameters of 1743 open clusters based on Gaia DR2. *Monthly*

Notices of the Royal Astronomical Society, 504(1):356–371, June 2021. doi: 10.1093/mnras/stab770.

O. J. Eggen and A. R. Sandage. New photoelectric observations of stars in the old galactic cluster M 67. *The American Astronomical Society*, 140:130–143, July 1964. doi: 10.1086/147901.

D. W. Evans, M. Riello, F. De Angeli, J. M. Carrasco, P. Montegriffo, C. Fabricius, C. Jordi, L. Palaversa, C. Diener, G. Busso, C. Cacciari, F. van Leeuwen, P. W. Burgess, M. Davidson, D. L. Harrison, S. T. Hodgkin, E. Pancino, P. J. Richards, G. Altavilla, L. Balaguer-Núñez, M. A. Barstow, M. Bellazzini, A. G. A. Brown, M. Castellani, G. Cocozza, F. De Luise, A. Delgado, C. Ducourant, S. Galleti, G. Gilmore, G. Giuffrida, B. Holl, A. Kewley, S. E. Koposov, S. Marinoni, P. M. Marrese, P. J. Osborne, A. Piersimoni, J. Portell, L. Pulone, S. Ragaini, N. Sanna, D. Terrett, N. A. Walton, T. Wevers, and Ł. Wyrzykowski. Gaia Data Release 2. Photometric content and validation. *Astronomy & Astrophysics*, 616:A4, Aug. 2018. doi: 10.1051/0004-6361/201832756.

C. Fabricius, X. Luri, F. Arenou, C. Babusiaux, A. Helmi, T. Muraveva, C. Reylé, F. Spoto, A. Vallenari, T. Antoja, E. Balbinot, C. Barache, N. Bauchet, A. Bragaglia, D. Busonero, T. Cantat-Gaudin, J. M. Carrasco, S. Diakité, M. Fabrizio, F. Figueras, A. Garcia-Gutierrez, A. Garofalo, C. Jordi, P. Kervella, S. Khanna, N. Leclerc, E. Licata, S. Lambert, P. M. Marrese, A. Masip, P. Ramos, N. Robichon, A. C. Robin, M. Romero-Gómez, S. Rubele, and M. Weiler. Gaia Early Data Release 3. Catalogue validation. *Astronomy & Astrophysics*, 649:A5, May 2021. doi: 10.1051/0004-6361/202039834.

F. R. Ferraro, B. Paltrinieri, F. Fusi Pecci, C. Cacciari, B. Dorman, R. T. Rood, R. Buonanno, C. E. Corsi, D. Burgarella, and M. Laget. HST observations of blue Straggler stars in the core of the globular cluster M 3. *Astronomy & Astrophysics*, 324:915–928, Aug. 1997. doi: 10.48550/arXiv.astro-ph/9703026.

F. R. Ferraro, N. D'Amico, A. Possenti, R. P. Mignani, and B. Paltrinieri. Blue Stragglers, Young White Dwarfs, and UV-Excess Stars in the Core of 47 Tucanae. *The American Astronomical Society*, 561(1):337–345, Nov. 2001. doi: 10.1086/322773.

F. R. Ferraro, G. Beccari, E. Dalessandro, B. Lanzoni, A. Sills, R. T. Rood, F. F. Pecci, A. I. Karakas, P. Miocchi, and S. Bovinelli. Two distinct sequences of blue straggler stars in the globular cluster M 30. , 462(7276):1028–1031, Dec. 2009. doi: 10.1038/nature08607.

F. R. Ferraro, B. Lanzoni, E. Dalessandro, G. Beccari, M. Pasquato, P. Miocchi, R. T. Rood, S. Sigurdsson, A. Sills, E. Vesperini, M. Mapelli, R. Contreras, N. Sanna, and A. Mucciarelli. Dynamical age differences among coeval star clusters as revealed by blue stragglers. , 492(7429):393–395, Dec. 2012. doi: 10.1038/nature11686.

F. R. Ferraro, B. Lanzoni, S. Raso, D. Nardiello, E. Dalessandro, E. Vesperini, G. Piotto, C. Pallanca, G. Beccari, A. Bellini, M. Libralato, J. Anderson, A. Aparicio, L. R. Bedin, S. Cassisi, A. P. Milone, S. Ortolani, A. Renzini, M. Salaris, and R. P. van der Marel. The Hubble Space Telescope UV Legacy Survey of Galactic Globular Clusters. XV. The Dynamical Clock: Reading Cluster Dynamical Evolution from the Segregation Level of Blue Straggler Stars. *The American Astronomical Society*, 860(1):36, June 2018. doi: 10.3847/1538-4357/aac01c.

F. R. Ferraro, B. Lanzoni, E. Vesperini, M. Cadelano, D. Deras, and C. Pallanca. Empirical Measurement of the Dynamical Ages of Three Globular Clusters and Some Considerations on the Use of the Dynamical Clock. *The American Astronomical Society*, 950(2): 145, June 2023. doi: 10.3847/1538-4357/accd5c.

G. Fiorentino, B. Lanzoni, E. Dalessandro, F. R. Ferraro, G. Bono, and M. Marconi. Blue Straggler Masses from Pulsation Properties. I. The Case of NGC 6541. *The American Astronomical Society*, 783(1):34, Mar. 2014. doi: 10.1088/0004-637X/783/1/34.

F. Fusi Pecci, F. R. Ferraro, and C. Cacciari. Blue Stragglers in Galactic Globular Clusters: A Revised Catalog, the Special Case of M3; and Some General Remarks. In R. A. Saffer, editor, *Blue Stragglers*, volume 53 of *Astronomical Society of the Pacific Conference Series*, page 97, Jan. 1993.

Gaia Collaboration, T. Prusti, J. H. J. de Bruijne, A. G. A. Brown, A. Vallenari, C. Babusiaux, C. A. L. Bailer-Jones, U. Bastian, M. Biermann, D. W. Evans, L. Eyer, F. Jansen,

C. Jordi, S. A. Klioner, U. Lammers, L. Lindegren, X. Luri, F. Mignard, D. J. Milligan, C. Panem, V. Poinsignon, D. Pourbaix, S. Randich, G. Sarri, P. Sartoretti, H. I. Siddiqui, C. Soubiran, V. Valette, F. van Leeuwen, N. A. Walton, C. Aerts, F. Arenou, M. Cropper, R. Drimmel, E. Høg, D. Katz, M. G. Lattanzi, W. O'Mullane, E. K. Grebel, A. D. Holland, C. Huc, X. Passot, L. Bramante, C. Cacciari, J. Castañeda, L. Chaoul, N. Cheek, F. De Angeli, C. Fabricius, R. Guerra, J. Hernández, A. Jean-Antoine-Piccolo, E. Masana, R. Messineo, N. Mowlavi, K. Nienartowicz, D. Ordóñez-Blanco, P. Panuzzo, J. Portell, P. J. Richards, M. Riello, G. M. Seabroke, P. Tanga, F. Thévenin, J. Torra, S. G. Els, G. Gracia-Abril, G. Comoretto, M. Garcia-Reinaldos, T. Lock, E. Mercier, M. Altmann, R. Andrae, T. L. Astraatmadja, I. Bellas-Velidis, K. Benson, J. Berthier, R. Blomme, G. Busso, B. Carry, A. Cellino, G. Clementini, S. Cowell, O. Creevey, J. Cuypers, M. Davidson, J. De Ridder, A. de Torres, L. Delchambre, A. Dell'Oro, C. Ducourant, Y. Frémat, M. García-Torres, E. Gosset, J. L. Halbwachs, N. C. Hambly, D. L. Harrison, M. Hauser, D. Hestroffer, S. T. Hodgkin, H. E. Huckle, A. Hutton, G. Jasniewicz, S. Jordan, M. Kontizas, A. J. Korn, A. C. Lanzafame, M. Manteiga, A. Moitinho, K. Muinonen, J. Osinde, E. Pancino, T. Pauwels, J. M. Petit, A. Recio-Blanco, A. C. Robin, L. M. Sarro, C. Siopis, M. Smith, K. W. Smith, A. Sozzetti, W. Thuillot, W. van Reeven, Y. Viala, U. Abbas, A. Abreu Aramburu, S. Accart, J. J. Aguado, P. M. Allan, W. Allasia, G. Altavilla, M. A. Álvarez, J. Alves, R. I. Anderson, A. H. Andrei, E. Anglada Varela, E. Antiche, T. Antoja, S. Antón, B. Arcay, A. Atzei, L. Ayache, N. Bach, S. G. Baker, L. Balaguer-Núñez, C. Barache, C. Barata, A. Barbier, F. Barblan, M. Baroni, D. Barrado y Navascués, M. Barros, M. A. Barstow, U. Becciani, M. Bellazzini, G. Bellei, A. Bello García, V. Belokurov, P. Bendjoya, A. Berihuete, L. Bianchi, O. Bienaymé, F. Billebaud, N. Blagorodnova, S. Blanco-Cuaresma, T. Boch, A. Bombrun, R. Borrachero, S. Bouquillon, G. Bourda, H. Bouy, A. Bragaglia, M. A. Breddels, N. Brouillet, T. Brüsemeister, B. Bucciarelli, F. Budnik, P. Burgess, R. Burgon, A. Burlacu, D. Busonero, R. Buzzi, E. Caffau, J. Cambras, H. Campbell, R. Cancelliere, T. Cantat-Gaudin, T. Carlucci, J. M. Carrasco, M. Castellani, P. Charlot, J. Charnas, P. Charvet, F. Chassat, A. Chiavassa, M. Clotet, G. Cocozza, R. S. Collins, P. Collins, G. Costigan, F. Crifo, N. J. G. Cross, M. Crosta, C. Crowley, C. Dafonte,

Y. Damerdji, A. Dapergolas, P. David, M. David, P. De Cat, F. de Felice, P. de Laverny, F. De Luise, R. De March, D. de Martino, R. de Souza, J. Debosscher, E. del Pozo, M. Delbo, A. Delgado, H. E. Delgado, F. di Marco, P. Di Matteo, S. Diakite, E. Distefano, C. Dolding, S. Dos Anjos, P. Drazinos, J. Durán, Y. Dzigan, E. Ecale, B. Edvardsson, H. Enke, M. Erdmann, D. Escolar, M. Espina, N. W. Evans, G. Eynard Bontemps, C. Fabre, M. Fabrizio, S. Faigler, A. J. Falcão, M. Farràs Casas, F. Faye, L. Federici, G. Fedorets, J. Fernández-Hernández, P. Fernique, A. Fienga, F. Figueras, F. Filippi, K. Findeisen, A. Fonti, M. Fouesneau, E. Fraile, M. Fraser, J. Fuchs, R. Furnell, M. Gai, S. Galleti, L. Galluccio, D. Garabato, F. García-Sedano, P. Garé, A. Garofalo, N. Garralda, P. Gavras, J. Gerssen, R. Geyer, G. Gilmore, S. Girona, G. Giuffrida, M. Gomes, A. González-Marcos, J. González-Núñez, J. J. González-Vidal, M. Granvik, A. Guerrier, P. Guillout, J. Guiraud, A. Gúrpide, R. Gutiérrez-Sánchez, L. P. Guy, R. Haigron, D. Hatzidimitriou, M. Haywood, U. Heiter, A. Helmi, D. Hobbs, W. Hofmann, B. Holl, G. Holland, J. A. S. Hunt, A. Hypki, V. Icardi, M. Irwin, G. Jevardat de Fombelle, P. Jofré, P. G. Jonker, A. Jorissen, F. Julbe, A. Karampelas, A. Kochoska, R. Kohley, K. Kolenberg, E. Kontizas, S. E. Koposov, G. Kordopatis, P. Koubsky, A. Kowalczyk, A. Krone-Martins, M. Kudryashova, I. Kull, R. K. Bachchan, F. Lacoste-Seris, A. F. Lanza, J. B. Lavigne, C. Le Poncin-Lafitte, Y. Lebreton, T. Lebzelter, S. Leccia, N. Leclerc, I. Lecoeur-Taibi, V. Lemaitre, H. Lenhardt, F. Leroux, S. Liao, E. Licata, H. E. P. Lindstrøm, T. A. Lister, E. Livanou, A. Lobel, W. Löffler, M. López, A. Lopez-Lozano, D. Lorenz, T. Loureiro, I. MacDonald, T. Magalhães Fernandes, S. Managau, R. G. Mann, G. Mantelet, O. Marchal, J. M. Marchant, M. Marconi, J. Marie, S. Marinoni, P. M. Marrese, G. Marschalkó, D. J. Marshall, J. M. Martín-Fleitas, M. Martino, N. Mary, G. Matijevič, T. Mazeh, P. J. McMillan, S. Messina, A. Mestre, D. Michalik, N. R. Millar, B. M. H. Miranda, D. Molina, R. Molinaro, M. Molinaro, L. Molnár, M. Moniez, P. Montegriffo, D. Monteiro, R. Mor, A. Mora, R. Morbidelli, T. Morel, S. Morgenthaler, T. Morley, D. Morris, A. F. Mulone, T. Muraveva, I. Musella, J. Narbonne, G. Nelemans, L. Nicastro, L. Noval, C. Ordénovic, J. Ordieres-Meré, P. Osborne, C. Pagani, I. Pagano, F. Pailler, H. Palacin, L. Palaversa, P. Parsons, T. Paulsen, M. Pecoraro, R. Pedrosa, H. Pentikäinen, J. Pereira, B. Pichon, A. M. Piersimoni, F. X. Pineau,

E. Plachy, G. Plum, E. Poujoulet, A. Prša, L. Pulone, S. Ragaini, S. Rago, N. Rambaux, M. Ramos-Lerate, P. Ranalli, G. Rauw, A. Read, S. Regibo, F. Renk, C. Reylé, R. A. Ribeiro, L. Rimoldini, V. Ripepi, A. Riva, G. Rixon, M. Roelens, M. Romero-Gómez, N. Rowell, F. Royer, A. Rudolph, L. Ruiz-Dern, G. Sadowski, T. Sagristà Sellés, J. Sahlmann, J. Salgado, E. Salguero, M. Sarasso, H. Savietto, A. Schnorhk, M. Schultheis, E. Sciacca, M. Segol, J. C. Segovia, D. Segransan, E. Serpell, I. C. Shih, R. Smareglia, R. L. Smart, C. Smith, E. Solano, F. Solitro, R. Sordo, S. Soria Nieto, J. Souchay, A. Spagna, F. Spoto, U. Stampa, I. A. Steele, H. Steidelmüller, C. A. Stephenson, H. Stoev, F. F. Suess, M. Süveges, J. Surdej, L. Szabados, E. Szegedi-Elek, D. Tapiador, F. Taris, G. Tauran, M. B. Taylor, R. Teixeira, D. Terrett, B. Tingley, S. C. Trager, C. Turon, A. Ulla, E. Utrilla, G. Valentini, A. van Elteren, E. Van Hemelryck, M. van Leeuwen, M. Varadi, A. Vecchiato, J. Veljanoski, T. Via, D. Vicente, S. Vogt, H. Voss, V. Votruba, S. Voutsinas, G. Walmsley, M. Weiler, K. Weingrill, D. Werner, T. Wevers, G. Whitehead, Ł. Wyrzykowski, A. Yoldas, M. Žerjal, S. Zucker, C. Zurbach, T. Zwitter, A. Alecu, M. Allen, C. Allende Prieto, A. Amorim, G. Anglada-Escudé, V. Arsenijevic, S. Azaz, P. Balm, M. Beck, H. H. Bernstein, L. Bigot, A. Bijaoui, C. Blasco, M. Bonfigli, G. Bono, S. Boudreault, A. Bressan, S. Brown, P. M. Brunet, P. Bunclark, R. Buonanno, A. G. Butkevich, C. Carret, C. Carrion, L. Chemin, F. Chéreau, L. Corcione, E. Darmigny, K. S. de Boer, P. de Teodoro, P. T. de Zeeuw, C. Delle Luche, C. D. Domingues, P. Dubath, F. Fodor, B. Frézouls, A. Fries, D. Fustes, D. Fyfe, E. Gallardo, J. Gallegos, D. Gardiol, M. Gebran, A. Gomboc, A. Gómez, E. Grux, A. Gueguen, A. Heyrovsky, J. Hoar, G. Iannicola, Y. Isasi Parache, A. M. Janotto, E. Joliet, A. Jonckheere, R. Keil, D. W. Kim, P. Klagyivik, J. Klar, J. Knude, O. Kochukhov, I. Kolka, J. Kos, A. Kutka, V. Lainey, D. LeBouquin, C. Liu, D. Loreggia, V. V. Makarov, M. G. Marseille, C. Martayan, O. Martinez-Rubi, B. Massart, F. Meynadier, S. Mignot, U. Munari, A. T. Nguyen, T. Nordlander, P. Ocvirk, K. S. O'Flaherty, A. Olias Sanz, P. Ortiz, J. Osorio, D. Oszkiewicz, A. Ouzounis, M. Palmer, P. Park, E. Pasquato, C. Peltzer, J. Peralta, F. Péturaud, T. Pieniluoma, E. Pigozzi, J. Poels, G. Prat, T. Prod'homme, F. Raison, J. M. Rebordao, D. Risquez, B. Rocca-Volmerange, S. Rosen, M. I. Ruiz-Fuertes, F. Russo, S. Sembay, I. Serraller Vizcaino,

A. Short, A. Siebert, H. Silva, D. Sinachopoulos, E. Slezak, M. Soffel, D. Sosnowska, V. Straižys, M. ter Linden, D. Terrell, S. Theil, C. Tiede, L. Troisi, P. Tsalmantza, D. Tur, M. Vaccari, F. Vachier, P. Valles, W. Van Hamme, L. Veltz, J. Virtanen, J. M. Wallut, R. Wichmann, M. I. Wilkinson, H. Ziaeepour, and S. Zschocke. The Gaia mission. *Astronomy & Astrophysics*, 595:A1, Nov. 2016. doi: 10.1051/0004-6361/201629272.

Gaia Collaboration, A. G. A. Brown, A. Vallenari, T. Prusti, J. H. J. de Bruijne, C. Babusiaux, C. A. L. Bailer-Jones, M. Biermann, D. W. Evans, L. Eyer, F. Jansen, C. Jordi, S. A. Klioner, U. Lammers, L. Lindegren, X. Luri, F. Mignard, C. Panem, D. Pourbaix, S. Randich, P. Sartoretti, H. I. Siddiqui, C. Soubiran, F. van Leeuwen, N. A. Walton, F. Arenou, U. Bastian, M. Cropper, R. Drimmel, D. Katz, M. G. Lattanzi, J. Bakker, C. Cacciari, J. Castañeda, L. Chaoul, N. Cheek, F. De Angeli, C. Fabricius, R. Guerra, B. Holl, E. Masana, R. Messineo, N. Mowlavi, K. Nienartowicz, P. Panuzzo, J. Portell, M. Riello, G. M. Seabroke, P. Tanga, F. Thévenin, G. Gracia-Abril, G. Comoretto, M. Garcia-Reinaldos, D. Teyssier, M. Altmann, R. Andrae, M. Audard, I. Bellas-Velidis, K. Benson, J. Berthier, R. Blomme, P. Burgess, G. Busso, B. Carry, A. Cellino, G. Clementini, M. Clotet, O. Creevey, M. Davidson, J. De Ridder, L. Delchambre, A. Dell'Oro, C. Ducourant, J. Fernández-Hernández, M. Fouesneau, Y. Frémat, L. Galluccio, M. García-Torres, J. González-Núñez, J. J. González-Vidal, E. Gosset, L. P. Guy, J. L. Halbwachs, N. C. Hambly, D. L. Harrison, J. Hernández, D. Hestroffer, S. T. Hodgkin, A. Hutton, G. Jasniewicz, A. Jean-Antoine-Piccolo, S. Jordan, A. J. Korn, A. Krone-Martins, A. C. Lanzafame, T. Lebzelter, W. Löffler, M. Manteiga, P. M. Marrese, J. M. Martín-Fleitas, A. Moitinho, A. Mora, K. Muinonen, J. Osinde, E. Pancino, T. Pauwels, J. M. Petit, A. Recio-Blanco, P. J. Richards, L. Rimoldini, A. C. Robin, L. M. Sarro, C. Siopis, M. Smith, A. Sozzetti, M. Süveges, J. Torra, W. van Reeven, U. Abbas, A. Abreu Aramburu, S. Accart, C. Aerts, G. Altavilla, M. A. Álvarez, R. Alvarez, J. Alves, R. I. Anderson, A. H. Andrei, E. Anglada Varela, E. Antiche, T. Antoja, B. Arcay, T. L. Astraatmadja, N. Bach, S. G. Baker, L. Balaguer-Núñez, P. Balm, C. Barache, C. Barata, D. Barbato, F. Barblan, P. S. Barklem, D. Barrado, M. Barros, M. A. Barstow, S. Bartholomé Muñoz, J. L. Bassilana, U. Becciani, M. Bellazzini, A. Berihuete, S. Bertone, L. Bianchi, O. Bienaymé, S. Blanco-Cuaresma, T. Boch, C. Boeche, A. Bom-

brun, R. Borrachero, D. Bossini, S. Bouquillon, G. Bourda, A. Bragaglia, L. Bramante, M. A. Breddels, A. Bressan, N. Brouillet, T. Brüsemeister, E. Brugaletta, B. Bucciarelli, A. Burlacu, D. Busonero, A. G. Butkevich, R. Buzzi, E. Caffau, R. Cancelliere, G. Cannizzaro, T. Cantat-Gaudin, R. Carballo, T. Carlucci, J. M. Carrasco, L. Casamiquela, M. Castellani, A. Castro-Ginard, P. Charlot, L. Chemin, A. Chiavassa, G. Cocozza, G. Costigan, S. Cowell, F. Crifo, M. Crosta, C. Crowley, J. Cuypers, C. Dafonte, Y. Damerdji, A. Dapergolas, P. David, M. David, P. de Laverny, F. De Luise, R. De March, D. de Martino, R. de Souza, A. de Torres, J. Debosscher, E. del Pozo, M. Delbo, A. Delgado, H. E. Delgado, P. Di Matteo, S. Diakite, C. Diener, E. Distefano, C. Dolding, P. Drazinos, J. Durán, B. Edvardsson, H. Enke, K. Eriksson, P. Esquej, G. Eynard Bontemps, C. Fabre, M. Fabrizio, S. Faigler, A. J. Falcão, M. Farràs Casas, L. Federici, G. Fedorets, P. Fernique, F. Figueras, F. Filippi, K. Findeisen, A. Fonti, E. Fraile, M. Fraser, B. Frézouls, M. Gai, S. Galleti, D. Garabato, F. García-Sedano, A. Garofalo, N. Garralda, A. Gavel, P. Gavras, J. Gerssen, R. Geyer, P. Giacobbe, G. Gilmore, S. Girona, G. Giuffrida, F. Glass, M. Gomes, M. Granvik, A. Gueguen, A. Guerrier, J. Guiraud, R. Gutiérrez-Sánchez, R. Haigron, D. Hatzidimitriou, M. Hauser, M. Haywood, U. Heiter, A. Helmi, J. Heu, T. Hilger, D. Hobbs, W. Hofmann, G. Holland, H. E. Huckle, A. Hypki, V. Icardi, K. Janßen, G. Jevardat de Fombelle, P. G. Jonker, Á. L. Juhász, F. Julbe, A. Karampelas, A. Kewley, J. Klar, A. Kochoska, R. Kohley, K. Kolenberg, M. Kontizas, E. Kontizas, S. E. Koposov, G. Kordopatis, Z. Kostrzewa-Rutkowska, P. Koubsky, S. Lambert, A. F. Lanza, Y. Lasne, J. B. Lavigne, Y. Le Fustec, C. Le Poncin-Lafitte, Y. Lebreton, S. Leccia, N. Leclerc, I. Lecoeur-Taibi, H. Lenhardt, F. Leroux, S. Liao, E. Licata, H. E. P. Lindstrøm, T. A. Lister, E. Livanou, A. Lobel, M. López, S. Managau, R. G. Mann, G. Mantelet, O. Marchal, J. M. Marchant, M. Marconi, S. Marinoni, G. Marschalkó, D. J. Marshall, M. Martino, G. Marton, N. Mary, D. Massari, G. Matijevič, T. Mazeh, P. J. McMillan, S. Messina, D. Michalik, N. R. Millar, D. Molina, R. Molinaro, L. Molnár, P. Montegriffo, R. Mor, R. Morbidelli, T. Morel, D. Morris, A. F. Mulone, T. Muraveva, I. Musella, G. Nelemans, L. Nicastro, L. Noval, W. O'Mullane, C. Ordénovic, D. Ordóñez-Blanco, P. Osborne, C. Pagani, I. Pagano, F. Pailler, H. Palacin, L. Palaversa, A. Panahi, M. Pawlak, A. M. Piersimoni, F. X.

Pineau, E. Plachy, G. Plum, E. Poggio, E. Poujoulet, A. Prša, L. Pulone, E. Racero, S. Ragaini, N. Rambaux, M. Ramos-Lerate, S. Regibo, C. Reylé, F. Riclet, V. Ripepi, A. Riva, A. Rivard, G. Rixon, T. Roegiers, M. Roelens, M. Romero-Gómez, N. Rowell, F. Royer, L. Ruiz-Dern, G. Sadowski, T. Sagristà Sellés, J. Sahlmann, J. Salgado, E. Salguero, N. Sanna, T. Santana-Ros, M. Sarasso, H. Savietto, M. Schultheis, E. Sciacca, M. Segol, J. C. Segovia, D. Ségransan, I. C. Shih, L. Siltala, A. F. Silva, R. L. Smart, K. W. Smith, E. Solano, F. Solitro, R. Sordo, S. Soria Nieto, J. Souchay, A. Spagna, F. Spoto, U. Stampa, I. A. Steele, H. Steidelmüller, C. A. Stephenson, H. Stoev, F. F. Suess, J. Surdej, L. Szabados, E. Szegedi-Elek, D. Tapiador, F. Taris, G. Tauran, M. B. Taylor, R. Teixeira, D. Terrett, P. Teyssandier, W. Thuillot, A. Titarenko, F. Torra Clotet, C. Turon, A. Ulla, E. Utrilla, S. Uzzi, M. Vaillant, G. Valentini, V. Valette, A. van Elteren, E. Van Hemelryck, M. van Leeuwen, M. Vaschetto, A. Vecchiato, J. Veljanoski, Y. Viala, D. Vicente, S. Vogt, C. von Essen, H. Voss, V. Votruba, S. Voutsinas, G. Walmsley, M. Weiler, O. Wertz, T. Wevers, Ł. Wyrzykowski, A. Yoldas, M. Žerjal, H. Ziaeepour, J. Zorec, S. Zschocke, S. Zucker, C. Zurbach, and T. Zwitter. Gaia Data Release 2. Summary of the contents and survey properties. *Astronomy & Astrophysics*, 616:A1, Aug. 2018. doi: 10.1051/0004-6361/201833051.

Gaia Collaboration, A. G. A. Brown, A. Vallenari, T. Prusti, J. H. J. de Bruijne, C. Babusiaux, M. Biermann, O. L. Creevey, D. W. Evans, L. Eyer, A. Hutton, F. Jansen, C. Jordi, S. A. Klioner, U. Lammers, L. Lindegren, X. Luri, F. Mignard, C. Panem, D. Pourbaix, S. Randich, P. Sartoretti, C. Soubiran, N. A. Walton, F. Arenou, C. A. L. Bailer-Jones, U. Bastian, M. Cropper, R. Drimmel, D. Katz, M. G. Lattanzi, F. van Leeuwen, J. Bakker, C. Cacciari, J. Castañeda, F. De Angeli, C. Ducourant, C. Fabricius, M. Fouesneau, Y. Frémat, R. Guerra, A. Guerrier, J. Guiraud, A. Jean-Antoine Piccolo, E. Masana, R. Messineo, N. Mowlavi, C. Nicolas, K. Nienartowicz, F. Pailler, P. Panuzzo, F. Riclet, W. Roux, G. M. Seabroke, R. Sordo, P. Tanga, F. Thévenin, G. Gracia-Abril, J. Portell, D. Teyssier, M. Altmann, R. Andrae, I. Bellas-Velidis, K. Benson, J. Berthier, R. Blomme, E. Brugaletta, P. W. Burgess, G. Busso, B. Carry, A. Cellino, N. Cheek, G. Clementini, Y. Damerdji, M. Davidson, L. Delchambre, A. Dell'Oro, J. Fernández-Hernández, L. Galluccio, P. García-Lario, M. Garcia-Reinaldos, J. González-Núñez,

E. Gosset, R. Haigron, J. L. Halbwachs, N. C. Hambly, D. L. Harrison, D. Hatzidimitriou, U. Heiter, J. Hernández, D. Hestroffer, S. T. Hodgkin, B. Holl, K. Janßen, G. Jevardat de Fombelle, S. Jordan, A. Krone-Martins, A. C. Lanzafame, W. Löffler, A. Lorca, M. Manteiga, O. Marchal, P. M. Marrese, A. Moitinho, A. Mora, K. Muinonen, P. Osborne, E. Pancino, T. Pauwels, J. M. Petit, A. Recio-Blanco, P. J. Richards, M. Riello, L. Rimoldini, A. C. Robin, T. Roegiers, J. Rybizki, L. M. Sarro, C. Siopis, M. Smith, A. Sozzetti, A. Ulla, E. Utrilla, M. van Leeuwen, W. van Reeven, U. Abbas, A. Abreu Aramburu, S. Accart, C. Aerts, J. J. Aguado, M. Ajaj, G. Altavilla, M. A. Álvarez, J. Álvarez Cid-Fuentes, J. Alves, R. I. Anderson, E. Anglada Varela, T. Antoja, M. Audard, D. Baines, S. G. Baker, L. Balaguer-Núñez, E. Balbinot, Z. Balog, C. Barache, D. Barbato, M. Barros, M. A. Barstow, S. Bartolomé, J. L. Bassilana, N. Bauchet, A. Baudesson-Stella, U. Becciani, M. Bellazzini, M. Bernet, S. Bertone, L. Bianchi, S. Blanco-Cuaresma, T. Boch, A. Bombrun, D. Bossini, S. Bouquillon, A. Bragaglia, L. Bramante, E. Breedt, A. Bressan, N. Brouillet, B. Bucciarelli, A. Burlacu, D. Busonero, A. G. Butkevich, R. Buzzi, E. Caffau, R. Cancelliere, H. Cánovas, T. Cantat-Gaudin, R. Carballo, T. Carlucci, M. I. Carnerero, J. M. Carrasco, L. Casamiquela, M. Castellani, A. Castro-Ginard, P. Castro Sampol, L. Chaoul, P. Charlot, L. Chemin, A. Chiavassa, M. R. L. Cioni, G. Comoretto, W. J. Cooper, T. Cornez, S. Cowell, F. Crifo, M. Crosta, C. Crowley, C. Dafonte, A. Dapergolas, M. David, P. David, P. de Laverny, F. De Luise, R. De March, J. De Ridder, R. de Souza, P. de Teodoro, A. de Torres, E. F. del Peloso, E. del Pozo, M. Delbo, A. Delgado, H. E. Delgado, J. B. Delisle, P. Di Matteo, S. Diakite, C. Diener, E. Distefano, C. Dolding, D. Eappachen, B. Edvardsson, H. Enke, P. Esquej, C. Fabre, M. Fabrizio, S. Faigler, G. Fedorets, P. Fernique, A. Fienga, F. Figueras, C. Fouron, F. Fragkoudi, E. Fraile, F. Franke, M. Gai, D. Garabato, A. Garcia-Gutierrez, M. García-Torres, A. Garofalo, P. Gavras, E. Gerlach, R. Geyer, P. Giacobbe, G. Gilmore, S. Girona, G. Giuffrida, R. Gomel, A. Gomez, I. Gonzalez-Santamaria, J. J. González-Vidal, M. Granvik, R. Gutiérrez-Sánchez, L. P. Guy, M. Hauser, M. Haywood, A. Helmi, S. L. Hidalgo, T. Hilger, N. Hładczuk, D. Hobbs, G. Holland, H. E. Huckle, G. Jasniewicz, P. G. Jonker, J. Juaristi Campillo, F. Julbe, L. Karbevska, P. Kervella, S. Khanna, A. Kochoska, M. Kontizas,

G. Kordopatis, A. J. Korn, Z. Kostrzewa-Rutkowska, K. Kruszyńska, S. Lambert, A. F. Lanza, Y. Lasne, J. F. Le Campion, Y. Le Fustec, Y. Lebreton, T. Lebzelter, S. Leccia, N. Leclerc, I. Lecoeur-Taibi, S. Liao, E. Licata, E. P. Lindstrøm, T. A. Lister, E. Livanou, A. Lobel, P. Madrero Pardo, S. Managau, R. G. Mann, J. M. Marchant, M. Marconi, M. M. S. Marcos Santos, S. Marinoni, F. Marocco, D. J. Marshall, L. Martin Polo, J. M. Martín-Fleitas, A. Masip, D. Massari, A. Mastrobuono-Battisti, T. Mazeh, P. J. McMillan, S. Messina, D. Michalik, N. R. Millar, A. Mints, D. Molina, R. Molinaro, L. Molnár, P. Montegriffo, R. Mor, R. Morbidelli, T. Morel, D. Morris, A. F. Mulone, D. Munoz, T. Muraveva, C. P. Murphy, I. Musella, L. Noval, C. Ordénovic, G. Orrù, J. Osinde, C. Pagani, I. Pagano, L. Palaversa, P. A. Palicio, A. Panahi, M. Pawlak, X. Peñalosa Esteller, A. Penttilä, A. M. Piersimoni, F. X. Pineau, E. Plachy, G. Plum, E. Poggio, E. Poretti, E. Poujoulet, A. Prša, L. Pulone, E. Racero, S. Ragaini, M. Rainer, C. M. Raiteri, N. Rambaux, P. Ramos, M. Ramos-Lerate, P. Re Fiorentin, S. Regibo, C. Reylé, V. Ripepi, A. Riva, G. Rixon, N. Robichon, C. Robin, M. Roelens, L. Rohrbasser, M. Romero-Gómez, N. Rowell, F. Royer, K. A. Rybicki, G. Sadowski, A. Sagristà Sellés, J. Sahlmann, J. Salgado, E. Salguero, N. Samaras, V. Sanchez Gimenez, N. Sanna, R. Santoveña, M. Sarasso, M. Schultheis, E. Sciacca, M. Segol, J. C. Segovia, D. Ségransan, D. Semeux, S. Shahaf, H. I. Siddiqui, A. Siebert, L. Siltala, E. Slezak, R. L. Smart, E. Solano, F. Solitro, D. Souami, J. Souchay, A. Spagna, F. Spoto, I. A. Steele, H. Steidelmüller, C. A. Stephenson, M. Süveges, L. Szabados, E. Szegedi-Elek, F. Taris, G. Tauran, M. B. Taylor, R. Teixeira, W. Thuillot, N. Tonello, F. Torra, J. Torra, C. Turon, N. Unger, M. Vaillant, E. van Dillen, O. Vanel, A. Vecchiato, Y. Viala, D. Vicente, S. Voutsinas, M. Weiler, T. Wevers, Ł. Wyrzykowski, A. Yoldas, P. Yvard, H. Zhao, J. Zorec, S. Zucker, C. Zurbach, and T. Zwitter. Gaia Early Data Release 3. Summary of the contents and survey properties. *Astronomy & Astrophysics*, 649:A1, May 2021. doi: 10.1051/0004-6361/202039657.

Gaia Collaboration, A. Vallenari, A. G. A. Brown, T. Prusti, J. H. J. de Bruijne, F. Arenou, C. Babusiaux, M. Biermann, O. L. Creevey, C. Ducourant, D. W. Evans, L. Eyer, R. Guerra, A. Hutton, C. Jordi, S. A. Klioner, U. L. Lammers, L. Lindegren, X. Luri, F. Mignard, C. Panem, D. Pourbaix, S. Randich, P. Sartoretti, C. Soubiran,

P. Tanga, N. A. Walton, C. A. L. Bailer-Jones, U. Bastian, R. Drimmel, F. Jansen, D. Katz, M. G. Lattanzi, F. van Leeuwen, J. Bakker, C. Cacciari, J. Castañeda, F. De Angeli, C. Fabricius, M. Fouesneau, Y. Frémat, L. Galluccio, A. Guerrier, U. Heiter, E. Masana, R. Messineo, N. Mowlavi, C. Nicolas, K. Nienartowicz, F. Pailler, P. Panuzzo, F. Riclet, W. Roux, G. M. Seabroke, R. Sordo, F. Thévenin, G. Gracia-Abril, J. Portell, D. Teyssier, M. Altmann, R. Andrae, M. Audard, I. Bellas-Velidis, K. Benson, J. Berthier, R. Blomme, P. W. Burgess, D. Busonero, G. Busso, H. Cánovas, B. Carry, A. Cellino, N. Cheek, G. Clementini, Y. Damerdji, M. Davidson, P. de Teodoro, M. Nuñez Campos, L. Delchambre, A. Dell'Oro, P. Esquej, J. Fernández-Hernández, E. Fraile, D. Garabato, P. García-Lario, E. Gosset, R. Haigron, J. L. Halbwachs, N. C. Hambly, D. L. Harrison, J. Hernández, D. Hestroffer, S. T. Hodgkin, B. Holl, K. Janßen, G. Jevardat de Fombelle, S. Jordan, A. Krone-Martins, A. C. Lanzafame, W. Löffler, O. Marchal, P. M. Marrese, A. Moitinho, K. Muinonen, P. Osborne, E. Pancino, T. Pauwels, A. Recio-Blanco, C. Reylé, M. Riello, L. Rimoldini, T. Roegiers, J. Rybizki, L. M. Sarro, C. Siopis, M. Smith, A. Sozzetti, E. Utrilla, M. van Leeuwen, U. Abbas, P. Ábrahám, A. Abreu Aramburu, C. Aerts, J. J. Aguado, M. Ajaj, F. Aldea-Montero, G. Altavilla, M. A. Álvarez, J. Alves, F. Anders, R. I. Anderson, E. Anglada Varela, T. Antoja, D. Baines, S. G. Baker, L. Balaguer-Núñez, E. Balbinot, Z. Balog, C. Barache, D. Barbato, M. Barros, M. A. Barstow, S. Bartolomé, J. L. Bassilana, N. Bauchet, U. Becciani, M. Bellazzini, A. Berihuete, M. Bernet, S. Bertone, L. Bianchi, A. Binnenfeld, S. Blanco-Cuaresma, A. Blazere, T. Boch, A. Bombrun, D. Bossini, S. Bouquillon, A. Bragaglia, L. Bramante, E. Breedt, A. Bressan, N. Brouillet, E. Brugaletta, B. Bucciarelli, A. Burlacu, A. G. Butkevich, R. Buzzi, E. Caffau, R. Cancelliere, T. Cantat-Gaudin, R. Carballo, T. Carlucci, M. I. Carnerero, J. M. Carrasco, L. Casamiquela, M. Castellani, A. Castro-Ginard, L. Chaoul, P. Charlot, L. Chemin, V. Chiaramida, A. Chiavassa, N. Chornay, G. Comoretto, G. Contursi, W. J. Cooper, T. Cornez, S. Cowell, F. Crifo, M. Cropper, M. Crosta, C. Crowley, C. Dafonte, A. Dapergolas, M. David, P. David, P. de Laverny, F. De Luise, R. De March, J. De Ridder, R. de Souza, A. de Torres, E. F. del Peloso, E. del Pozo, M. Delbo, A. Delgado, J. B. Delisle, C. Demouchy, T. E. Dharmawardena, P. Di Matteo, S. Diakite, C. Diener,

E. Distefano, C. Dolding, B. Edvardsson, H. Enke, C. Fabre, M. Fabrizio, S. Faigler, G. Fedorets, P. Fernique, A. Fienga, F. Figueras, Y. Fournier, C. Fouron, F. Fragkoudi, M. Gai, A. Garcia-Gutierrez, M. Garcia-Reinaldos, M. García-Torres, A. Garofalo, A. Gavel, P. Gavras, E. Gerlach, R. Geyer, P. Giacobbe, G. Gilmore, S. Girona, G. Giuffrida, R. Gomel, A. Gomez, J. González-Núñez, I. González-Santamaría, J. J. González-Vidal, M. Granvik, P. Guillout, J. Guiraud, R. Gutiérrez-Sánchez, L. P. Guy, D. Hatzidimitriou, M. Hauser, M. Haywood, A. Helmer, A. Helmi, M. H. Sarmiento, S. L. Hidalgo, T. Hilger, N. Hładczuk, D. Hobbs, G. Holland, H. E. Huckle, K. Jardine, G. Jasniewicz, A. Jean-Antoine Piccolo, Ó. Jiménez-Arranz, A. Jorissen, J. Juaristi Campillo, F. Julbe, L. Karbevska, P. Kervella, S. Khanna, M. Kontizas, G. Kordopatis, A. J. Korn, Á. Kóspál, Z. Kostrzewa-Rutkowska, K. Kruszyńska, M. Kun, P. Laizeau, S. Lambert, A. F. Lanza, Y. Lasne, J. F. Le Campion, Y. Lebreton, T. Lebzelter, S. Leccia, N. Leclerc, I. Lecoeur-Taibi, S. Liao, E. L. Licata, H. E. P. Lindstrøm, T. A. Lister, E. Livanou, A. Lobel, A. Lorca, C. Loup, P. Madrero Pardo, A. Magdaleno Romeo, S. Managau, R. G. Mann, M. Manteiga, J. M. Marchant, M. Marconi, J. Marcos, M. M. S. Marcos Santos, D. Marín Pina, S. Marinoni, F. Marocco, D. J. Marshall, L. Martin Polo, J. M. Martín-Fleitas, G. Marton, N. Mary, A. Masip, D. Massari, A. Mastrobuono-Battisti, T. Mazeh, P. J. McMillan, S. Messina, D. Michalik, N. R. Millar, A. Mints, D. Molina, R. Molinaro, L. Molnár, G. Monari, M. Monguió, P. Montegriffo, A. Montero, R. Mor, A. Mora, R. Morbidelli, T. Morel, D. Morris, T. Muraveva, C. P. Murphy, I. Musella, Z. Nagy, L. Noval, F. Ocaña, A. Ogden, C. Ordenovic, J. O. Osinde, C. Pagani, I. Pagano, L. Palaversa, P. A. Palicio, L. Pallas-Quintela, A. Panahi, S. Payne-Wardenaar, X. Peñalosa Esteller, A. Penttilä, B. Pichon, A. M. Piersimoni, F. X. Pineau, E. Plachy, G. Plum, E. Poggio, A. Prša, L. Pulone, E. Racero, S. Ragaini, M. Rainer, C. M. Raiteri, N. Rambaux, P. Ramos, M. Ramos-Lerate, P. Re Fiorentin, S. Regibo, P. J. Richards, C. Rios Diaz, V. Ripepi, A. Riva, H. W. Rix, G. Rixon, N. Robichon, A. C. Robin, C. Robin, M. Roelens, H. R. O. Rogues, L. Rohrbasser, M. Romero-Gómez, N. Rowell, F. Royer, D. Ruz Mieres, K. A. Rybicki, G. Sadowski, A. Sáez Núñez, A. Sagristà Sellés, J. Sahlmann, E. Salguero, N. Samaras, V. Sanchez Gimenez, N. Sanna, R. Santoveña, M. Sarasso, M. Schultheis, E. Sciacca, M. Segol,

J. C. Segovia, D. Ségransan, D. Semeux, S. Shahaf, H. I. Siddiqui, A. Siebert, L. Siltala, A. Silvelo, E. Slezak, I. Slezak, R. L. Smart, O. N. Snaith, E. Solano, F. Solitro, D. Souami, J. Souchay, A. Spagna, L. Spina, F. Spoto, I. A. Steele, H. Steidelmüller, C. A. Stephenson, M. Süveges, J. Surdej, L. Szabados, E. Szegedi-Elek, F. Taris, M. B. Taylor, R. Teixeira, L. Tolomei, N. Tonello, F. Torra, J. Torra, G. Torralba Elipe, M. Trabucchi, A. T. Tsounis, C. Turon, A. Ulla, N. Unger, M. V. Vaillant, E. van Dillen, W. van Reeven, O. Vanel, A. Vecchiato, Y. Viala, D. Vicente, S. Voutsinas, M. Weiler, T. Wevers, Ł. Wyrzykowski, A. Yoldas, P. Yvard, H. Zhao, J. Zorec, S. Zucker, and T. Zwitter. Gaia Data Release 3. Summary of the content and survey properties. *Astronomy & Astrophysics*, 674:A1, June 2023. doi: 10.1051/0004-6361/202243940.

A. M. Geller, R. D. Mathieu, H. C. Harris, and R. D. McClure. WIYN Open Cluster Study. XXXII. Stellar Radial Velocities in the Old Open Cluster NGC 188. *The Astronomical Journal*, 135(6):2264–2278, June 2008. doi: 10.1088/0004-6256/135/6/2264.

J. I. González Hernández and P. Bonifacio. A new implementation of the infrared flux method using the 2MASS catalogue. *Astronomy & Astrophysics*, 497(2):497–509, Apr. 2009. doi: 10.1051/0004-6361/200810904.

N. M. Gosnell, R. D. Mathieu, A. M. Geller, A. Sills, N. Leigh, and C. Knigge. Implications for the Formation of Blue Straggler Stars from HST Ultraviolet Observations of NGC 188. *The American Astronomical Society*, 814(2):163, Dec. 2015. doi: 10.1088/0004-637X/814/2/163.

W. E. Harris. A New Catalog of Globular Clusters in the Milky Way. *arXiv e-prints*, art. arXiv:1012.3224, Dec. 2010. doi: 10.48550/arXiv.1012.3224.

J. G. Hills and C. A. Day. Stellar Collisions in Globular Clusters. , 17:87, Feb. 1976.

F. Hoyle. *Frontiers of astronomy.* 1955.

J. R. Hurley, C. A. Tout, and O. R. Pols. Evolution of binary stars and the effect of tides on binary populations. *Monthly Notices of the Royal Astronomical Society*, 329(4): 897–928, Feb. 2002. doi: 10.1046/j.1365-8711.2002.05038.x.

J. R. Hurley, O. R. Pols, S. J. Aarseth, and C. A. Tout. A complete N-body model of the old open cluster M67. *Monthly Notices of the Royal Astronomical Society*, 363(1): 293–314, Oct. 2005. doi: 10.1111/j.1365-2966.2005.09448.x.

V. V. Jadhav and A. Subramaniam. Blue straggler stars in open clusters using Gaia: dependence on cluster parameters and possible formation pathways. *Monthly Notices of the Royal Astronomical Society*, 507(2):1699–1709, Oct. 2021. doi: 10.1093/mnras/stab2264.

H. L. Johnson and A. R. Sandage. The galactic cluster M 67 and its significance for stellar evolution. *The American Astronomical Society*, 121:616, May 1955. doi: 10.1086/146027.

B. Lanzoni, N. Sanna, F. R. Ferraro, E. Valenti, G. Beccari, R. P. Schiavon, R. T. Rood, M. Mapelli, and S. Sigurdsson. A Panchromatic Study of the Globular Cluster NGC 1904. I. The Blue Straggler Population. *The American Astronomical Society*, 663(2): 1040–1048, July 2007. doi: 10.1086/518688.

B. Lanzoni, F. R. Ferraro, E. Alessandrini, E. Dalessandro, E. Vesperini, and S. Raso. Refining the Dynamical Clock for Star Clusters. , 833(2):L29, Dec. 2016. doi: 10.3847/2041-8213/833/2/L29.

N. Leigh, A. Sills, and C. Knigge. Dissecting the colour-magnitude diagram: a homogeneous catalogue of stellar populations in globular clusters. *Monthly Notices of the Royal Astronomical Society*, 415(4):3771–3782, Aug. 2011. doi: 10.1111/j.1365-2966.2011.18995.x.

C. Li, J. Zhong, S. Qin, and L. Chen. The new detection of blue straggler stars in 50 open clusters using Gaia DR3. *Astronomy & Astrophysics*, 672:A81, Apr. 2023. doi: 10.1051/0004-6361/202244998.

C. J. Lombardi, James, F. A. Rasio, and S. L. Shapiro. On Blue Straggler Formation by Direct Collisions of Main-Sequence Stars. , 445:L117, June 1995. doi: 10.1086/187903.

M. Mapelli, S. Sigurdsson, M. Colpi, F. R. Ferraro, A. Possenti, R. T. Rood, A. Sills, and

G. Beccari. The Contribution of Primordial Binaries to the Blue Straggler Population in 47 Tucanae. , 605(1):L29–L32, Apr. 2004. doi: 10.1086/386370.

M. Mapelli, S. Sigurdsson, F. R. Ferraro, M. Colpi, A. Possenti, and B. Lanzoni. The radial distribution of blue straggler stars and the nature of their progenitors. *Monthly Notices of the Royal Astronomical Society*, 373(1):361–368, Nov. 2006. doi: 10.1111/j.1365-2966.2006.11038.x.

M. Mapelli, E. Ripamonti, G. Battaglia, E. Tolstoy, M. J. Irwin, B. Moore, and S. Sigurdsson. Blue straggler stars in dwarf spheroidal galaxies - II. Sculptor and Fornax. *Monthly Notices of the Royal Astronomical Society*, 396(3):1771–1782, July 2009. doi: 10.1111/j.1365-2966.2009.14861.x.

P. Marigo, L. Girardi, A. Bressan, M. A. T. Groenewegen, L. Silva, and G. L. Granato. Evolution of asymptotic giant branch stars. II. Optical to far-infrared isochrones with improved TP-AGB models. *Astronomy & Astrophysics*, 482(3):883–905, May 2008. doi: 10.1051/0004-6361:20078467.

G. Mathys. Properties of blue stragglers in young OB associations. , 71:201–219, Nov. 1987.

W. H. McCrea. Extended main-sequence of some stellar clusters. *Monthly Notices of the Royal Astronomical Society*, 128:147, Jan. 1964. doi: 10.1093/mnras/128.2.147.

J. C. Mermilliod and E. Paunzen. Analysing the database for stars in open clusters. I. General methods and description of the data. *Astronomy & Astrophysics*, 410:511–518, Nov. 2003. doi: 10.1051/0004-6361:20031112.

A. P. Milone, G. Piotto, L. R. Bedin, A. Aparicio, J. Anderson, A. Sarajedini, A. F. Marino, A. Moretti, M. B. Davies, B. Chaboyer, A. Dotter, M. Hempel, A. Marín-Franch, S. Majewski, N. E. Q. Paust, I. N. Reid, A. Rosenberg, and M. Siegel. The ACS survey of Galactic globular clusters. XII. Photometric binaries along the main sequence. *Astronomy & Astrophysics*, 540:A16, Apr. 2012a. doi: 10.1051/0004-6361/201016384.

A. P. Milone, G. Piotto, L. R. Bedin, I. R. King, J. Anderson, A. F. Marino, A. Bellini, R. Gratton, A. Renzini, P. B. Stetson, S. Cassisi, A. Aparicio, A. Bragaglia, E. Carretta, F. D'Antona, M. Di Criscienzo, S. Lucatello, M. Monelli, and A. Pietrinferni. Multiple Stellar Populations in 47 Tucanae. *The American Astronomical Society*, 744(1):58, Jan. 2012b. doi: 10.1088/0004-637X/744/1/5810.1086/141918.

A. P. Milone, L. R. Bedin, G. Piotto, A. F. Marino, S. Cassisi, A. Bellini, H. Jerjen, A. Pietrinferni, A. Aparicio, and R. M. Rich. Multiple stellar populations in Magellanic Cloud clusters - III. The first evidence of an extended main sequence turn-off in a young cluster: NGC 1856. *Monthly Notices of the Royal Astronomical Society*, 450(4):3750–3764, July 2015. doi: 10.1093/mnras/stv829.

Y. Momany, E. V. Held, I. Saviane, S. Zaggia, L. Rizzi, and M. Gullieuszik. The blue plume population in dwarf spheroidal galaxies. Genuine blue stragglers or young stellar population? *Astronomy & Astrophysics*, 468(3):973–978, June 2007. doi: 10.1051/0004-6361:20067024.

P. Montegriffo, F. De Angeli, R. Andrae, M. Riello, E. Pancino, N. Sanna, M. Bellazzini, D. W. Evans, J. M. Carrasco, R. Sordo, G. Busso, C. Cacciari, C. Jordi, F. van Leeuwen, A. Vallenari, G. Altavilla, M. A. Barstow, A. G. A. Brown, P. W. Burgess, M. Castellani, S. Cowell, M. Davidson, F. De Luise, L. Delchambre, C. Diener, C. Fabricius, Y. Frémat, M. Fouesneau, G. Gilmore, G. Giuffrida, N. C. Hambly, D. L. Harrison, S. Hidalgo, S. T. Hodgkin, G. Holland, S. Marinoni, P. J. Osborne, C. Pagani, L. Palaversa, A. M. Piersimoni, L. Pulone, S. Ragaini, M. Rainer, P. J. Richards, N. Rowell, D. Ruz-Mieres, L. M. Sarro, N. A. Walton, and A. Yoldas. Gaia Data Release 3. External calibration of BP/RP low-resolution spectroscopic data. *Astronomy & Astrophysics*, 674:A3, June 2023. doi: 10.1051/0004-6361/202243880.

A. Mucciarelli, M. Bellazzini, and D. Massari. Exploiting the Gaia EDR3 photometry to derive stellar temperatures. *Astronomy & Astrophysics*, 653:A90, Sept. 2021. doi: 10.1051/0004-6361/202140979.

D. Nardiello, M. Libralato, G. Piotto, J. Anderson, A. Bellini, A. Aparicio, L. R. Bedin,

S. Cassisi, V. Granata, I. R. King, F. Lucertini, A. F. Marino, A. P. Milone, S. Ortolani, I. Platais, and R. P. van der Marel. The Hubble Space Telescope UV Legacy Survey of Galactic Globular Clusters - XVII. Public Catalogue Release. *Monthly Notices of the Royal Astronomical Society*, 481(3):3382–3393, Dec. 2018. doi: 10.1093/mnras/sty2515.

H. B. Perets and D. C. Fabrycky. On the Triple Origin of Blue Stragglers. *The American Astronomical Society*, 697(2):1048–1056, June 2009. doi: 10.1088/0004-637X/697/2/1048.

G. Piotto, A. P. Milone, L. R. Bedin, J. Anderson, I. R. King, A. F. Marino, D. Nardiello, A. Aparicio, B. Barbuy, A. Bellini, T. M. Brown, S. Cassisi, A. M. Cool, A. Cunial, E. Dalessandro, F. D'Antona, F. R. Ferraro, S. Hidalgo, B. Lanzoni, M. Monelli, S. Ortolani, A. Renzini, M. Salaris, A. Sarajedini, R. P. van der Marel, E. Vesperini, and M. Zoccali. The Hubble Space Telescope UV Legacy Survey of Galactic Globular Clusters. I. Overview of the Project and Detection of Multiple Stellar Populations. *The Astronomical Journal*, 149(3):91, Mar. 2015. doi: 10.1088/0004-6256/149/3/91.

G. W. Preston, T. C. Beers, and S. A. Shectman. The Space Density and Kinematics of Blue Metal-Poor Main Sequence Stars Near the Solar Circle. *The Astronomical Journal*, 108:538, Aug. 1994. doi: 10.1086/117089.

M. J. Rain, J. A. Ahumada, and G. Carraro. A new, Gaia-based, catalogue of blue straggler stars in open clusters. *Astronomy & Astrophysics*, 650:A67, June 2021. doi: 10.1051/0004-6361/202040072.

K. K. Rao, K. Vaidya, M. Agarwal, and S. Bhattacharya. Determination of dynamical ages of open clusters through the A^+ parameter - I. *Monthly Notices of the Royal Astronomical Society*, 508(4):4919–4937, Dec. 2021. doi: 10.1093/mnras/stab2894.

K. K. Rao, S. Bhattacharya, K. Vaidya, and M. Agarwal. Discovery of double BSS sequences in the old Galactic open cluster Berkeley 17. *Monthly Notices of the Royal Astronomical Society*, 518(1):L7–L12, Jan. 2023a. doi: 10.1093/mnrasl/slac122.

K. K. Rao, K. Vaidya, M. Agarwal, S. Balan, and S. Bhattacharya. Determination of

dynamical ages of open clusters through the A^+ parameter – II. *arXiv e-prints*, art. arXiv:2309.02746, Sept. 2023b. doi: 10.48550/arXiv.2309.02746.

S. Raso, F. R. Ferraro, E. Dalessandro, B. Lanzoni, D. Nardiello, A. Bellini, and E. Vesperini. The "UV-route" to Search for Blue Straggler Stars in Globular Clusters: First Results from the HST UV Legacy Survey. *The American Astronomical Society*, 839(1): 64, Apr. 2017. doi: 10.3847/1538-4357/aa6891.

M. Riello, F. De Angeli, D. W. Evans, P. Montegriffo, J. M. Carrasco, G. Busso, L. Palaversa, P. W. Burgess, C. Diener, M. Davidson, N. Rowell, C. Fabricius, C. Jordi, M. Bellazzini, E. Pancino, D. L. Harrison, C. Cacciari, F. van Leeuwen, N. C. Hambly, S. T. Hodgkin, P. J. Osborne, G. Altavilla, M. A. Barstow, A. G. A. Brown, M. Castellani, S. Cowell, F. De Luise, G. Gilmore, G. Giuffrida, S. Hidalgo, G. Holland, S. Marinoni, C. Pagani, A. M. Piersimoni, L. Pulone, S. Ragaini, M. Rainer, P. J. Richards, N. Sanna, N. A. Walton, M. Weiler, and A. Yoldas. Gaia Early Data Release 3. Photometric content and validation. *Astronomy & Astrophysics*, 649:A3, May 2021. doi: 10.1051/0004-6361/202039587.

C. Rodrigo and E. Solano. The SVO Filter Profile Service. In *XIV.0 Scientific Meeting (virtual) of the Spanish Astronomical Society*, page 182, July 2020.

C. Rodrigo, E. Solano, and A. Bayo. SVO Filter Profile Service Version 1.0. IVOA Working Draft 15 October 2012, Oct. 2012.

A. R. Sandage. The color-magnitude diagram for the globular cluster M 3. *The Astronomical Journal*, 58:61–75, Jan. 1953. doi: 10.1086/106822.

A. Sarajedini. A Survey of Galactic Globular Clusters for Blue Straggler Stars. In R. A. Saffer, editor, *Blue Stragglers*, volume 53 of *Astronomical Society of the Pacific Conference Series*, page 14, Jan. 1993.

A. Sarajedini, L. R. Bedin, B. Chaboyer, A. Dotter, M. Siegel, J. Anderson, A. Aparicio, I. King, S. Majewski, A. Marín-Franch, G. Piotto, I. N. Reid, and A. Rosenberg. The ACS Survey of Galactic Globular Clusters. I. Overview and Clusters without Previous

Hubble Space Telescope Photometry. *The Astronomical Journal*, 133(4):1658–1672, Apr. 2007. doi: 10.1086/511979.

M. J. Sarna and J. P. De Greve. Chemical Evolution of Algols. , 37:11, Mar. 1996.

H. Schild. The evolutionary status of OB stars with peculiar nitrogen spectra. *Astronomy & Astrophysics*, 146:113–118, May 1985.

E. F. Schlafly, A. M. Meisner, and G. M. Green. The unWISE Catalog: Two Billion Infrared Sources from Five Years of WISE Imaging. , 240(2):30, Feb. 2019. doi: 10.3847/1538-4365/aafbea.

Y. Shao and X.-D. Li. Nonconservative Mass Transfer in Massive Binaries and the Formation of Wolf-Rayet+O Binaries. *The American Astronomical Society*, 833(1):108, Dec. 2016. doi: 10.3847/1538-4357/833/1/108.

M. M. Shara, R. A. Saffer, and M. Livio. The First Direct Measurement of the Mass of a Blue Straggler in the Core of a Globular Cluster: BSS 19 in 47 Tucanae. , 489(1): L59–L62, Nov. 1997. doi: 10.1086/310952.

A. Sills, A. Karakas, and J. Lattanzio. Blue Stragglers After the Main Sequence. *The American Astronomical Society*, 692(2):1411–1420, Feb. 2009. doi: 10.1088/0004-637X/692/2/1411.

M. Simunovic. *The blue straggler star populations in galactic globular clusters*. PhD thesis, Ruprecht-Karls University of Heidelberg, Germany, Jan. 2017.

M. Simunovic and T. H. Puzia. Blue straggler star populations in globular clusters - II. Proper-motion cleaned HST catalogues of BSSs in 38 Galactic GCs. *Monthly Notices of the Royal Astronomical Society*, 462(3):3401–3418, Nov. 2016. doi: 10.1093/mnras/stw1884.

M. Simunovic, T. H. Puzia, and A. Sills. The Blue Straggler Star Population in NGC 1261: Evidence for a Post-core-collapse Bounce State. , 795(1):L10, Nov. 2014. doi: 10.1088/2041-8205/795/1/L10.

N. Sindhu, A. Subramaniam, V. V. Jadhav, S. Chatterjee, A. M. Geller, C. Knigge, N. Leigh, T. H. Puzia, M. Shara, and M. Simunovic. UVIT Open Cluster Study. I. Detection of a White Dwarf Companion to a Blue Straggler in M67: Evidence of Formation through Mass Transfer. *The American Astronomical Society*, 882(1):43, Sept. 2019. doi: 10.3847/1538-4357/ab31a8.

M. F. Skrutskie, R. M. Cutri, R. Stiening, M. D. Weinberg, S. Schneider, J. M. Carpenter, C. Beichman, R. Capps, T. Chester, J. Elias, J. Huchra, J. Liebert, C. Lonsdale, D. G. Monet, S. Price, P. Seitzer, T. Jarrett, J. D. Kirkpatrick, J. E. Gizis, E. Howard, T. Evans, J. Fowler, L. Fullmer, R. Hurt, R. Light, E. L. Kopan, K. A. Marsh, H. L. McCallon, R. Tam, S. Van Dyk, and S. Wheelock. The Two Micron All Sky Survey (2MASS). *The Astronomical Journal*, 131(2):1163–1183, Feb. 2006. doi: 10.1086/498708.

K. Stępień and M. Kiraga. Model computations of blue stragglers and W UMa-type stars in globular clusters. *Astronomy & Astrophysics*, 577:A117, May 2015. doi: 10.1051/0004-6361/201425550.

A. Subramaniam, N. Sindhu, S. N. Tandon, N. Kameswara Rao, J. Postma, P. Côté, J. B. Hutchings, S. K. Ghosh, K. George, V. Girish, R. Mohan, J. Murthy, K. Sankarasubramanian, C. S. Stalin, F. Sutaria, C. Mondal, and S. Sahu. A Hot Companion to a Blue Straggler in NGC 188 as Revealed by the Ultra-Violet Imaging Telescope (UVIT) on ASTROSAT. , 833(2):L27, Dec. 2016. doi: 10.3847/2041-8213/833/2/L27.

A. Subramaniam, S. Pandey, V. V. Jadhav, and S. Sahu. UVIT/AstroSat studies of blue straggler stars and post-mass transfer systems in star clusters: detection of one more blue lurker in M67. *Journal of Astrophysics and Astronomy*, 41(1):45, Dec. 2020. doi: 10.1007/s12036-020-09668-1.

M. B. Taylor. TOPCAT & STIL: Starlink Table/VOTable Processing Software. In P. Shopbell, M. Britton, and R. Ebert, editors, *Astronomical Data Analysis Software and Systems XIV*, volume 347 of *Astronomical Society of the Pacific Conference Series*, page 29, Dec. 2005.

B. Tian, L. Deng, Z. Han, and X. B. Zhang. The blue stragglers formed via mass transfer in old open clusters. *Astronomy & Astrophysics*, 455(1):247–254, Aug. 2006. doi: 10.1051/0004-6361:20064879.

A. Tokovinin, S. Thomas, M. Sterzik, and S. Udry. Tertiary companions to close spectroscopic binaries. *Astronomy & Astrophysics*, 450(2):681–693, May 2006. doi: 10.1051/0004-6361:20054427.

E. Vasiliev and H. Baumgardt. Gaia EDR3 view on galactic globular clusters. *Monthly Notices of the Royal Astronomical Society*, 505(4):5978–6002, Aug. 2021. doi: 10.1093/mnras/stab1475.

C. Wang, Y. Huang, H. Yuan, H. Zhang, M. Xiang, and X. Liu. The Value-added Catalog for LAMOST DR8 Low-resolution Spectra. , 259(2):51, Apr. 2022. doi: 10.3847/1538-4365/ac4df7.

M. Xiang, H.-W. Rix, Y.-S. Ting, R.-P. Kudritzki, C. Conroy, E. Zari, J.-R. Shi, N. Przybilla, M. Ramirez-Tannus, A. Tkachenko, S. Gebruers, and X.-W. Liu. Stellar labels for hot stars from low-resolution spectra. I. The HotPayne method and results for 330 000 stars from LAMOST DR6. *Astronomy & Astrophysics*, 662:A66, June 2022. doi: 10.1051/0004-6361/202141570.

X. Zhang, G. M. Green, and H.-W. Rix. Parameters of 220 million stars from Gaia BP/RP spectra. *Monthly Notices of the Royal Astronomical Society*, 524(2):1855–1884, Sept. 2023. doi: 10.1093/mnras/stad1941.

Appendix A

Blue Straggler Stars identified with Gaia DR3

A.1 Globular Clusters

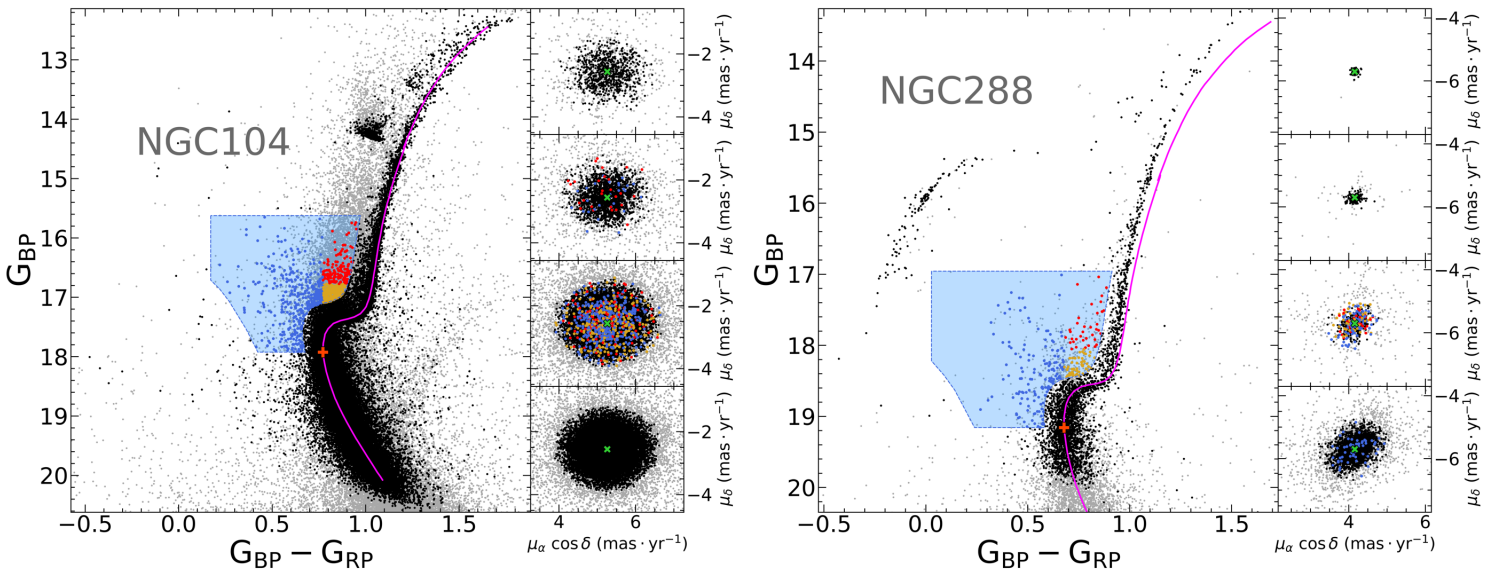

Figure A.1: Same as Figure 3.7, but for the rest of the GC sample.

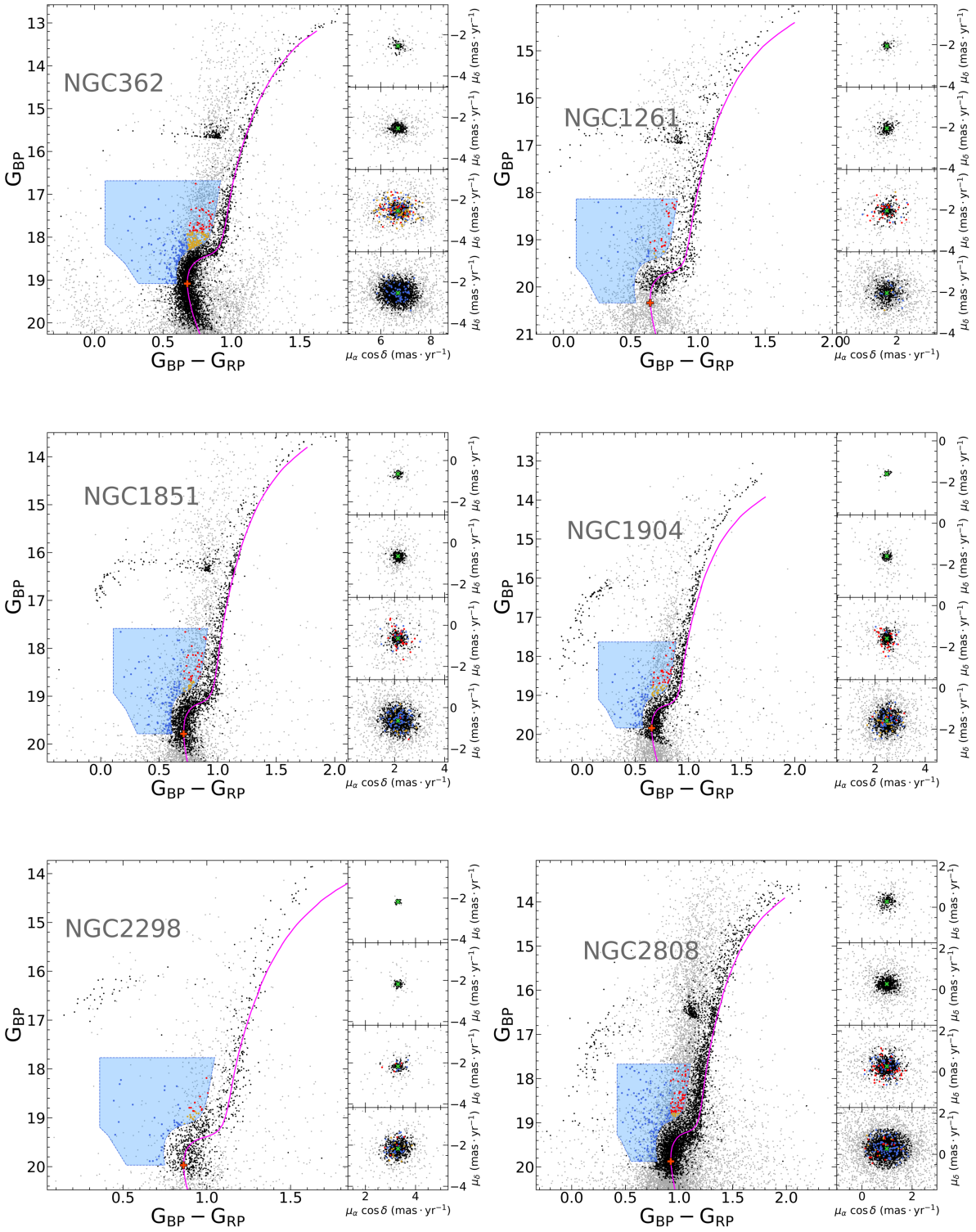

Figure A.2: Same as Figure 3.7, but for the rest of the GC sample.

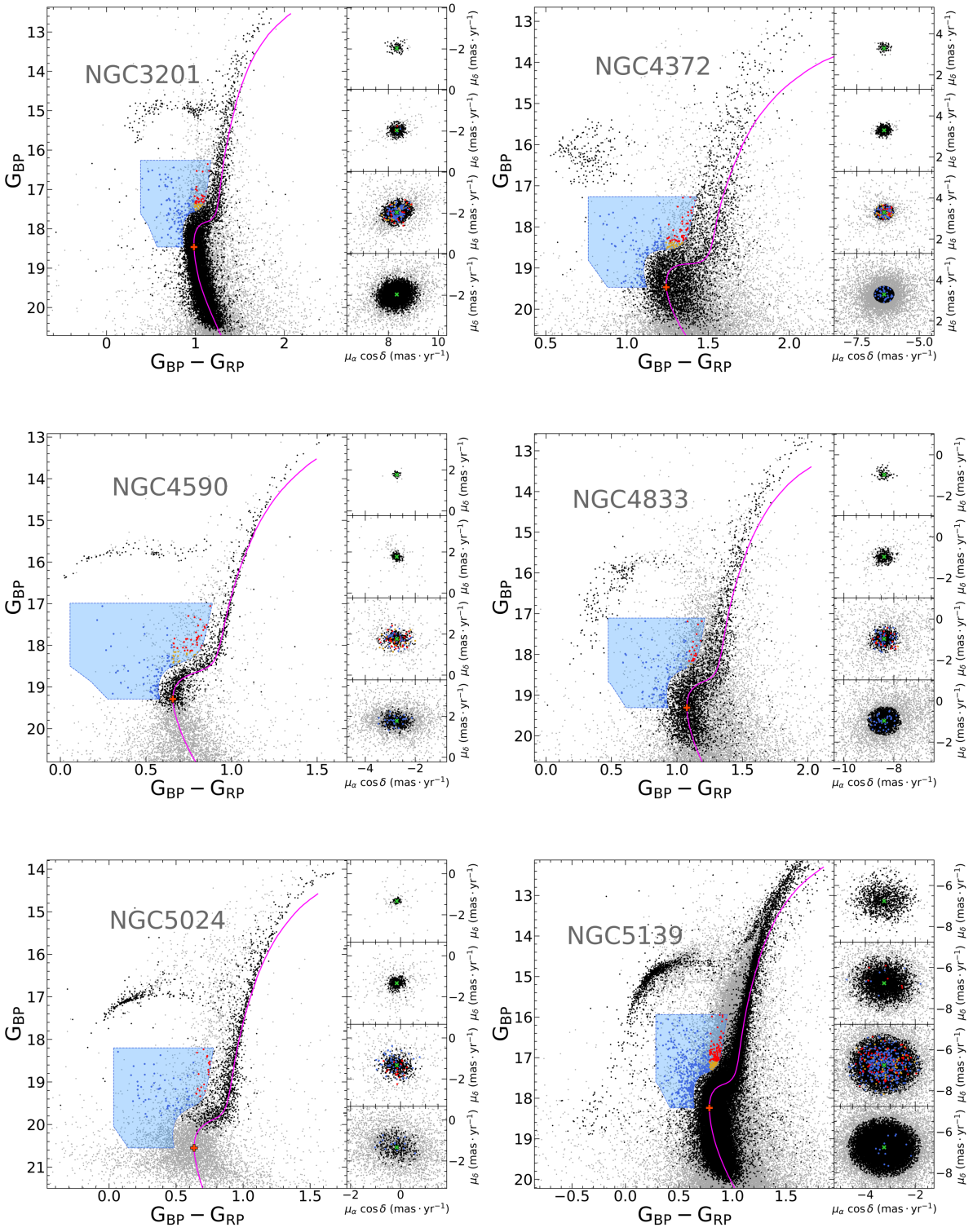

Figure A.3: Same as Figure 3.7, but for the rest of the GC sample.

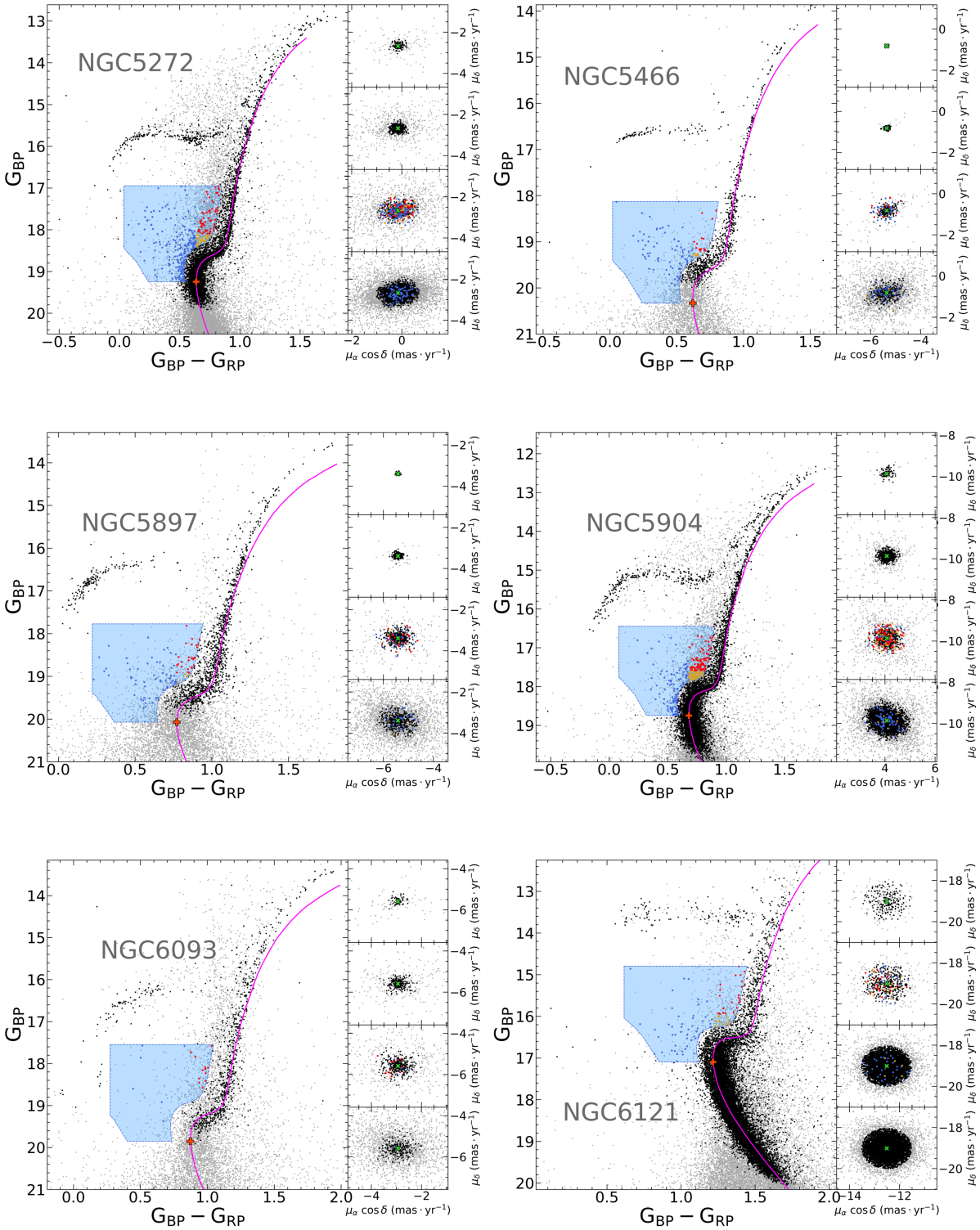

Figure A.4: Same as Figure 3.7, but for the rest of the GC sample.

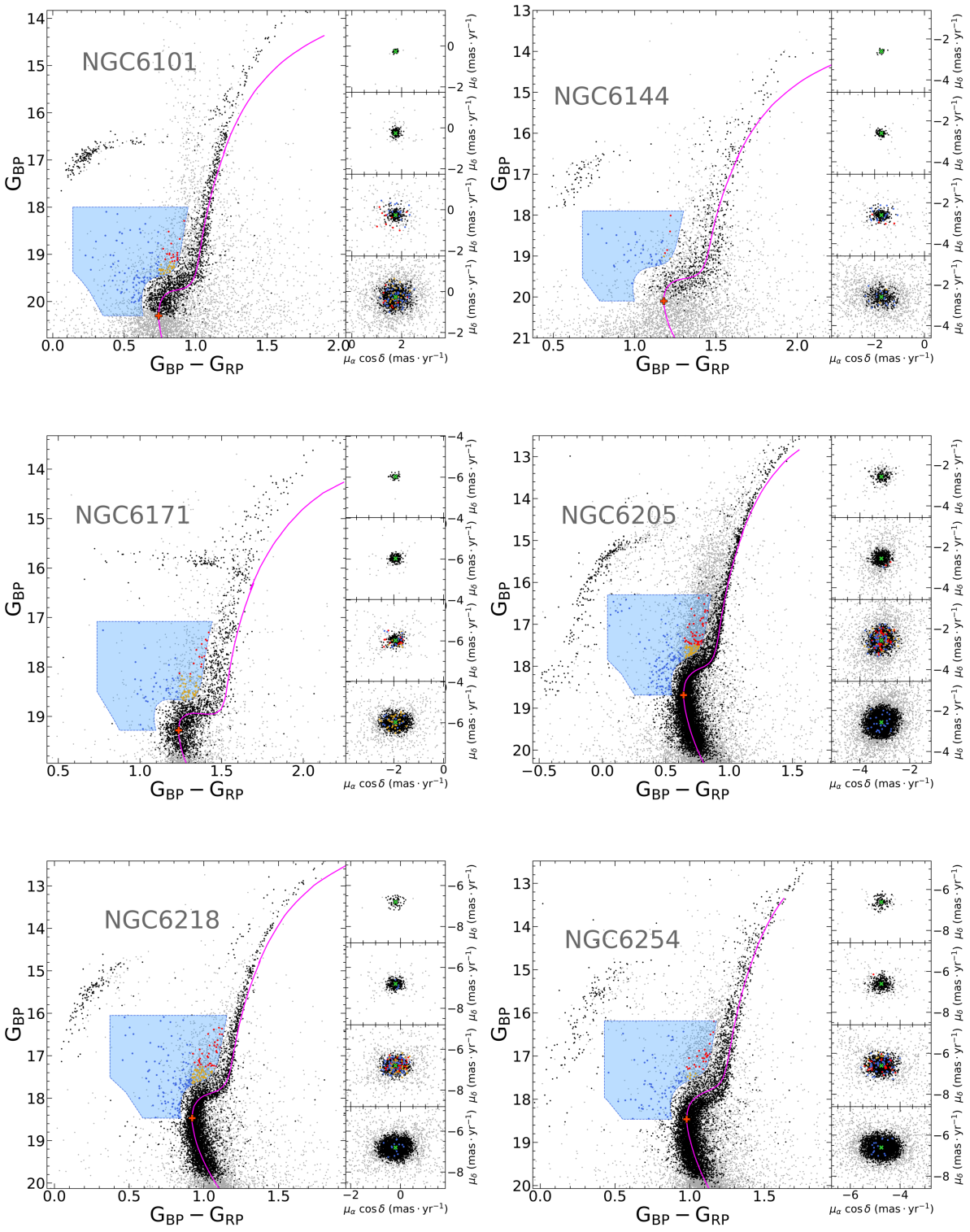

Figure A.5: Same as Figure 3.7, but for the rest of the GC sample.

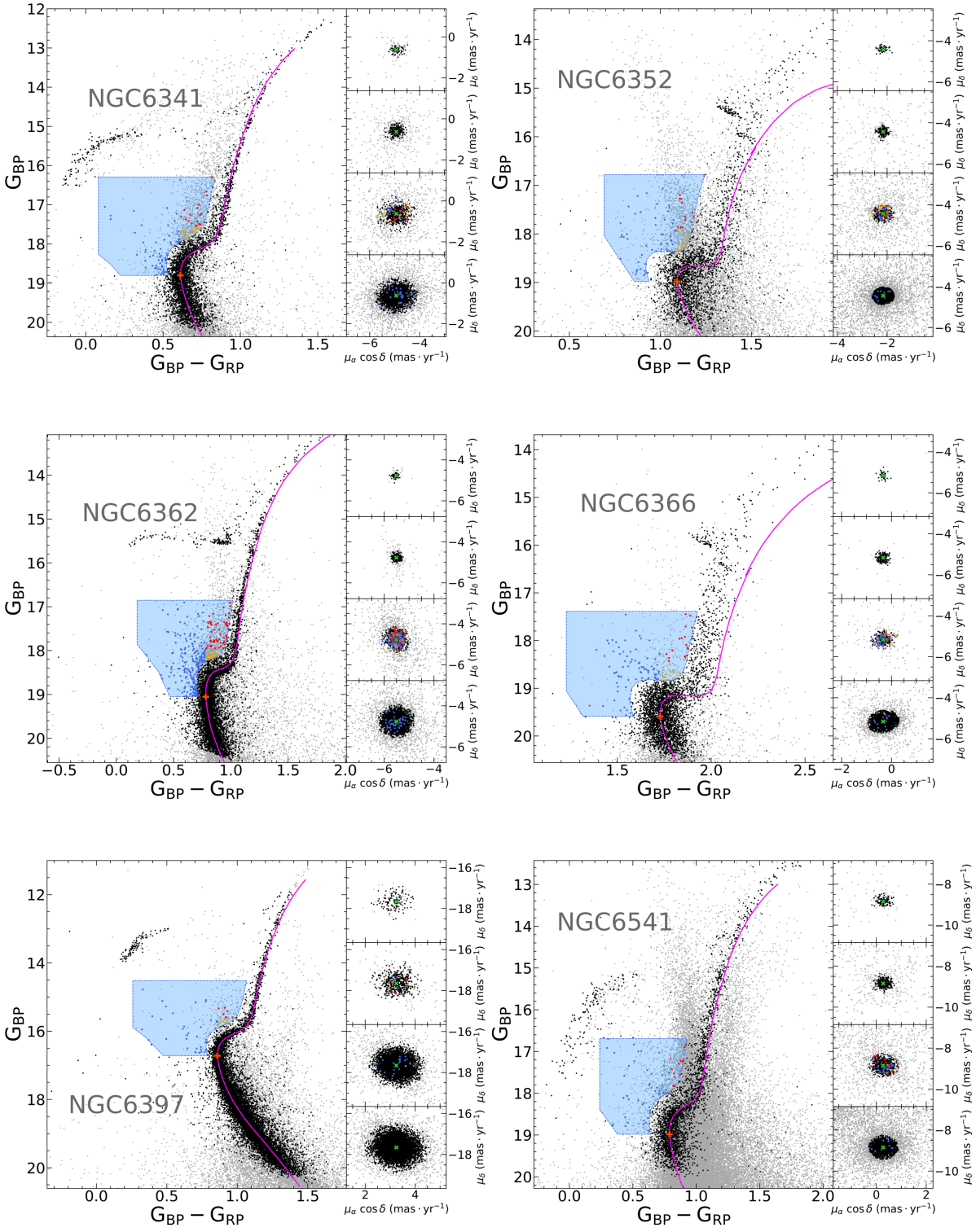

Figure A.6: Same as Figure 3.7, but for the rest of the GC sample.

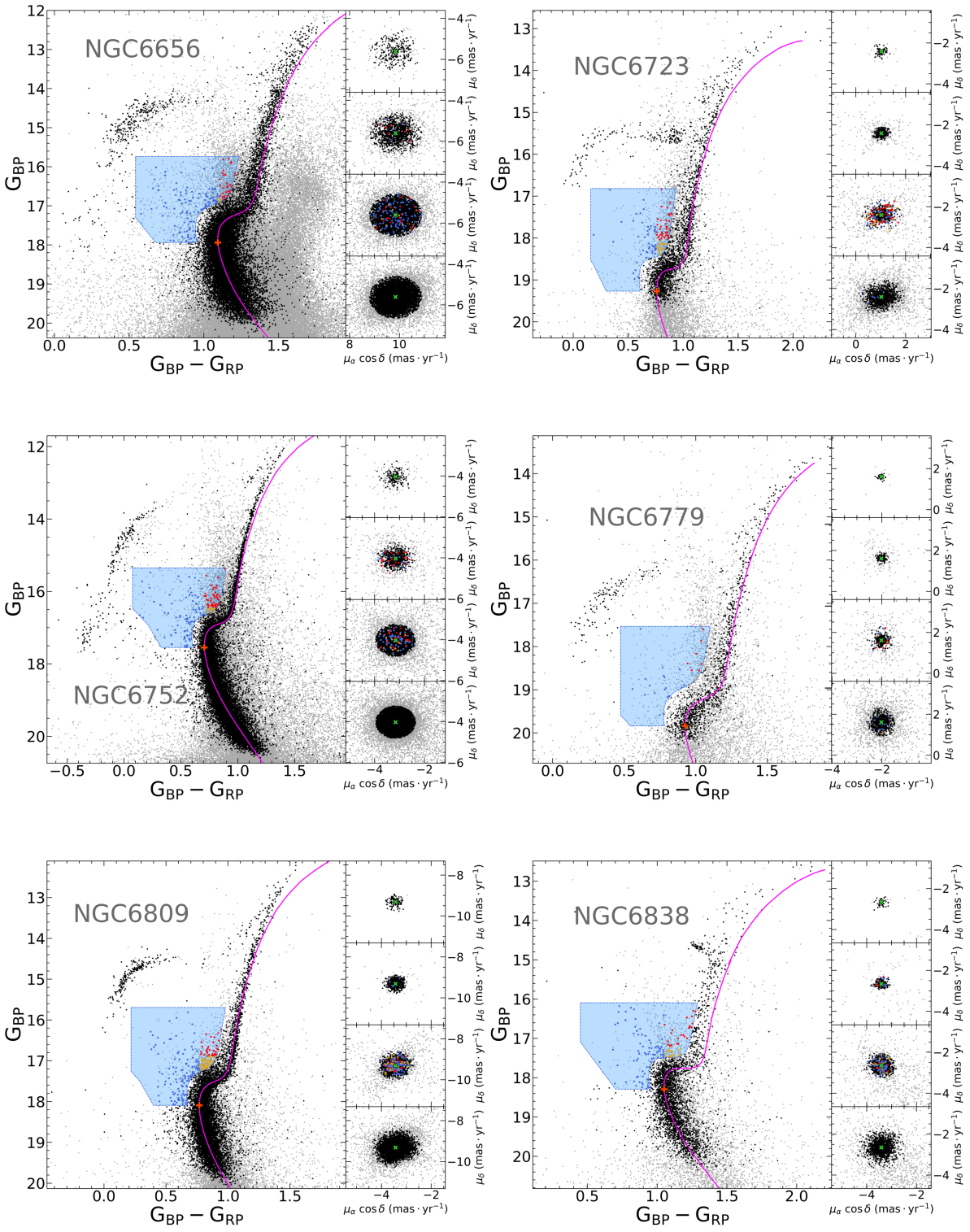

Figure A.7: Same as Figure 3.7, but for the rest of the GC sample.

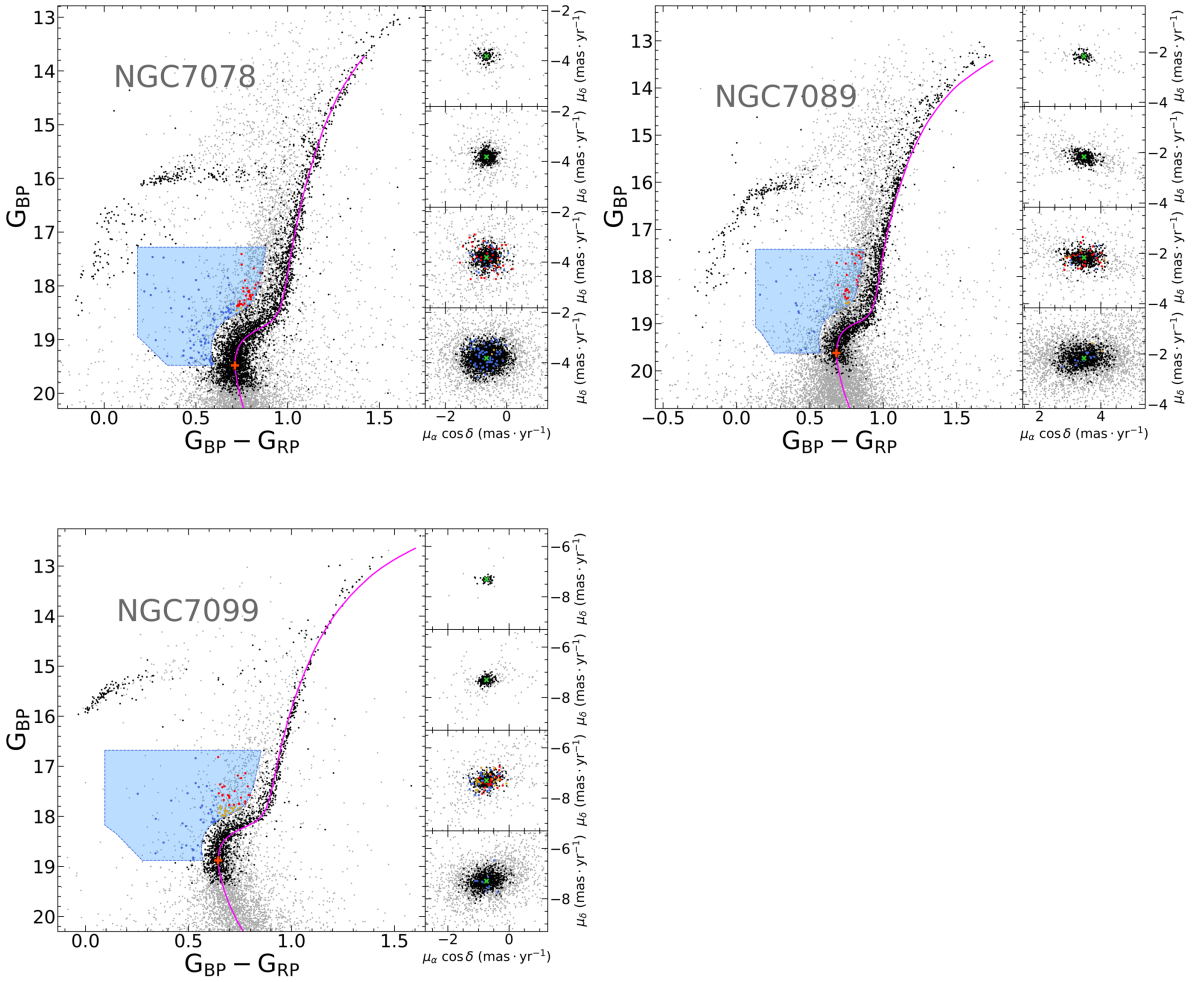

Figure A.8: Same as Figure 3.7, but for the rest of the GC sample.

A.2 Open Clusters

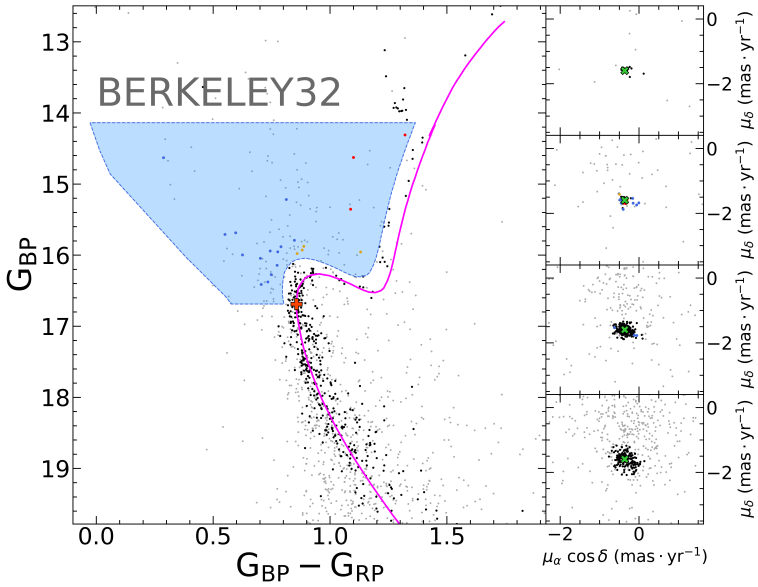

Figure A.9: Same as Figure 3.8, but for Berkeley32.

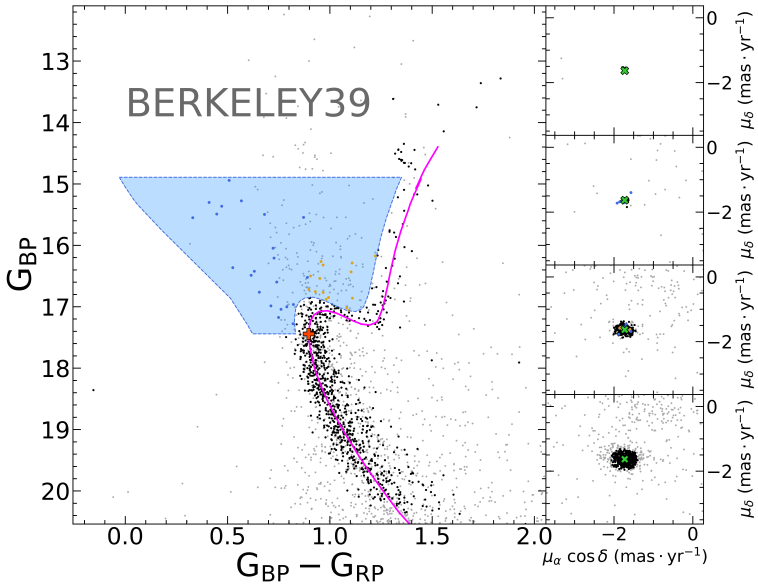

Figure A.10: Same as Figure 3.8, but for Berkeley39.

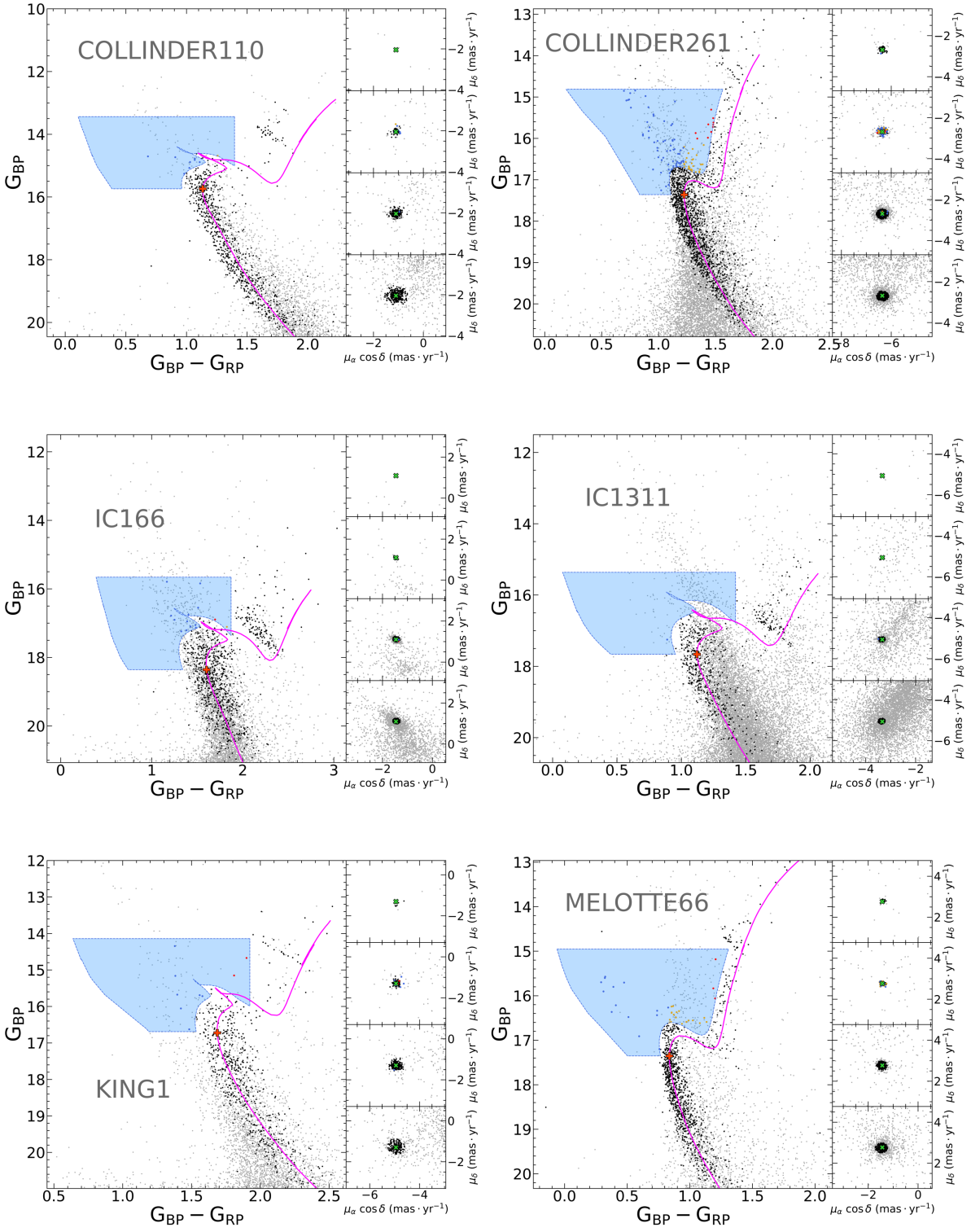

Figure A.11: Same as Figure 3.8, but for the rest of the OC sample.

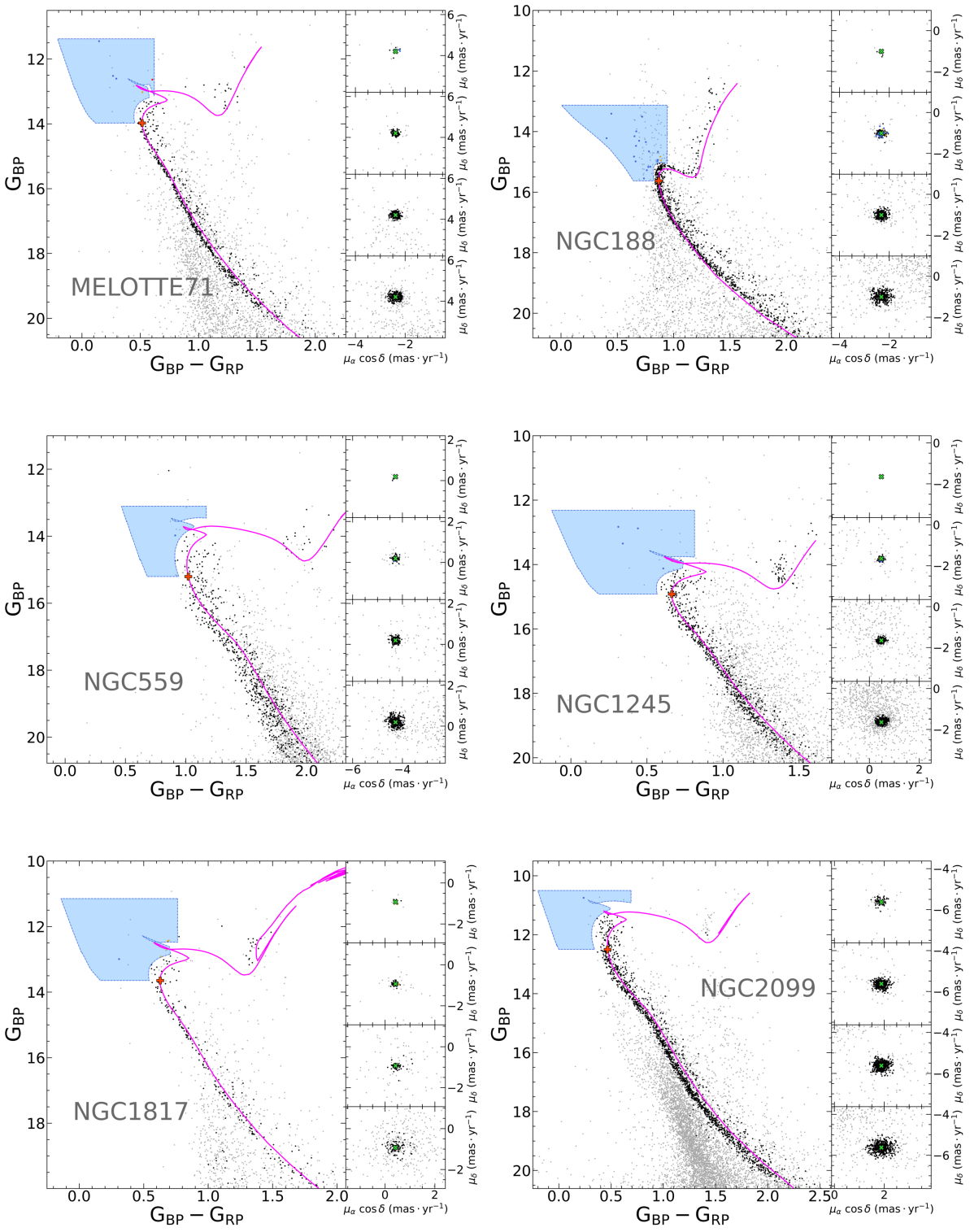

Figure A.12: Same as Figure 3.8, but for the rest of the OC sample.

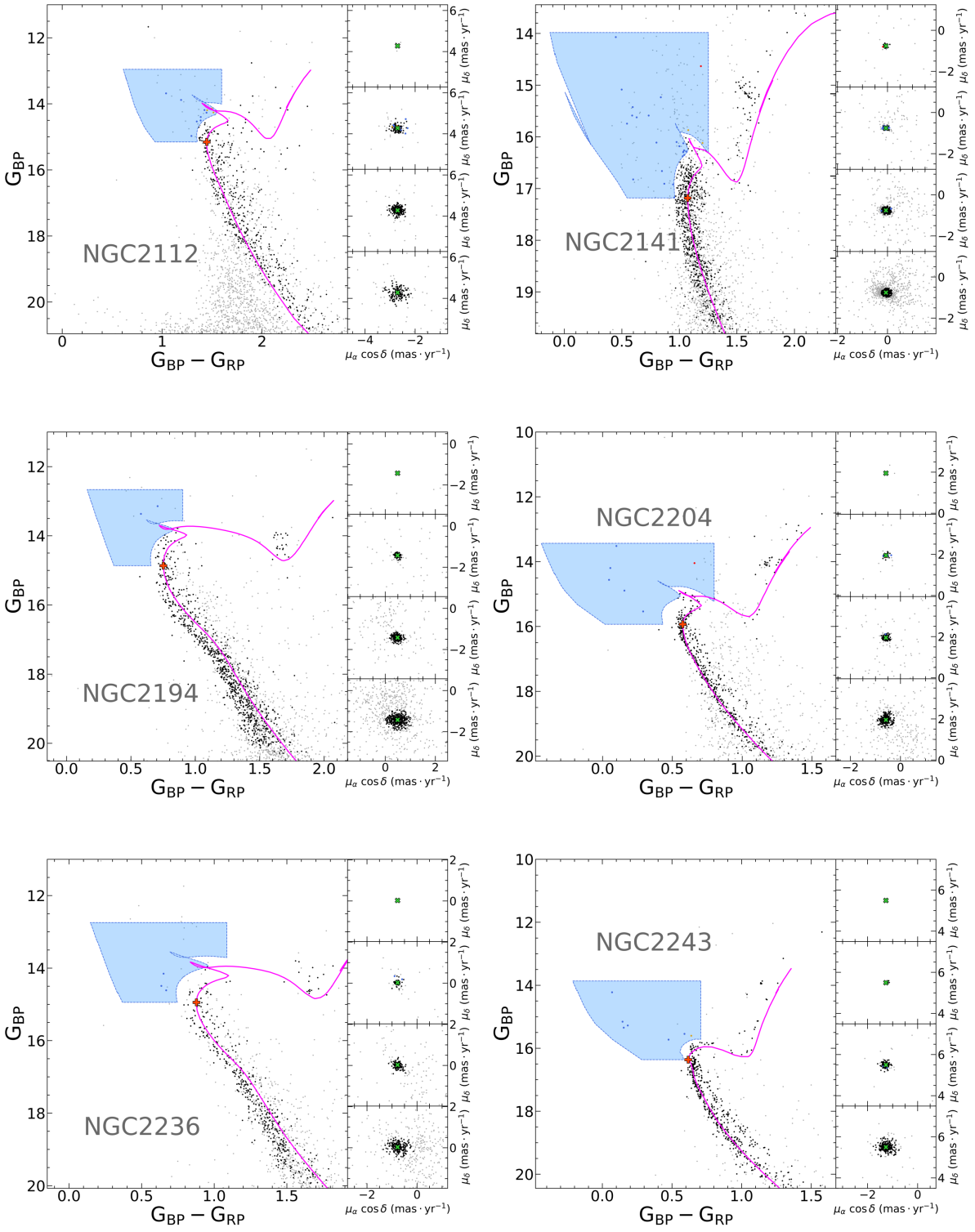

Figure A.13: Same as Figure 3.8, but for the rest of the OC sample.

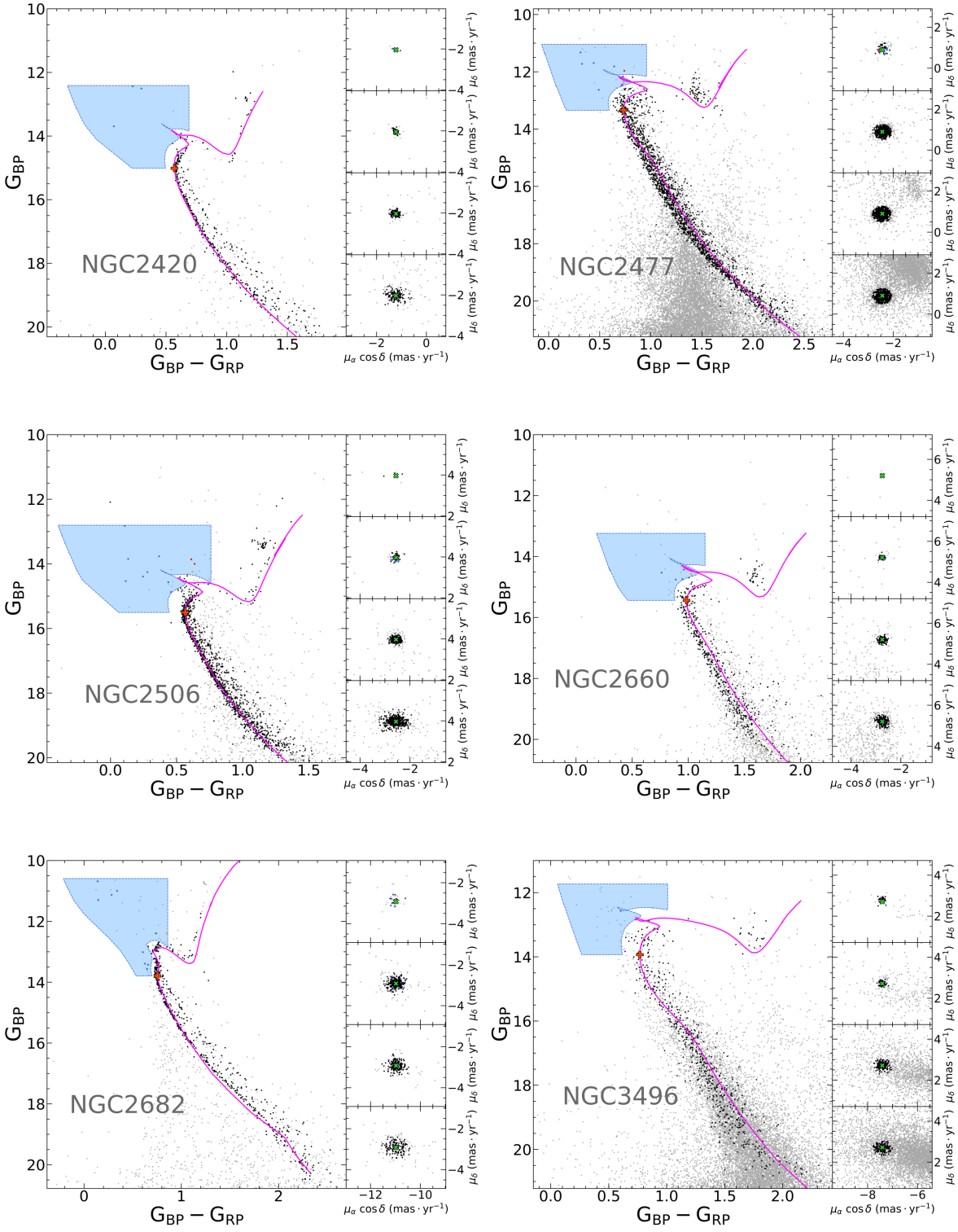

Figure A.14: Same as Figure 3.8, but for the rest of the OC sample.

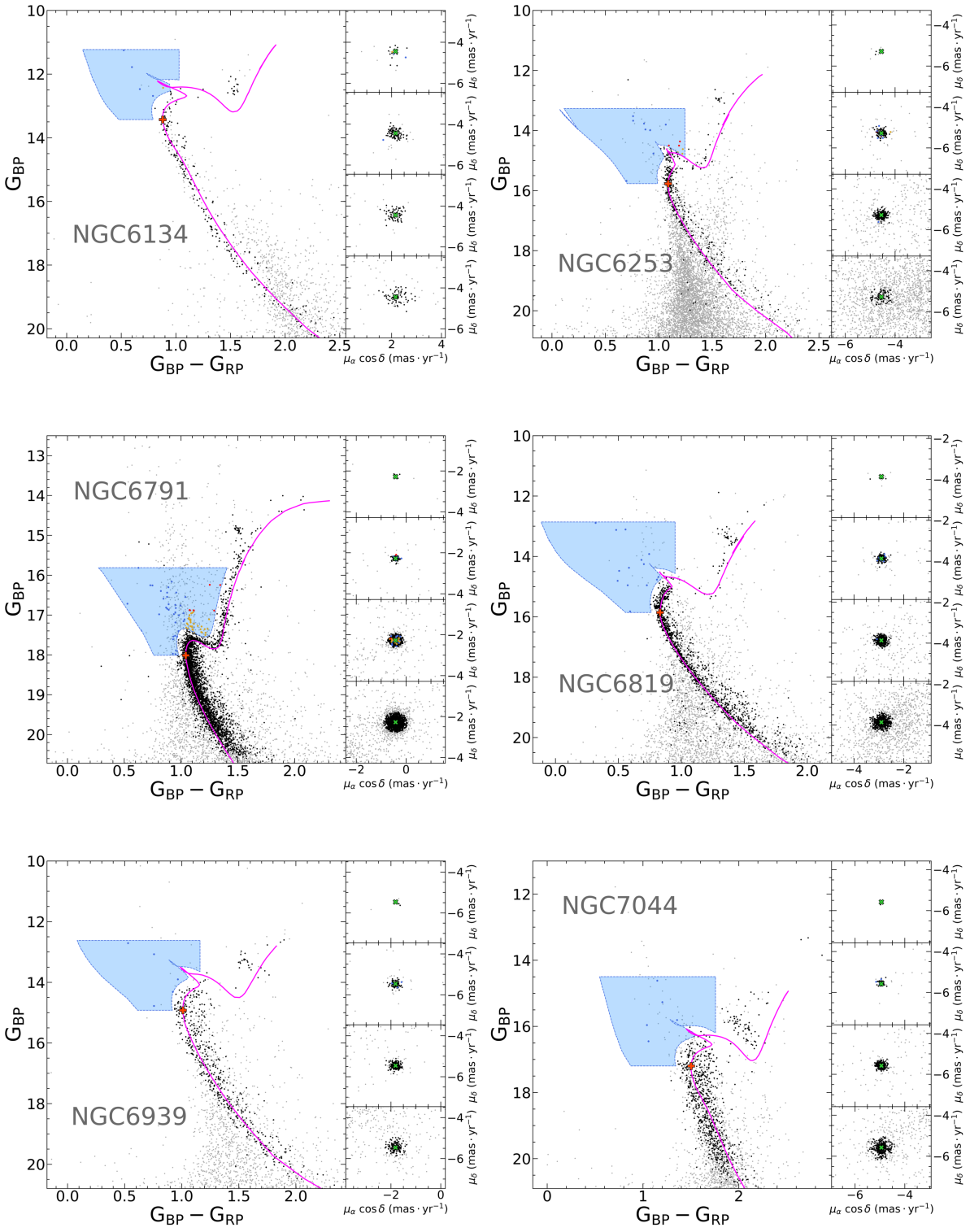

Figure A.15: Same as Figure 3.8, but for the rest of the OC sample.

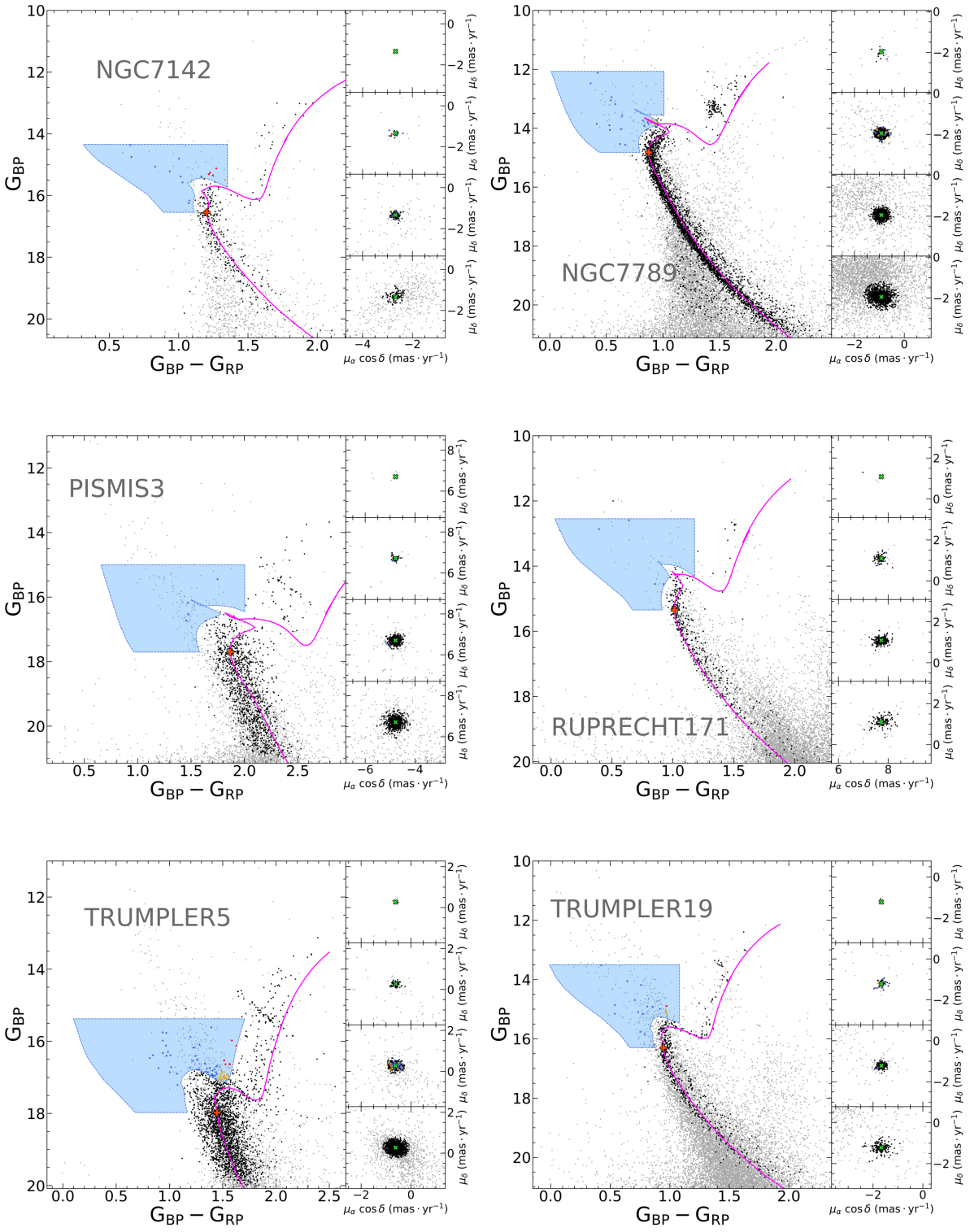

Figure A.16: Same as Figure 3.8, but for the rest of the OC sample.

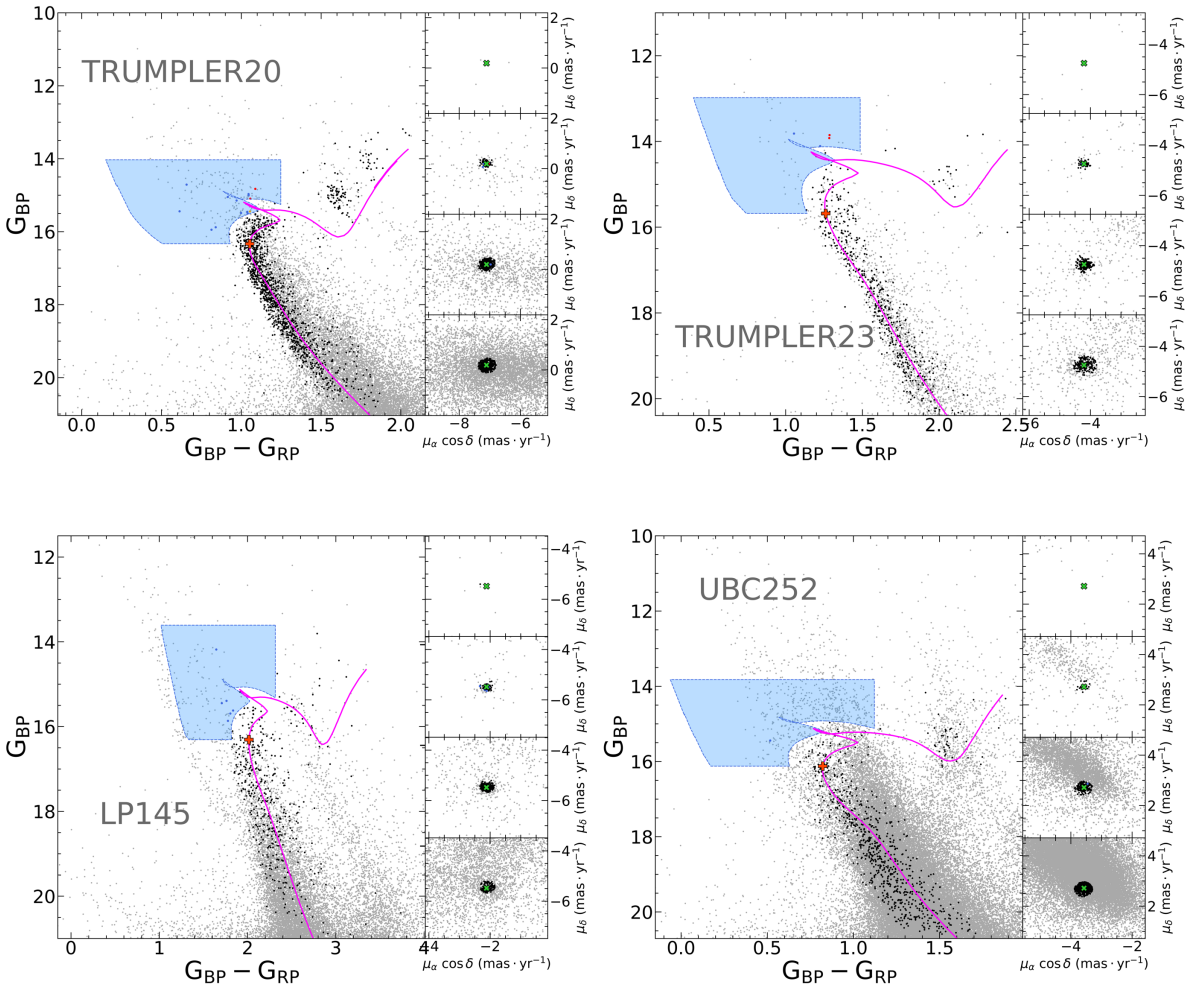

Figure A.17: Same as Figure 3.8, but for the rest of the OC sample.

Appendix B

Astrophysical Parameters of Yellow Straggler Stars and Red Straggler Stars

B.1 Effective Temperatures

Similar to equations (4.1) and (4.2), we derive the relations of $T_{\rm eff}$ obtained through color–temperature relations and XPP against $T_{\rm eff}$ found with isochrones for YSSs –with errors below 300 K in both components–, in units of K, as:

$$T_{\rm eff,\ IRFM} = 0.952\ \times T_{\rm eff,\ isochrone} - 204 \tag{B.1}$$

$$T_{\rm eff,\ xpp} = 1.017\ \times T_{\rm eff,\ isochrone} - 161 \tag{B.2}$$

And for RSSs:

$$T_{\rm eff,\ IRFM} = 0.897\ \times T_{\rm eff,\ isochrone} - 529 \tag{B.3}$$

$$T_{\rm eff,\ xpp} = 1.334\ \times T_{\rm eff,\ isochrone} - 1963 \tag{B.4}$$

Equations (B.1) and (B.2) are the best-fit for the top and bottom of Figure B.1, respectively. Equations (B.3) and (B.4) are the best-fit for the top and bottom of Figure

B.2, respectively.

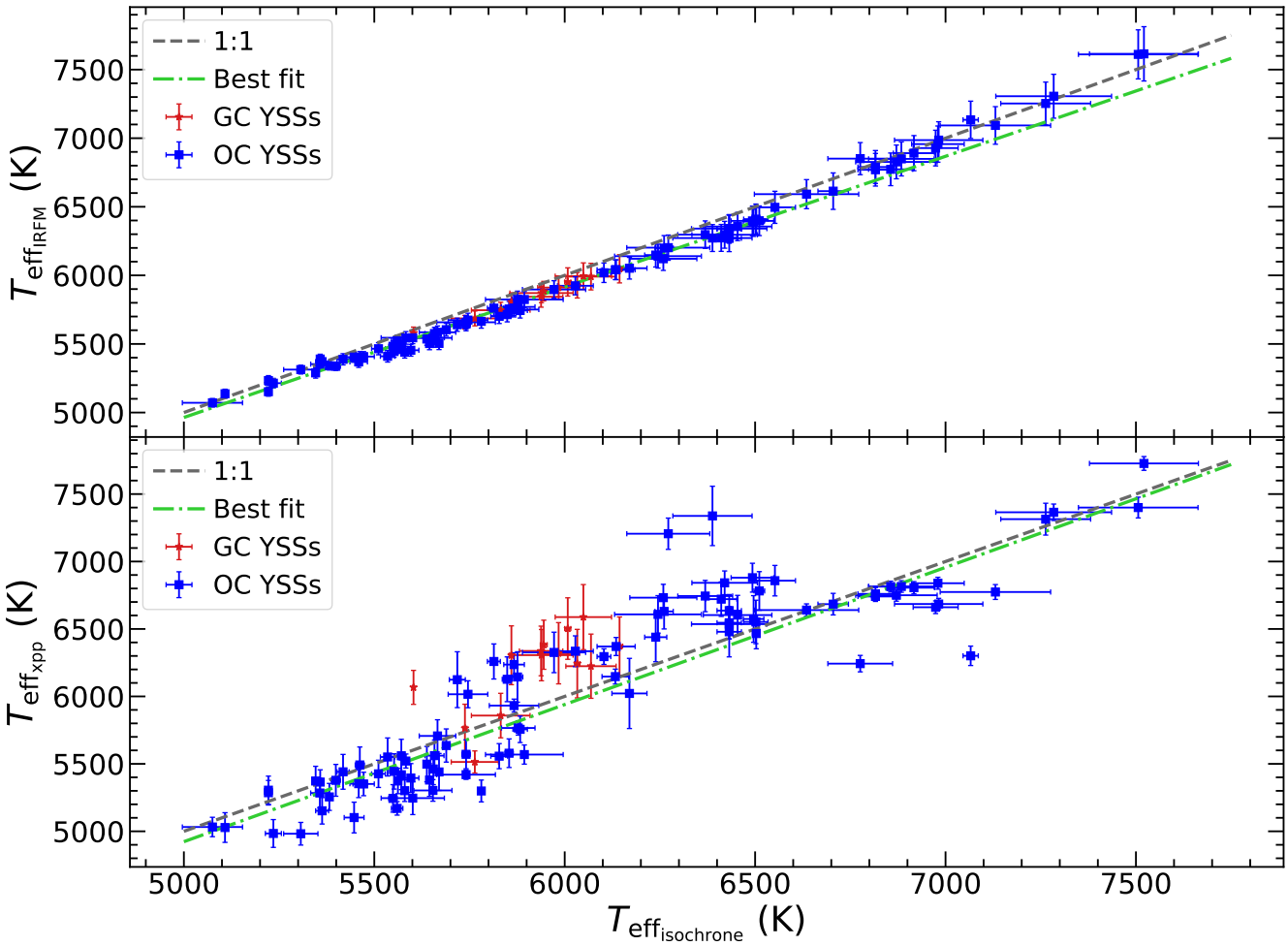

Figure B.1: Similar to Figure 4.2, but for YSSs.

Similar to equation (4.3), we derive the relations of T_{eff} found using color–temperature relations and those provided by XPP for YSSs, in K units, as:

$$T_{\mathrm{eff,\ xpp}} = 1.066\ \times T_{\mathrm{eff,\ IRFM}} - 371 \tag{B.5}$$

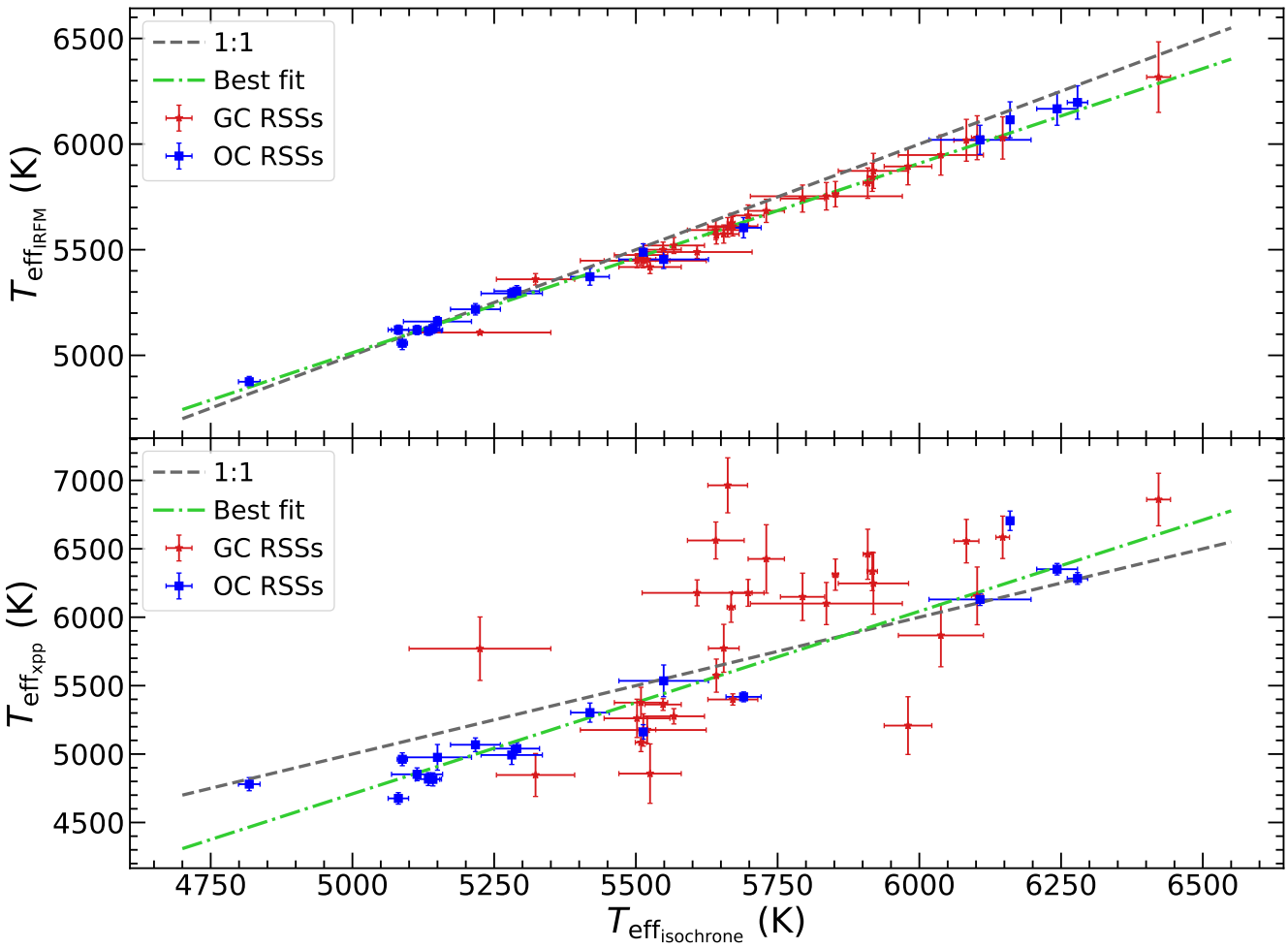

Figure B.2: Similar to Figure 4.2, but for YSSs.

And, finally, for RSSs:

$$T_{\mathrm{eff,\ xpp}} = 1.485\ \times T_{\mathrm{eff,\ IRFM}} - 2735 \tag{B.6}$$

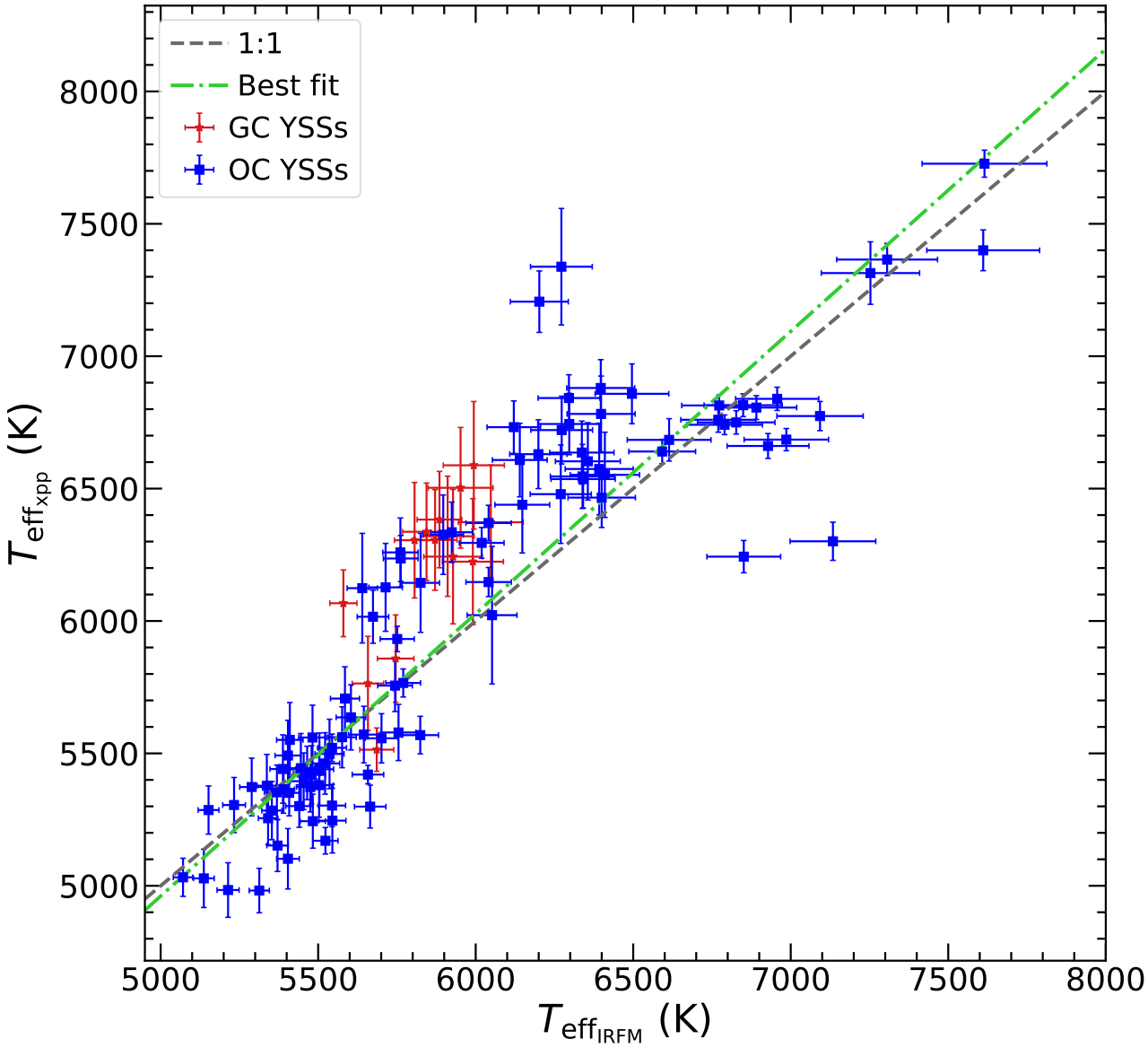

Figure B.3: Similar to Figure 4.3, but for YSSs.

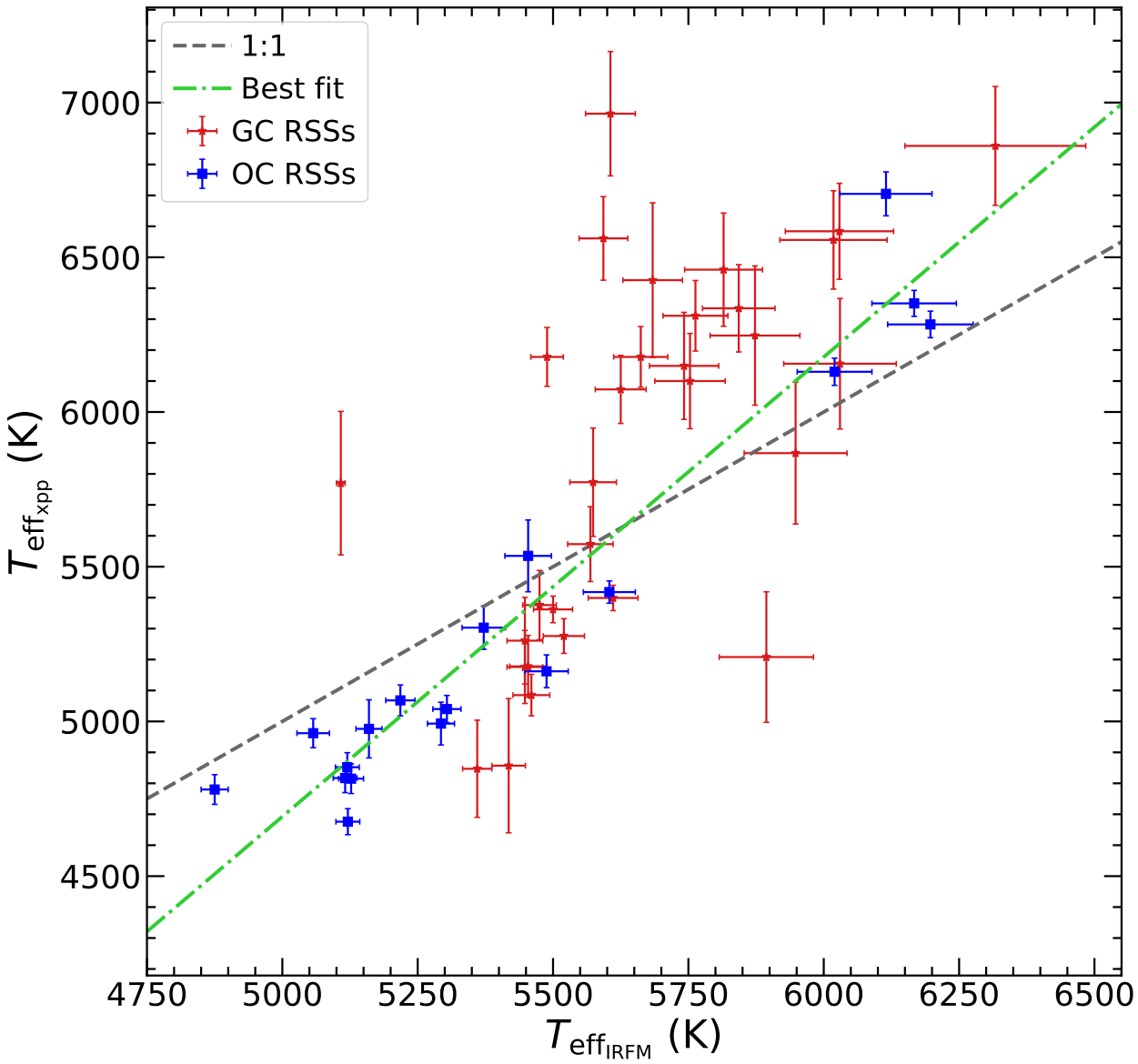

Figure B.4: Similar to Figure 4.3, but for RSSs.

B.2 Surface gravity

Surface gravity, log(g), for YSSs and RSSs were obtained from isochrone models and XPP. Similar as equation (4.4) for Figure 4.4, we derive relations for YSSs:

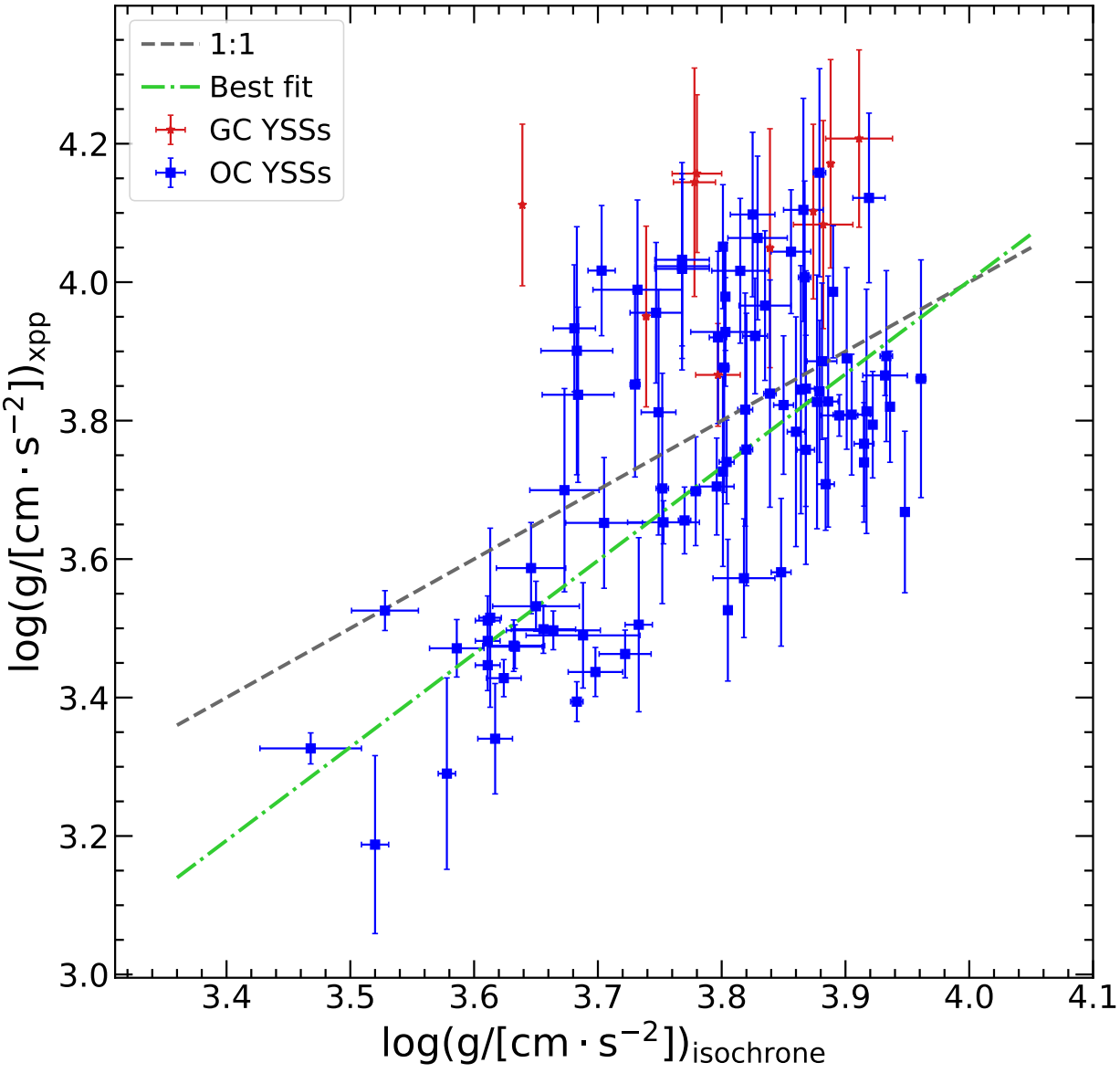

Figure B.5: Similar as Figure 4.4, but for YSSs.

$$\log(g)_{\rm xpp} = 1.347 \times \log(g)_{\rm isochrone} - 1.39 \tag{B.7}$$

and RSSs:

$$\log(g)_{\rm xpp} = 1.207 \times \log(g)_{\rm isochrone} - 0.80 \tag{B.8}$$

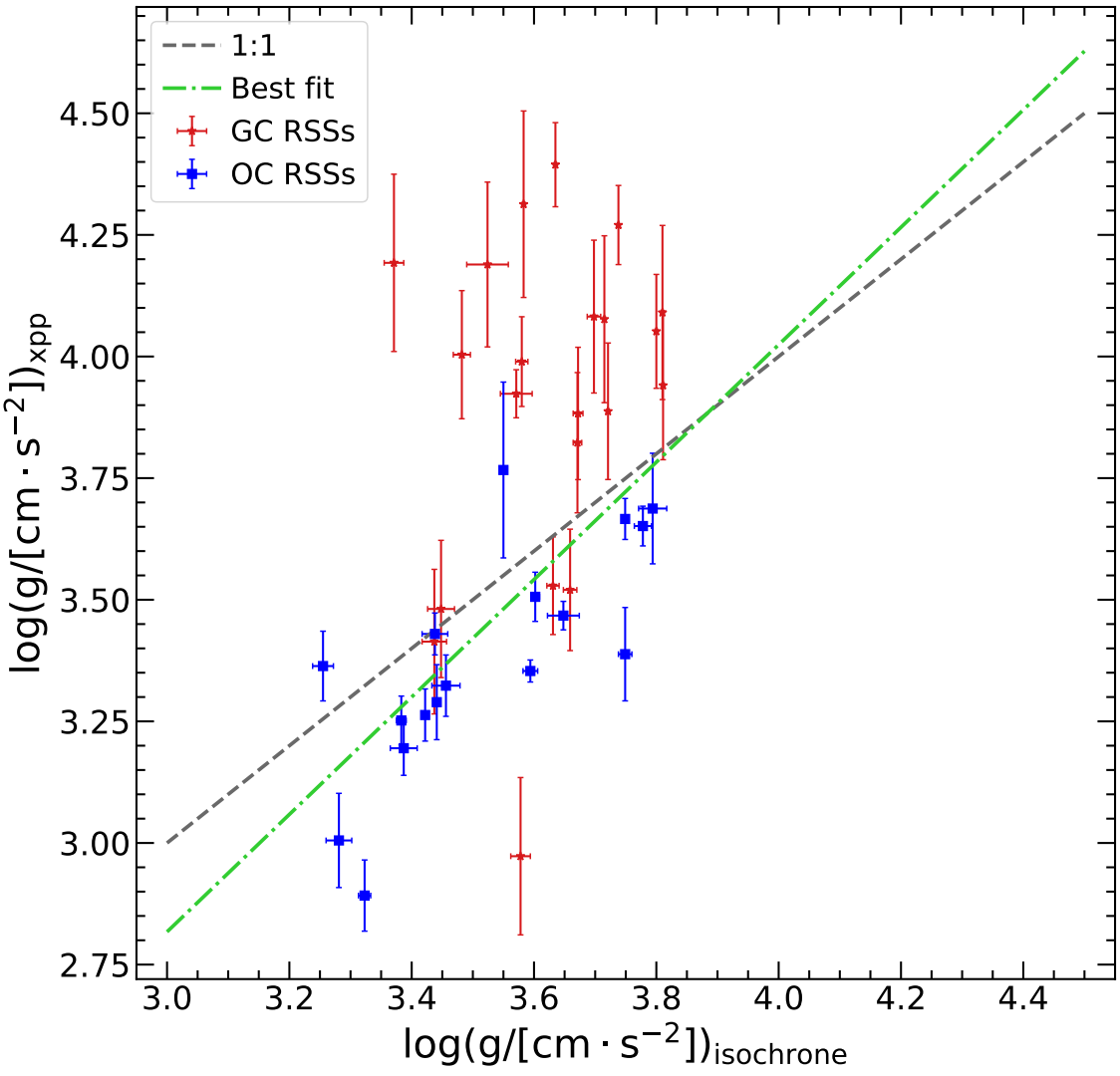

Figure B.6: Similar as Figure 4.4, but for RSSs.

Appendix C

Open Source Software/Scripts

Trying to make working with Gaia data more comfortable and accessible to people, is that we created some public/open source scripts to work with. Both codes apply Cordoni et al. (2018) algorithm presented in this work (Section 3.1), both written on Python3 Programming Language.

- The first one is a Jupyter Notebook, which is the option if the user prefers to read what is happening with the data instead of working with a "black box".

  Github repository link: `https://github.com/gunzf0x/astrogaia-jupyter`

- The second is a Command-Line Interface (CLI) script –designed for Debian based Operations Systems such as Ubuntu–, which is similar to its Jupyter version, but designed to work with Gaia data in a faster way. This will be soon available through `pip` command with: `pip3 install astrogaia`

  Github repository link: `https://github.com/gunzf0x/astrogaia-python`

Note that these links to the repositories may not work into the future. If you want to contact the author try sending an email to `ffcarrasco@uc.cl` or `fcarrasco@astro.puc.cl`